



MONASH University

**An Analysis of the Errors Associated
with the Estimation of Turbulent
Dissipation from PIV-type Data in
Wall-bounded Flows**

by

**Dinesh Kanhaiya Meena
Bhatia**

A thesis submitted for the degree of *Master of Engineering Science*
at Monash University in April 2018

April 2018

Abstract

This thesis discusses the impact of finite spatial and dimensional resolution of the velocity fields provided by most experimental measurement techniques, on the accuracy of the turbulent dissipation rate in channel flows. These characteristics introduce a bias error in the calculated turbulent dissipation rate, leading to its underestimation and consequentially an overestimation of the Kolmogorov length scale, the accuracy of which is critical in turbulence research.

To investigate the effect of finite spatial resolution, velocity fields obtained from direct numerical simulation (DNS) of a turbulent channel flow are spatially filtered successively along each of the three Cartesian directions and the effect of spatial filtering along each direction on the turbulent dissipation rate is reported. The analysis reveals that spatial filtering along the wall-normal direction has the largest effect on turbulent dissipation rate in the near wall region, while the spatial filtering along only the stream-wise direction has the least effect. The truncation error in the gradient calculation scheme is found to have a large effect on the accuracy of dissipation in the near wall region, its fractional contribution at large wall-normal filter sizes is as high as 40% of the total error.

All the components of the velocity gradient tensor needed to calculate the turbulent dissipation rate cannot be directly determined in most experimental techniques due to their limited dimensional resolution capabilities. In such cases, the missing components are modelled using various formulations. The dissipation calculated from unfiltered DNS velocity fields by using the existing formulations from literature is found to be highly inaccurate in the near-wall region when compared with the true value. A new model has been developed to estimate dissipation accurately in the near wall region when a limited number of components of the velocity gradient tensor are obtained from any experimental technique which provides either 2 component 2 direction (2C-2D) or 3 component 2 direction (3C-2D) velocity field measurements. When the dissipation is calculated using the new model, with the derivatives

calculated from the unfiltered DNS data, it has a maximum error of 20% of true value in the entire channel while the maximum error in Kolmogorov length scale was 5% of the true value.

The net error in the turbulent dissipation rate and Kolmogorov length scale due to limited spatial and dimensional resolution of velocity fields provided by any experimental technique which involve spatial filtering, was estimated by spatially filtering velocity fields at resolutions typical of various experimental techniques and then employing the existing and new models to calculate dissipation. The error introduced due to spatial filtering alone was found to be the dominant source of error in dissipation as compared to the error introduced due to the use of various models. The error arising from the use of the models depends on the size of the measurement volume and the choice of an appropriate model for wall-bounded flows can thus vary with Reynolds number and size of the measurement volume.

Table of contents

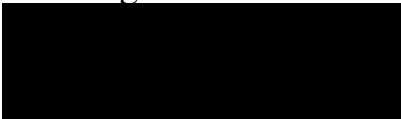
Acknowledgements	ix
List of figures	xi
List of tables	xvii
Nomenclature	xix
Introduction	xxiii
1 Challenges in Determination of Turbulent Dissipation Rate from Experiments	1
1.1 Effect of finite size of the measurement volume	1
1.2 Effect of limited dimensionality	4
1.3 Combined effect of spatial filtering and limited dimensionality	8
2 Channel Flow DNS dataset	11
2.1 Description of the DNS database	11
2.2 Turbulent Dissipation in Channel Flow	12
3 Computational Methodology	17
3.1 Gradient computation methods	17
3.2 Spatial filtering technique	18
3.2.1 Study of spatial filtering methods	18
4 Effect of Spatial Filtering on Dissipation	23
4.1 Effect of truncation error on turbulent dissipation rate	24
4.2 Effect of filter size in the wall-normal (y) direction	25
4.3 Effect of filter size in the span-wise (z) direction	34

4.4	Effect of filter size in the stream-wise (x) direction	39
5	Effect of Dimensionally Limited Data on Dissipation	47
5.1	Existing models	47
5.1.1	Local axisymmetry model	47
5.1.2	Weak local isotropy model	51
5.1.3	Evaluation of performance of the existing models	51
5.2	Local homogeneity model	53
6	Combined Effect of Spatial Filtering and Limited Dimensionality on Turbulent Dissipation Rate	59
6.1	1C-1D Velocity Fields	60
6.2	2C-2D Velocity Fields	63
6.3	3C-2D Velocity Fields	67
7	Discussion and Conclusions	73
Appendix A	Formulation of True Error in Dissipation due to Spatial Filtering	81
Appendix B	Results	85
B.1	Effect of Spatial Filtering: Contribution of error from various components .	85
B.1.1	Effect of filter size in the wall-normal direction	85
B.1.2	Effect of filter size in the span-wise direction	87
B.1.3	Effect of filter size in the stream-wise direction	89
	Bibliography	91

Declaration

I hereby declare that this thesis contains no material which has been accepted for the award of any other degree or diploma at any university or equivalent institution and that, to the best of my knowledge and belief, this thesis contains no material previously published or written by another person, except where due reference is made in text of the thesis.

Signature:

A solid black rectangular box used to redact the signature of the author.

Name: Dinesh Kanhaiya Meena Bhatia

Date: April 2018

Acknowledgements

The path of academic achievement is rarely completed without the support of mentors, colleagues, family, and friends, my current work is no exception.

I would first like to thank my supervisor Prof. Julio Soria for not only giving me an opportunity to work with his group but also for being a strict and supportive mentor always encouraging me to push my boundaries and to transcend my perceived limits. In addition, I am incredibly grateful to Prof. Soria for the economic support without which this work wouldn't have been possible.

I would like to extend my sincere thanks to my co-supervisor Dr. Callum Atkinson for his constant guidance and his support in helping me break the mould and change my perception of academic research. I also wish to thank my colleagues at Laboratory of Turbulence Research in Aerospace and Combustion for their friendship, advice, and support.

Finally, I have to thank my parents and sister for giving me the support and freedom through my struggles with the challenges posed by my research.

List of figures

2.1	Joint PDF of $\partial u/\partial x$ and $-(\partial v/\partial y + \partial w/\partial z)$ of one DNS field	13
2.2	Fractional contribution of various velocity gradient terms to dissipation . .	14
2.3	Distribution of dissipation and Kolmogorov length scale along the channel height for unfiltered velocity fields	15
2.4	Distribution of Integral fraction (χ) along the channel height for DNS dataset	16
3.1	Schematic of clustering of grid points within the filter window (green box) in the near wall region	19
3.2	Schematic representation of volume weighted averaging filter	19
3.3	Comparison of the mean turbulent dissipation rate calculated from unfiltered velocity fields with velocity fields spatially filtered using volume weighted averaging method with filter of size $f_x^+ \times f_y^+ \times f_z^+ = 8 \times 8 \times 8$	20
3.4	Comparison of the mean turbulent dissipation rate for filtered and unfiltered velocity fields. The filtering operation is performed by applying a box-filter (Eq. 3.3) and using the numerical integration method, the filter size is $f_x^+ \times f_y^+ \times f_z^+ = 8 \times 8 \times 8$	21
4.1	Profiles of the mean turbulent dissipation rate in wall-units ε^+ for the unfiltered case (black) and various wall-normal filter sizes (f_y^+); $f_x^+ = 0$, $f_z^+ = 0$	27
4.2	Effect of increasing the filter size in the wall-normal direction (f_y^+) on normalized dissipation (r_ε) at various wall-normal locations; $f_x^+ = 0$, $f_z^+ = 0$	28
4.3	Effect of increasing the filter size in the wall-normal direction (f_y^+) on normalized Kolmogorov length scale (r_η) at various wall-normal heights; $f_x^+ = 0$, $f_z^+ = 0$	28

4.4	Contribution of truncation error to the total error is dissipation for various wall-normal filter sizes (f_y^+); $f_x^+ = 0$, $f_z^+ = 0$	29
4.5	Profiles of integral error ($\tilde{\xi}$) for various wall-normal filter sizes (f_y^+), $f_x^+ = 0$, $f_z^+ = 0$	30
4.6	Contribution of error in various gradient terms to the error in dissipation (α_r) for different wall-normal filter sizes ($f_y^+ = 0$); $f_x^+ = 0$, $f_z^+ = 0$	31
4.7	Effect of increasing the filter size in the wall-normal direction (f_y^+) on α_r (solid lines) and r_c (dashed)	31
4.8	Effect of increasing the filter size in the wall-normal direction on normalized Kolmogorov length scale (r_η) at various wall-normal heights: (a) $f_x^+ = 16$, $f_z^+ = 12$, (b) $f_x^+ = 16$, $f_z^+ = 20$	32
4.9	Consolidated results of the effect of filtering along wall-normal direction on the error in total dissipation in the channel ($\tilde{\beta}(h)$) and minimum Kolmogorov length scale ($\tilde{\eta}_{min}/\eta_{min}$)	34
4.10	Profiles of the mean turbulent dissipation rate in wall-units ε^+ for the unfiltered case (black) and various span-wise filter sizes (f_z^+), $f_x^+ = 0$, $f_y^+ = 0$	35
4.11	Effect of increasing the filter size in the span-wise direction (f_z^+) on normalized dissipation (r_ε) at various wall-normal locations; $f_x^+ = 0$, $f_y^+ = 0$	36
4.12	Contribution of truncation error to the total error in dissipation for various span-wise filter sizes(f_z^+); $f_x^+ = 0$, $f_y^+ = 0$	36
4.13	Profiles of Integral error ($\tilde{\xi}$) for various span-wise filter sizes (f_z^+); $f_x^+ = 0$, $f_y^+ = 0$	37
4.14	Contribution of error in various terms to the error in dissipation (α_r) for different span-wise filter sizes (f_z^+); $f_x^+ = 0$, $f_y^+ = 0$	37
4.15	Effect of spatial filter size in the span-wise direction (f_z^+) on normalized Kolmogorov length scale (r_η) at various wall-normal heights: (a) $f_x^+ = 0$, $f_y^+ = 0$, (b) $f_x^+ = 0$, $f_y^+ = 8$, (c) $f_x^+ = 24$, $f_y^+ = 24$	38

4.16	Consolidated results of the effect of filtering along span-wise direction on the error in total dissipation in the channel ($\tilde{\beta}(h)$) and minimum Kolmogorov length scale ($\tilde{\eta}_{min}/\eta_{min}$)	39
4.17	Profiles of the mean turbulent dissipation rate in wall-units ε^+ for the unfiltered case (black) and various stream-wise filter sizes (f_x^+), $f_y^+ = 0$, $f_z^+ = 0$	40
4.18	Effect of increasing the filter size in the stream-wise direction (f_x^+) on normalized dissipation rate (r_ε); $f_y^+ = 0$, $f_z^+ = 0$	41
4.19	Effect of spatial filtering alone on normalized turbulent dissipation rate (r_{ε_T}) for various stream-wise filter sizes (f_x^+), $f_y^+ = 0$, $f_z^+ = 0$	42
4.20	Contribution of truncation error to total error for various stream-wise filter sizes (f_x^+), $f_y^+ = 0$, $f_z^+ = 0$	42
4.21	Profiles of integral error ($\tilde{\xi}$) for various stream-wise filter sizes (f_x^+), $f_y^+ = 0$, $f_z^+ = 0$	43
4.22	Effect of increasing the filter size in the stream-wise direction (f_x^+) on α_r (solid lines) and r_c (dashed)	43
4.23	Effect of increasing the filter size in the stream-wise direction direction (f_x^+) on normalized Kolmogorov length scale (r_η) at various wall-normal heights : (a) $f_y^+ = 0$, $f_z^+ = 0$, (b) $f_y^+ = 8$, $f_z^+ = 8$, (c) $f_y^+ = 16$, $f_z^+ = 24$	44
4.24	Consolidated results of the effect of filtering along stream-wise direction on the error in total dissipation in the channel ($\tilde{\beta}(h)$) and minimum Kolmogorov length scale ($\tilde{\eta}_{min}/\eta_{min}$)	45
5.1	Distribution of the normalized turbulent dissipation rate (r_ε^m) along the channel height for 1C-1D and 2C-2D velocity field formulations based on local isotropy, local axisymmetry and weak local isotropy assumptions; $r_\varepsilon^m = 1$ (black dash)	52
5.2	Distribution of the normalized turbulent dissipation rate (r_ε^m) along the channel height for 3C-2D velocity field formulations based on local axisymmetry and weak local isotropy assumptions; x-y plane formulation	52

5.3	Distribution of the normalized turbulent dissipation rate (r_ε^m) along the channel height for 3C-2D velocity field formulations based on local axisymmetry and weak local isotropy assumptions; y-z plane formulation	53
5.4	Profiles of the normalized turbulent dissipation rate (r_ε^m), normalized Kolmogorov length scale (r_η^m) and Integral ratio (β^m) calculated using 2C-2D velocity field formulations of local homogeneity assumption, weak local isotropy assumption and blend formulation	56
5.5	Profiles of the normalized turbulent dissipation rate (r_ε^m), normalized Kolmogorov length scale (r_η^m) and Integral ratio (β^m) calculated using 3C-2D velocity field formulations of weak local isotropy assumption, local homogeneity assumption and blend formulation; solid lines (x-y plane formulation), dashed (y-z plane formulation)	57
6.1	Effect of span-wise wire length(l) on normalised dissipation rate (r_ε^m) and normalised Kolmogorov length scale (r_η^m) calculated using the local isotropy formulation	61
6.2	Profiles of the normalised turbulent dissipation rate (r_ε^m) and normalised Kolmogorov length scale (r_η^m) for various measurement volume sizes calculated using 2C-2D velocity field Local axisymmetry-x formulation for various measurement volume sizes	64
6.3	Profiles of the normalised turbulent dissipation rate (r_ε^m) and normalised Kolmogorov length scale (r_η^m) for various measurement volume sizes calculated using 2C-2D velocity field Local axisymmetry-y formulation for various measurement volume sizes	65
6.4	Profiles of the normalised turbulent dissipation rate (r_ε^m) and normalised Kolmogorov length scale (r_η^m) for various measurement volume sizes calculated using 2C-2D velocity field Weak local isotropy formulation for various measurement volume sizes	65

6.5	Profiles of the normalised turbulent dissipation rate (r_{ε}^m) and normalised Kolmogorov length scale (r_{η}^m) for various measurement volume sizes calculated using 2C-2D velocity field Blend formulation for various measurement volume sizes	66
6.6	Profiles of the normalised turbulent dissipation rate (r_{ε}^m) and normalised Kolmogorov length scale (r_{η}^m) for various measurement volume sizes calculated using x - y plane Local axisymmetry- x formulation: 3C-2D velocity fields . . .	67
6.7	Profiles of the normalised turbulent dissipation rate (r_{ε}^m) and normalised Kolmogorov length scale (r_{η}^m) for various measurement volume sizes calculated using x - y plane Local axisymmetry- y formulation: 3C-2D velocity fields . .	68
6.8	Profiles of the normalised turbulent dissipation rate (r_{ε}^m) and normalised Kolmogorov length scale (r_{η}^m) for various measurement volume sizes calculated using x - y plane Weak local isotropy formulation: 3C-2D velocity fields . . .	68
6.9	Profiles of the normalised turbulent dissipation rate (r_{ε}^m) and normalised Kolmogorov length scale (r_{η}^m) for various measurement volume sizes calculated using x - y plane Blend formulation: 3C-2D velocity fields	69
6.10	Profiles of the normalised turbulent dissipation rate (r_{ε}^m) and normalised Kolmogorov length scale (r_{η}^m) for various measurement volume sizes calculated using y - z plane Local axisymmetry- y formulation: 3C-2D velocity fields . .	69
6.11	Profiles of the normalised turbulent dissipation rate (r_{ε}^m) and normalised Kolmogorov length scale (r_{η}^m) for various measurement volume sizes calculated using y - z plane Weak local isotropy formulation: 3C-2D velocity fields . . .	70
6.12	Profiles of the normalised turbulent dissipation rate (r_{ε}^m) and normalised Kolmogorov length scale (r_{η}^m) for various measurement volume sizes calculated using y - z plane Blend formulation: 3C-2D velocity fields	70
7.1	Turbulent dissipation rate in wall units and integral fraction (χ) for a range of Reynolds number obtained from channel flow DNS of Lee and Moser (2015)	76
B.1	Effect of increasing the filter size in the wall-normal direction (f_y^+) on α_r (solid lines) and r_c (dashed)	86

B.2	Effect of increasing the filter size in the span-wise direction (f_z^+) on α_r (solid lines) and r_c (dashed)	88
B.3	Effect of increasing the filter size in the stream-wise direction (f_x^+) on α_r (solid lines) and r_c (dashed)	90

List of tables

2.1	Numerical details of DNS dataset	12
4.1	Filter size combinations used for study of the effect of spatial filter size in the wall-normal direction (f_y^+), the quantity in brackets is the corresponding grid spacing	26
4.2	Filter size combinations used to study the effect of filter size along the span-wise direction (f_z^+) direction, the quantities in brackets are the corresponding grid spacings	34
4.3	Filter size combinations used for study of the effect of filter size in the stream-wise direction (f_x^+) direction, the quantities in brackets are the corresponding grid spacings	40
6.1	Consolidated results of net effect of wire length and use of the 1C-1D velocity field, Local Isotropy Formulation (ISO) formulation	62
6.2	Estimate of minimum Kolmogorov length scale expressed as a fraction of the true value calculated using Eq. 6.1, the stream-wise velocity is assumed to be measured using a hot-wire anemometer at $y^+ = 8$ and the wall-normal derivative is calculated using the second-order central difference scheme . .	63
6.3	Interrogation window/spatial filter sizes and grid spacing of the velocity fields used to evaluate net error in the turbulent dissipation rate due to limited dimensionality and spatial filtering in experimental measurements using PIV	64
6.4	Consolidated results of 2C-2D velocity field formulations of various models: LA- x , LA- y : Local Axisymmetry about x , Local Axisymmetry about y ; WLI : Weak Local Isotropy; Bl : Blend	66

6.5	Consolidated results for x - y plane 3C-2D velocity field formulations of various models	71
6.6	Consolidated results for y - z plane 3C-2D velocity field formulations of various models	71
7.1	Distribution of dissipation in channel flow for various Reynolds number . . .	77

Nomenclature

Greek Symbols

β Integral Ratio

χ Integral Fraction

$\nabla \cdot \mathbf{U}$ Divergence of the velocity

ε Mean Turbulent Dissipation Rate

η Kolmogorov Length Scale

ε^m Mean Turbulent Dissipation Rate calculated using a model

$\tilde{\Delta}_x, \tilde{\Delta}_z$ Grid spacing in the spatially filtered velocity fields along the x , y and z directions

$\tilde{\varepsilon}$ Mean Turbulent Dissipation Rate calculated from spatially filtered velocity fields

$\tilde{\varepsilon}^m$ Mean Turbulent Dissipation Rate calculated using a model from spatially filtered velocity fields

γ Error in various terms of dissipation due to truncation error

ν Fluid Kinematic Viscosity

ρ Fluid Density

$\Delta x, \Delta z$ Grid spacing of the unfiltered velocity fields along the x and z directions

$\Delta y_{min}, \Delta y_{max}$ Minimum and maximum grid spacing of the unfiltered velocity fields along the y direction

Γ Error in the mean turbulent dissipation rate due to truncation error expressed as a fraction of the total error

$\tilde{\epsilon}_T$	Mean Turbulent Dissipation Rate for filtered velocity fields and zero truncation error
τ_w	wall shear stress
u_τ	Friction Velocity: $u_\tau = \sqrt{\tau_w/\rho}$
ξ	Integral Error

Superscripts

m	The quantity is calculated using a model
-----	--

Other Symbols

b	blend function
\mathcal{C}	Central Derivative Filter
\mathcal{F}	Spatial Filter
h	Channel half height
Re	Reynolds number
Re_τ	Reynolds number based on friction velocity : $Re_\tau = u_\tau h/\nu$
u'_i	Fluctuating velocity component : $u'_1 = u; u'_2 = v; u'_3 = w$

Acronyms / Abbreviations

1C-1D	One-component , one-direction
1D	One-dimensional
2C-2D	Two-component , two-direction
2D	Two-dimensional
3C-2D	Three-component , two-direction
3C-3D	Three-component , three-direction

3D Three-dimensional

DNS Direct Numerical Simulation

DPSPIV Dual Plane Stereo Particle Image Velocimetry

f_x, f_y, f_z Size of filter or measurement volume along x, y and z directions

HWA Hot-wire anemometry

LES Large Eddy Simulation

LH Local Homogeneity

\tilde{g} Spatially filtered value of an unfiltered variable g

PIV Particle Image Velocimetry

$r_a = \tilde{a}/a$ Ratio of filtered value of variable a to its unfiltered value

RANS Reynolds Averaged Navier Stokes

SGS Sub Grid Scale

s_{ij} Fluctuating strain-rate tensor

SPIV Stereo Particle Image Velocimetry

TBL Turbulent Boundary Layer

TPIV Tomographic Particle Image Velocimetry

VA Volume Averaging

W_i Fraction of the filter window volume overlapping with cell i

Introduction

*"Big whirls have little whirls that feed on their velocity,
and little whirls have smaller whirls and so on to viscosity
- in the molecular sense."*

These poetic lines by Richardson (1922) succinctly summarise the turbulent kinetic energy cascade in fluid flows, where the kinetic energy first enters turbulence through the process of production, at the largest scales, and is transferred successively to smaller scales, up to the scales at which Reynolds number (Re) is small enough ($\sim \mathcal{O}(1)$) for molecular viscosity to be effective in dissipating the turbulent kinetic energy (Pope, 2001). This placement of dissipation at the end of the energy cascade, the rate of which is determined by production of turbulent kinetic energy in a statistically stationary flow, makes the rate of production (\mathcal{P}) and dissipation (ε) the source and sink of turbulent kinetic energy respectively, each playing a fundamental role in the study of turbulent flow processes.

The dissipation rate of turbulent kinetic energy is primarily a small-scale phenomenon, hence its accurate determination is critical for the modelling of many small-scale processes (Gerolymos and Vallet, 2016; Lee and Reynolds, 1987; Sreenivasan and Antonia, 1997). For example, models of chemical and turbulent mixing processes in tanks and combustion chambers rely on the accurate determination of the mean turbulent dissipation rate and its distribution across the domain of interest. (Delafosse et al., 2011; Doron et al., 2001; Gabriele et al., 2009; Sharp and Adrian, 2001; Sheng et al., 2000).

Wall-bounded turbulent flows in general and turbulent boundary layers (TBL) in particular have received a lot of attention due to their importance in the determination of efficiency and safety of many industrial systems. A deeper understanding of the mechanisms of turbulent transport of momentum and Reynolds stresses requires the study of budgets of Reynolds

stresses and turbulent kinetic energy, which amongst other quantities, need the accurate determination of turbulent dissipation rate.

In the domain of numerical simulation of turbulent flows, Reynolds Averaged Navier Stokes (RANS) equations based solvers employ turbulence models which often require accurate determination of turbulent dissipation rate for their validation. Large Eddy Simulations (LES) resolve the large scales in a flow and model the effect of small, unresolved scales using various sub-grid scale (SGS) models; the validation of these models is dependent on the accurate determination of turbulent dissipation rate in various flow configurations.

The dissipation rate of turbulent kinetic energy can be obtained by direct numerical simulation (DNS) of the governing Navier-Stokes equations for fluid flow. DNS requires accurate resolution of the entire range of length and time scales in a flow; from largest to the Kolmogorov scale. The range of scales in a flow increase with Reynolds number, the computational costs of DNS scaling with $\sim Re^3$ (Davidson, 2015), as a result, these simulations are limited to simple configurations and to Reynolds numbers which much lower than those encountered in industrial and natural flows.

Due to the high computational costs associated with the DNS of turbulent flows, high Reynolds number turbulence research is often conducted with the aid of experimental measurements which have their own challenges. The velocities obtained from every measurement technique have associated errors and uncertainties, the analysis of these errors and corrections to be applied to the measured velocities have been the subject of extensive research (Abdel-Rahman et al., 1987; Comte-Bellot, 1976; Corrsin, 1963; Forliti et al., 2000; Huang et al., 1997). Even in the limit of no measurement errors in the velocity, the accuracy of dissipation determined from experimental measurements is affected by two factors:

- 1) Velocity fields obtained from experimental measurements are spatially filtered due to the finite size of the probe or measurement volume (Spatial filtering).
- 2) Most measurement techniques provide velocity fields from which limited components of the velocity gradient tensor can be obtained (Limited dimensionality); in such cases, the turbulent dissipation rate is determined with the aid of models which are found to provide an inaccurate estimate of dissipation in wall-bounded flows.

Spatial filtering and limited dimensionality of the measured velocity fields, which are characteristics common to most measurement techniques, thus lead to a bias error in the turbulent dissipation rate obtained from experimental measurements. Although some literature is available which addresses some or all of these issues for various flows (Antonia et al., 1991; Bertens et al., 2015; Buxton et al., 2011; Xu and Chen, 2013), little information is available on the loss in accuracy of the dissipation (and hence Kolmogorov length scale) in wall-bounded flows.

Aims

The present study aims to determine the error induced in the turbulent dissipation rate (and the associated quantities) due to spatial filtering and limited dimensionality of the velocity fields obtained from experiments on wall-bounded turbulent flows. Channel flows being homogeneous along the stream-wise and span-wise directions, are a canonical case of wall-bounded turbulent flows, hence for the present study, the velocity fields sourced from DNS of a channel flow by Kitsios et al. (2015) will be used to:

- determine the error introduced in the turbulent dissipation rate due to spatial filtering as a function of filter size along each of the Cartesian directions.
- evaluate the accuracy of the turbulent dissipation rate calculated by various existing models which are used when limited components of the fluctuating velocity gradient tensor can be determined directly from measurements.
- determine the combined effect of both spatial filtering and limited dimensionality on the accuracy of the turbulent dissipation rate as a function of wall-normal distance.

Outline

The thesis is organized as follows:

- Chapter 1 is a brief overview of the existing research on the effect of spatial filtering and limited dimensionality on turbulent flow measurements with a specific focus on dissipation.
- Chapter 2 presents the distribution of the mean turbulent dissipation rate in a channel flow calculated from DNS data and investigates the contribution of various velocity gradients to dissipation in wall-bounded flows.
- Chapter 3 describes the filtering technique and other numerical methods used in this study.
- Chapter 4 discusses the effect of spatial filtering on the accuracy of the turbulent dissipation rate as a function of wall normal distance.
- Chapter 5 analyses the effectiveness of various existing models in accurately estimating dissipation in channel flows.
- Chapter 6 evaluates the net error in dissipation due to both spatial filtering and limited dimensionality.
- Chapter 7 provides a summary of the entire study and presents the conclusion from the findings of this research.

Chapter 1

Challenges in Determination of Turbulent Dissipation Rate from Experiments

Accurate determination of the turbulent dissipation rate from experimental measurements poses certain challenges. Apart from measurement noise, experimental measurements provide velocity fields which are spatially filtered and in most cases, are of limited dimensionality. The existing research on the effect of these aspects on the accuracy of turbulent dissipation rate is discussed in the following sections.

1.1 Effect of finite size of the measurement volume

Ideally, any measurement obtained from experiments should be point values, but the size of the measurement length in case of say, the wire in hot-wire anemometry and the interrogation window volume in case of PIV measurement techniques like planar particle image velocimetry (PIV), dual plane stereoscopic PIV (DPSPIV) or tomographic PIV (TPIV) is finite (and will be generically referred to as the measurement volume in the text henceforth). Due to the finite size of the measurement volume, velocities obtained from experimental measurements are an average over that volume, as a result, the information from length scales smaller than the size of the measurement volume is filtered out. Dissipation of turbulent kinetic energy takes place at the smallest scales in the flow, the Kolmogorov length scale (η) (Kolmogorov,

1941), measurement at such length scales is challenging, especially at large Reynolds numbers where the ratio of largest to smallest scales in the flow is substantial. It might be possible to employ very large experimental facilities and very small measurement volume to attenuate the problem of spatial filtering, but for most experimental facilities, spatial filtering of the velocity field is unavoidable, as a result, the velocity obtained from measurement volumes of finite size is an average over length scales which are several times larger than the Kolmogorov length scale. An average over lengths much larger than the Kolmogorov length scale filters out a substantial contribution to dissipation from small-scale turbulent velocity fluctuations (Buxton et al., 2011) which results in an underestimation of the turbulent dissipation rate (Antonia et al., 1994).

One dimensional (1D) spatial filtering in hot-wires (Chin et al., 2009; Corrsin and Kovasznay, 1949; Frenkiel, 1949; Philip et al., 2013; Segalini et al., 2011; Ueberoi and Kovasznay, 1953; Wyngaard, 1968), and two dimensional (2D) and three dimensional (3D) spatial filtering in PIV measurements (Atkinson et al., 2014; Buxton et al., 2011; Saikrishnan et al., 2006) have been the subjects of intense research. Studies on the effect of spatial filtering on velocity spectra and dissipation are well documented for different shear flows. Saikrishnan et al. (2006) highlighted that spatial averaging filters out small-scale structures and smooths the velocity fields thereby underestimating the instantaneous velocity gradients, resulting in an underestimation of the turbulent dissipation rate. Atkinson et al. (2014) demonstrated that a noiseless PIV measurement would underestimate the Reynolds stresses and turbulent velocity fluctuations, leading to an attenuation of the velocity power spectra at high wave-numbers. Since a substantial proportion of dissipation takes place in the high wave-number regime (small length scale fluctuations), the attenuation of velocity power spectra due to spatial filtering leads to an underestimation of the turbulent dissipation rate.

Data obtained from PIV measurements has been extensively used in determination of the turbulent dissipation rate (Baldi et al., 2002; Bertens et al., 2015; Buxton et al., 2011; De Jong et al., 2009; Delafosse et al., 2011; Doron et al., 2001; Gabriele et al., 2009; Saarenrinne and Piirto, 2000; Sharp and Adrian, 2001; Sheng et al., 2000). Buxton et al. (2011) studied the effect of PIV interrogation window size on fine-scale turbulence by spatially filtering the velocity fields obtained from DNS of a two-dimensional mixing layer. They reported

that the intermittency of dissipation is greatly reduced due to spatial filtering. Along with measurement noise, the errors in velocity derivatives due to spatial filtering introduced artificial compressibility into the results due to non-zero divergence ($\nabla \cdot \mathbf{U}$) of the measured velocity fields and presented a skewed picture of the dynamics of dissipation.

The study of Saarenrinne and Piirto (2000) revealed that an interrogation window size of the order of Kolmogorov length scale is needed for accurate estimation of the turbulent dissipation rate. The inability of most experimental techniques to provide adequate resolution of the flow, particularly at high Reynolds numbers, make the accurate measurement of turbulent dissipation rate from experimental measurements a challenging task. For example, the experiments in the Princeton Superpipe (Hultmark et al., 2012) employed a hot-wire with the smallest wire size in the world in terms of Kolmogorov length scale (η) and are still not able to achieve a probe size smaller than 10η , thus filtering a substantial portion of the dissipation spectrum. Additionally, it should be noted that the natural choice for expressing the interrogation window size is in terms of Kolmogorov length scale, but in flows where it is difficult to know the Kolmogorov length scale in advance, the optimal window size has to be determined iteratively.

Existing studies on the determination of the error introduced in the turbulent dissipation rate due to the finite size of the measurement volume are performed for either isotropic turbulence (Bertens et al., 2015; Xu and Chen, 2013), stirred tanks (Baldi et al., 2002; Delafosse et al., 2011; Gabriele et al., 2009; Sheng et al., 2000) or in regions far away from walls (Doron et al., 2001), while limited information is available for wall-bounded flows. Wall-bounded turbulent flow research is important due to its criticality in the design of many engineering systems. Wall-bounded turbulence is known to be highly anisotropic, large-scale anisotropy in the velocity gradients due to the presence of the wall, leads to finite anisotropy even in the smallest scales (Oberlack, 1997). The anisotropy of wall-bounded turbulence in general and the associated dissipation rate tensor in particular, have been reported in numerous studies (Gerolymos and Vallet, 2016; Lee and Reynolds, 1987; Mansour et al., 1988; Mazellier and Vassilicos, 2008, 2010). The anisotropy of wall-bounded turbulence has been attributed to the inhomogeneity in the wall-normal direction which is introduced by the mean flow (Buschmann and Gad-el Hak, 2006), the no-slip condition at the wall (Lumley, 1979) and

wall-echo (the reflective effect of the wall on pressure) (Chang III et al., 1999; Gerolymos et al., 2013; Kim, 1989). Hanjalic and Launder (1976) deduced that the isotropic part of the dissipation tensor is zero at the wall and varies as the square of the distance from the wall; thus most dissipation in the near wall region is contributed from the anisotropic part of the dissipation rate tensor. Due to this anisotropy in the near wall region, it is anticipated that the dissipation obtained from spatially filtered data will introduce an anisotropic error, i.e. it will depend on the direction of filtering. Hence, a structured approach of quantifying the error introduced in dissipation due to spatial filtering of the velocity fields along each of the stream-wise, wall-normal and span-wise directions is warranted.

1.2 Effect of limited dimensionality

In order to address the challenge posed by limited dimensionality to the accurate determination of dissipation from experimental data, let us look at the equation for turbulent dissipation rate.(Eq. 1.1)

$$\varepsilon = 2\nu \langle s_{ij} \cdot s_{ij} \rangle \quad (1.1)$$

here $\langle \cdot \rangle$ denotes the ensemble averaging, ν is the kinematic viscosity and s_{ij} is the strain rate tensor associated with the instantaneous turbulent velocity fluctuations and is given by

$$s_{ij} = \frac{1}{2} \left(\frac{\partial u'_i}{\partial x_j} + \frac{\partial u'_j}{\partial x_i} \right) \quad (1.2)$$

where u'_i is the turbulent fluctuating velocity along the direction x_i . Combining Eq. 1.1 and Eq. 1.2 and expansion of the terms leads to the equation of the mean turbulent dissipation rate (Eq.1.3)

$$\begin{aligned} \varepsilon = \nu \left\langle 2 \left(\frac{\partial u'_1}{\partial x_1} \right)^2 + 2 \left(\frac{\partial u'_2}{\partial x_2} \right)^2 + 2 \left(\frac{\partial u'_3}{\partial x_3} \right)^2 + \left(\frac{\partial u'_1}{\partial x_2} \right)^2 + \left(\frac{\partial u'_2}{\partial x_1} \right)^2 + \left(\frac{\partial u'_3}{\partial x_1} \right)^2 \right. \\ \left. + \left(\frac{\partial u'_1}{\partial x_3} \right)^2 + \left(\frac{\partial u'_2}{\partial x_3} \right)^2 + \left(\frac{\partial u'_3}{\partial x_2} \right)^2 + 2 \left(\frac{\partial u'_1}{\partial x_2} \frac{\partial u'_2}{\partial x_1} \right) + 2 \left(\frac{\partial u'_1}{\partial x_3} \frac{\partial u'_3}{\partial x_1} \right) + 2 \left(\frac{\partial u'_2}{\partial x_3} \frac{\partial u'_3}{\partial x_2} \right) \right\rangle \end{aligned} \quad (1.3)$$

When the alignment of the co-ordinate system is such that $x_1 = x$, $x_2 = y$ and $x_3 = w$ and $u'_1 = u'$, $u'_2 = v'$ and $u'_3 = w'$; the equation of the mean turbulent dissipation rate is expressed as Eq. 1.4.

$$\begin{aligned} \varepsilon = \nu \left\langle 2 \left(\frac{\partial u'}{\partial x} \right)^2 + 2 \left(\frac{\partial v'}{\partial y} \right)^2 + 2 \left(\frac{\partial w'}{\partial z} \right)^2 + \left(\frac{\partial u'}{\partial y} \right)^2 + \left(\frac{\partial v'}{\partial x} \right)^2 + \left(\frac{\partial w'}{\partial x} \right)^2 \right. \\ \left. + \left(\frac{\partial u'}{\partial z} \right)^2 + \left(\frac{\partial v'}{\partial z} \right)^2 + \left(\frac{\partial w'}{\partial y} \right)^2 + 2 \left(\frac{\partial u'}{\partial y} \frac{\partial v'}{\partial x} \right) + 2 \left(\frac{\partial u'}{\partial z} \frac{\partial w'}{\partial x} \right) + 2 \left(\frac{\partial v'}{\partial z} \frac{\partial w'}{\partial y} \right) \right\rangle \end{aligned} \quad (1.4)$$

Thus accurate measurement of all nine components of the fluctuating velocity gradient tensor is needed in order to directly determine turbulent dissipation rate from the velocity fields.

Most experimental techniques provide velocity fields which are either 1 component 1 direction (1C-1D)[Hot Wire Annemometry (HWA)], 2 component 2 direction (2C-2D) (Planar PIV) or 3 component 2 direction (3C-2D) (Stereoscopic PIV). In these cases, indirect methods are used which are models based on simplifying assumptions like homogeneous and/or isotropic turbulence (Doron et al., 2001; Elsner and Elsner, 1996; Saarenrinne and Piirto, 2000; Sheng et al., 2000). The most successful models available in the literature are presented in the following sections.

Local Isotropy Model

Kolmogorov (1941) formulated the theory of local isotropy which states that at infinite Reynolds number, small-scale turbulence is locally isotropic, i.e. it is statistically invariant under translations, rotations, and reflections of the coordinate system. Hence statistically,

isotropic turbulence is uniform in all directions. Hinze (1975) derived the derivative equivalences satisfied in isotropic turbulence, given in Eq. 1.5.

$$\begin{aligned}
 \left\langle \left(\frac{\partial u'_1}{\partial x_1} \right)^2 \right\rangle &= \left\langle \left(\frac{\partial u'_2}{\partial x_2} \right)^2 \right\rangle = \left\langle \left(\frac{\partial u'_3}{\partial x_3} \right)^2 \right\rangle \\
 \left\langle \left(\frac{\partial u'_1}{\partial x_2} \right)^2 \right\rangle &= \left\langle \left(\frac{\partial u'_2}{\partial x_1} \right)^2 \right\rangle = \left\langle \left(\frac{\partial u'_2}{\partial x_3} \right)^2 \right\rangle = \left\langle \left(\frac{\partial u'_3}{\partial x_2} \right)^2 \right\rangle = \left\langle \left(\frac{\partial u'_3}{\partial x_1} \right)^2 \right\rangle = \left\langle \left(\frac{\partial u'_1}{\partial x_3} \right)^2 \right\rangle \\
 &= 2 \left\langle \left(\frac{\partial u'_1}{\partial x_1} \right)^2 \right\rangle \\
 \left\langle \frac{\partial u'_1}{\partial x_2} \frac{\partial u'_2}{\partial x_1} \right\rangle &= \left\langle \frac{\partial u'_2}{\partial x_3} \frac{\partial u'_3}{\partial x_2} \right\rangle = \left\langle \frac{\partial u'_3}{\partial x_1} \frac{\partial u'_1}{\partial x_3} \right\rangle = -\frac{1}{2} \left\langle \left(\frac{\partial u'_1}{\partial x_1} \right)^2 \right\rangle
 \end{aligned} \tag{1.5}$$

Substituting Eq. 1.5 in Eq. 1.3 we get the formulation of dissipation for isotropic turbulence (ϵ_{ISO} , Eq. 1.6).

$$\epsilon_{ISO} = 15\nu \left\langle \left(\frac{\partial u_1}{\partial x_1} \right)^2 \right\rangle \tag{1.6}$$

When data is obtained using experimental techniques like single wire hot-wire anemometry (1C-1D), local isotropy of the smallest length scales in the flow is generally assumed and the dissipation is calculated using Eq. 1.6 (Elsner and Elsner, 1996).

Local axisymmetry model

George and Hussein (1991) proposed that small-scale turbulence can be considered to be locally axisymmetric. The prescribed derivative equivalence conditions to be satisfied in turbulence assumed to be axisymmetric about the x_1 direction are presented in Eq. 1.7

$$\begin{aligned}
\left\langle \left(\frac{\partial u'_1}{\partial x_2} \right)^2 \right\rangle &= \left\langle \left(\frac{\partial u'_1}{\partial x_3} \right)^2 \right\rangle \\
\left\langle \left(\frac{\partial u'_2}{\partial x_1} \right)^2 \right\rangle &= \left\langle \left(\frac{\partial u'_3}{\partial x_1} \right)^2 \right\rangle \\
\left\langle \left(\frac{\partial u'_2}{\partial x_2} \right)^2 \right\rangle &= \left\langle \left(\frac{\partial u'_3}{\partial x_3} \right)^2 \right\rangle \\
\left\langle \left(\frac{\partial u'_2}{\partial x_3} \right)^2 \right\rangle &= \left\langle \left(\frac{\partial u'_3}{\partial x_2} \right)^2 \right\rangle \\
\left\langle \left(\frac{\partial u'_2}{\partial x_2} \right)^2 \right\rangle &= \frac{1}{3} \left\langle \left(\frac{\partial u'_1}{\partial x_1} \right)^2 \right\rangle + \frac{1}{3} \left\langle \left(\frac{\partial u'_2}{\partial x_3} \right)^2 \right\rangle \\
\left\langle \frac{\partial u'_2}{\partial x_3} \frac{\partial u'_3}{\partial x_2} \right\rangle &= \frac{1}{6} \left\langle \left(\frac{\partial u'_1}{\partial x_1} \right)^2 \right\rangle - \frac{1}{3} \left\langle \left(\frac{\partial u'_2}{\partial x_3} \right)^2 \right\rangle \\
\left\langle \frac{\partial u'_1}{\partial x_2} \frac{\partial u'_2}{\partial x_1} \right\rangle &= \left\langle \frac{\partial u'_1}{\partial x_3} \frac{\partial u'_3}{\partial x_1} \right\rangle = -\frac{1}{2} \left\langle \left(\frac{\partial u'_1}{\partial x_1} \right)^2 \right\rangle
\end{aligned} \tag{1.7}$$

The 2C-2D formulations of dissipation were derived by George and Hussein (1991) by using the derivative equivalence relations in Eq. 1.7 to model the unknown terms. When measurements are performed in the 1-2 plane, the formulation of dissipation based on the assumption of local axisymmetry of turbulence about the x_1 axis is given by Eq. 1.8.

$$\varepsilon_{LA} = \nu \left\langle \left(\frac{\partial u'_1}{\partial x_1} \right)^2 + 8 \left(\frac{\partial u'_2}{\partial x_2} \right)^2 + 2 \left(\frac{\partial u'_1}{\partial x_2} \right)^2 + 2 \left(\frac{\partial u'_2}{\partial x_1} \right)^2 + 4 \left(\frac{\partial u'_1}{\partial x_2} \frac{\partial u'_2}{\partial x_1} \right) \right\rangle \tag{1.8}$$

Weak local isotropy model

Doron et al. (2001) modelled the dissipation in coastal ocean bottom boundary layer from 2C-2D PIV data by assuming weak local isotropy of turbulence. The model is based on the assumption that the out-of-plane cross gradients (gradients along directions perpendicular to the velocity component) are equal to the average in-plane cross-gradients (Eq. 1.9), these assumptions are weaker than those used in the local-isotropy model as they assume equivalence of only the cross-gradients.

$$\begin{aligned}
\left\langle \left(\frac{\partial u'_1}{\partial x_3} \right)^2 \right\rangle &= \left\langle \left(\frac{\partial u'_3}{\partial x_1} \right)^2 \right\rangle = \left\langle \left(\frac{\partial u'_2}{\partial x_3} \right)^2 \right\rangle = \left\langle \left(\frac{\partial u'_3}{\partial x_2} \right)^2 \right\rangle \\
&= \frac{1}{2} \left\langle \left(\frac{\partial u'_1}{\partial x_2} \right)^2 + \left(\frac{\partial u'_2}{\partial x_1} \right)^2 \right\rangle \\
\left\langle \frac{\partial u'_1}{\partial x_3} \frac{\partial u'_3}{\partial x} \right\rangle &= \left\langle \frac{\partial u'_2}{\partial x_3} \frac{\partial u'_3}{\partial x_3} \right\rangle = \left\langle \frac{\partial u'_1}{\partial x_2} \frac{\partial u'_2}{\partial x_1} \right\rangle
\end{aligned} \tag{1.9}$$

Using the assumption of weak local isotropy of turbulence, Doron et al. (2001) presented the formulation of dissipation which is given by Eq. 1.10

$$\begin{aligned}
\varepsilon_{WI} = \nu \left\langle 4 \left(\frac{\partial u'_1}{\partial x_1} \right)^2 + 4 \left(\frac{\partial u'_2}{\partial x_2} \right)^2 + 3 \left(\frac{\partial u'_1}{\partial x_2} \right)^2 + 3 \left(\frac{\partial u'_2}{\partial x_1} \right)^2 + 4 \left(\frac{\partial u'_1}{\partial x_1} \frac{\partial u'_2}{\partial x_2} \right) \right. \\
\left. + 6 \left(\frac{\partial u'_1}{\partial x_2} \frac{\partial u'_2}{\partial x_1} \right) \right\rangle \tag{1.10}
\end{aligned}$$

The adequacy of each of the above three models to estimate dissipation in wall-bounded flows will be discussed in chapter 5.

1.3 Combined effect of spatial filtering and limited dimensionality

Xu and Chen (2013) studied the effect of filter size on the turbulent dissipation rate in isotropic turbulence and reported that the accuracy of the turbulent dissipation rate calculated using above-described models decreases with increasing spatial filtering; although no information was provided on the individual contributions of spatial filtering and limited dimensionality to the error in the turbulent dissipation rate obtained from experiments. The effect of spatial filtering on the accuracy of the above described models is unknown and will depend on the response of error introduced in each of the derivative terms in Eq. 1.3 due to spatial filtering.

An estimate of bias error introduced in dissipation (ε) and Kolmogorov length scale (η) due to both spatial filtering and limited dimensionality is needed for the analysis of these

quantities and the dynamics of dissipation and turbulent kinetic energy. The existing studies on the impact of spatial filtering and limited dimensionality on the accuracy of turbulent dissipation rate are available only for simple flows without strong mean shear and away from any boundaries. Given that the nature of wall-bounded turbulence is characterized by strong anisotropy and inhomogeneity in the near wall region, even at the smallest scales; there is a strong need to investigate the individual and combined effect of spatial resolution and limited dimensionality on the accuracy of turbulent dissipation rate in wall-bounded flows.

Chapter 2

Channel Flow DNS dataset

Three-dimensional velocity fields obtained from DNS of fully developed turbulent channel flow by Kitsios et al. (2015) have been used to study the effect of spatial filtering and limited dimensionality on the turbulent dissipation rate in wall-bounded flows. The effects on the accuracy of the turbulent dissipation rate were evaluated by considering the unfiltered DNS data as the reference case. Details of the DNS are provided in section 2.1 and the dissipation for the baseline DNS case is presented in section 2.2

2.1 Description of the DNS database

The code used to generate the DNS data used in the current study solved the incompressible isothermal Navier-Stokes equations in spectral space. The simulation domain is oriented such that the stream-wise, wall-normal and span-wise directions are along the cartesian x, y and z directions respectively. The discretization is performed by using a collocated Chebyshev discretization in the wall-normal (y) direction, and Fourier expansions in the wall-parallel x - z plane. The code solves for the wall-normal vorticity and the Laplacian of the wall-normal velocity, further details of the code can be found in Kitsios et al. (2015).

The friction velocity based Reynolds number, $Re_\tau = u_\tau h / \nu = 950$ where $u_\tau = \sqrt{\tau_w / \rho}$ is the friction velocity, τ_w is the wall shear stress, ρ is the fluid density and h is the channel half width.

The domain and grid properties are listed in Table 2.1. The simulation domain was a rectangular box with the x, y, z extents of L_x, L_y and L_z respectively while N_x, N_y , and N_z

Table 2.1 Numerical details of DNS dataset

$Re\tau$	(L_x, L_y, L_z)	(N_x, N_y, N_z)	$(\Delta x^+, \Delta y_{min}^+, \Delta y_{max}^+, \Delta z^+)$
945	$(\pi, 2, \pi/2)$	(384, 385, 384)	(7.8, 0.03, 7.6, 3.9)

are the corresponding grid points along those directions. The uniform grid spacings along stream-wise x and span-wise z directions expressed in viscous/wall units (normalized by viscous length scale, ν/u_τ) are Δx^+ and Δz^+ respectively. The grid along the wall normal (y) direction was non-uniform having minimum grid spacing at the wall (Δy_{min}^+) and the cell spacing increasing until it approaches the maximum spacing (Δy_{max}^+) at the channel centerline.

2.2 Turbulent Dissipation in Channel Flow

To ensure the accuracy of the computed gradients, the joint probability distribution function (PDF) distribution of $\partial u/\partial x$ and $-(\partial v/\partial y + \partial w/\partial z)$ was evaluated. Ideally, these terms should be equal in an incompressible flow since their difference is the divergence ($\nabla \cdot \mathbf{U}$) which is zero in an incompressible flow. The gradients were computed in the spectral space. To mimic the accuracy and method of the gradient calculations in the DNS computations, the gradients along the stream-wise and span-wise directions were computed by performing a Fourier transform of the velocity fields along those directions, calculating the derivatives in Fourier space and performing an inverse Fourier transform of the derivatives to convert the data back to physical space. A similar approach was employed for calculating derivatives along the wall-normal direction, except that the transformation was into spectral space by performing Chebyshev polynomial fits of the velocity fields along the wall-normal direction. Since the terms of the joint PDF are equal in the ideal case, their ideal distribution should be a distribution with minimal spread around the 45° line. The accuracy of calculated gradients was ensured by confirming that the joint-PDF is close to the ideal which is demonstrated in Fig. 2.1; the joint-PDF for one random field, which has $384 \times 385 \times 384 \approx 5.7 \times 10^7$ grid points. Since the ideal value of divergence ($\nabla \cdot \mathbf{U}$) for incompressible flow is zero,

the accuracy of derivatives can be estimated by calculating the mean, median and standard deviation of divergence, the values of these quantities for the same field as the one used to plot the joint-PDF were -2.71×10^{-12} , 5.586×10^{-5} and 8.12×10^{-3} respectively, since the velocity data available was in single precision which has 7 decimal digits of precision, hence the accuracy level of the calculated gradients was deemed acceptable.

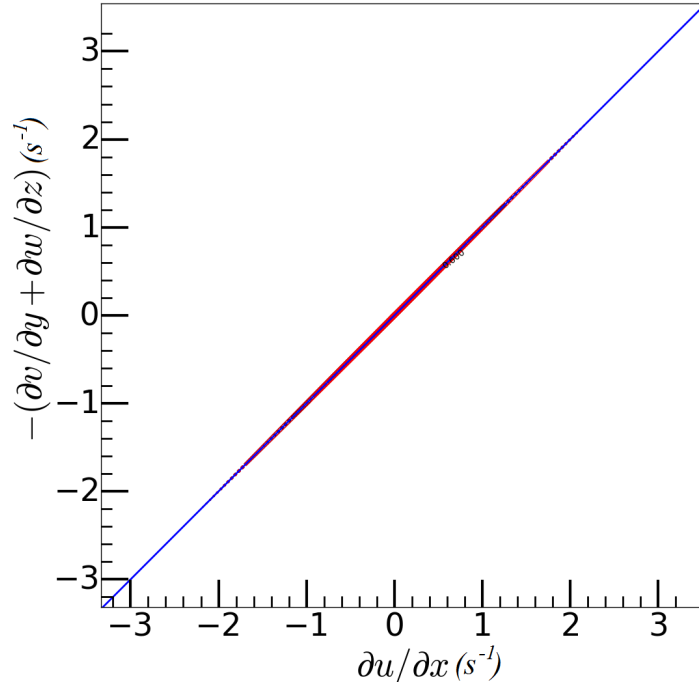


Fig. 2.1 Joint PDF of $\partial u/\partial x$ and $-(\partial v/\partial y + \partial w/\partial z)$ of one DNS field

We have seen in the equation used to calculate the mean turbulent dissipation rate (Eq.1.4), that the turbulent dissipation rate is composed of 12 terms which are calculated by multiplying different terms of the fluctuating velocity gradient tensor taken two at a time. Since these terms would be consistently evaluated and presented throughout the current text, the contribution of various terms to turbulent dissipation rate is non-dimensionalised and expressed using notation in Eq. 2.1, and presented in Fig. 2.2

$$\begin{aligned}
D_{ii} &= 2\nu \frac{\left\langle \left(\frac{\partial u'_i}{\partial x_i} \right)^2 \right\rangle}{\varepsilon} \\
C_{ij} &= \nu \frac{\left\langle \left(\frac{\partial u'_i}{\partial x_j} \right)^2 \right\rangle}{\varepsilon} \quad i \neq j \\
M_{ij} &= 2\nu \frac{\left\langle \left(\frac{\partial u'_i}{\partial x_j} \right) \left(\frac{\partial u'_j}{\partial x_i} \right) \right\rangle}{\varepsilon} \quad i \neq j
\end{aligned} \tag{2.1}$$

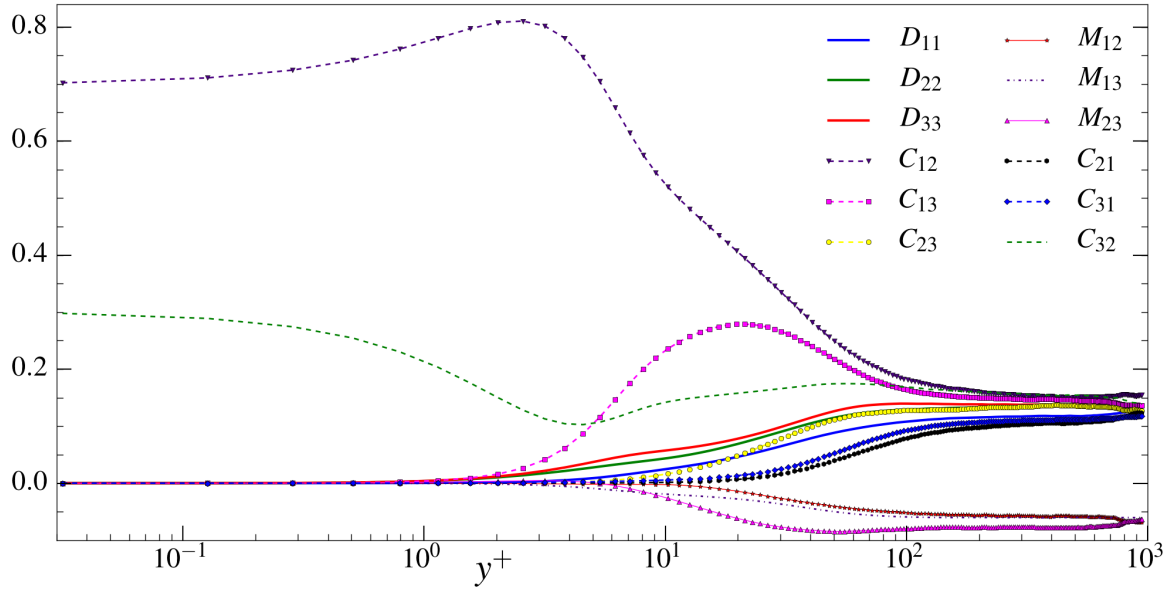


Fig. 2.2 Fractional contribution of various velocity gradient terms to dissipation

The contribution of various terms to dissipation is consistent with the observations from channel flow DNS of Antonia et al. (1991). As expected, the flow in the near wall region is highly anisotropic, the contribution to dissipation mainly comes from $(\partial u'/\partial y)^2 (C_{12})$, $(\partial w'/\partial y)^2 (C_{32})$ and $(\partial u'/\partial z)^2 (C_{13})$ in the region $y^+ \leq 20$; the dissipation exhibits an isotropic distribution only in the region $y^+ \geq 200$.

Kolmogorov length scale (η) is the characteristic length scale at which most of the turbulent dissipation takes place (Kolmogorov, 1941) and is given by Eq. 2.2.

$$\eta = (\nu^3/\varepsilon)^{1/4} \tag{2.2}$$

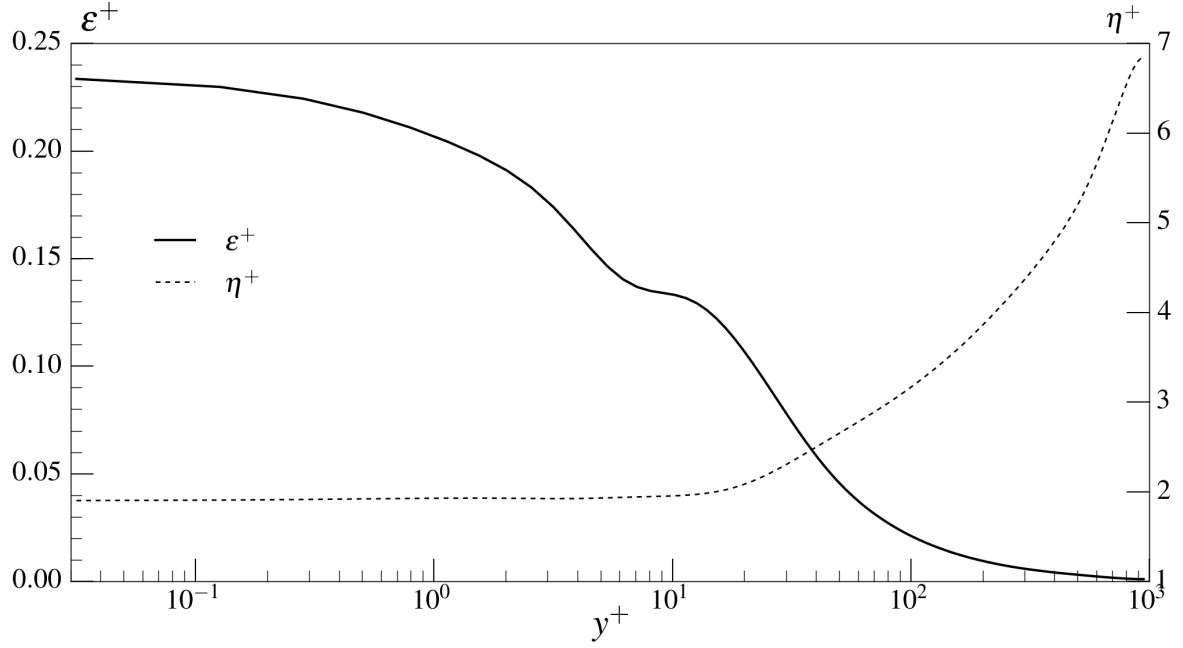


Fig. 2.3 Distribution of dissipation and Kolmogorov length scale along the channel height for unfiltered velocity fields

Fig. 2.3 presents the distribution of turbulent dissipation rate ε and Kolmogorov length scale η (expressed in wall units) in the wall-normal direction (from wall to channel center-line). The minimum Kolmogorov length scale (η) calculated using the reference DNS dataset velocity fields is $\sim 2^+$ units and is almost constant till a wall height of $\sim 10^+$ units. The turbulent dissipation rate varies from $\sim 0.24^+$ units at the wall to $\sim 0^+$ units at the channel center-line. The contribution of dissipation in different regions of the flow to total dissipation in the channel is evaluated with the help of integral fraction (χ), which is defined as the net dissipation from wall to a wall-normal distance, expressed as a fraction of the dissipation in the entire channel (Eq. 2.3). The distribution of χ as a function of wall-normal distance is shown in fig. 2.4.

$$\chi(y) = \frac{\int_0^y \varepsilon(y) dy}{\int_0^h \varepsilon(y) dy} \quad (2.3)$$

Thus, 50% of the total dissipation in the channel takes place between the wall and a wall-normal distance of $y^+ \sim 50$, while at $y^+ \sim 400$, the corresponding value is 90%. Thus any error in the dissipation in the near wall region would have a large impact on the overall error

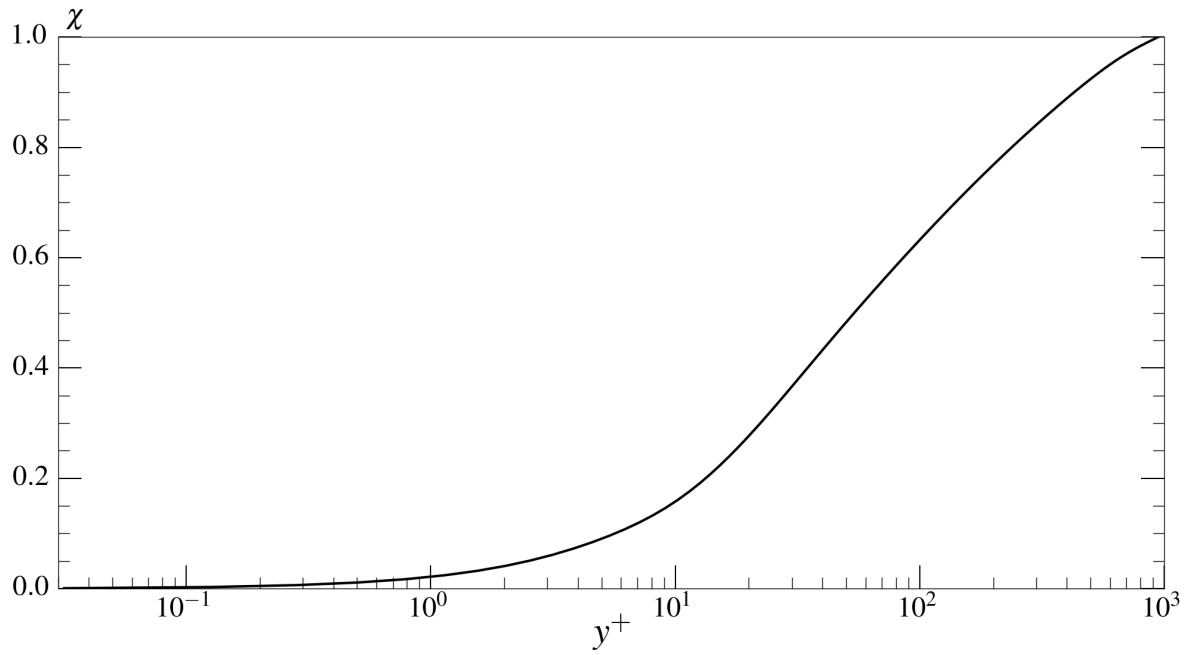


Fig. 2.4 Distribution of Integral fraction (χ) along the channel height for DNS dataset

in dissipation. The distribution of dissipation along the wall-normal direction is a function of Reynolds number (Lee and Moser, 2015) and the applicability of the results that will be presented for the current study, to different Reynolds numbers, is discussed in Chapter 7.

Chapter 3

Computational Methodology

This chapter provides the details of the computational method used for spatially filtering the DNS velocity fields and the method used for evaluating the velocity gradients of spatially filtered velocity fields. The details of gradient calculation methods for filtered velocity fields is provided in Section 3.1. Section 3.2 discusses the existing methods used for spatially filtering the velocity fields followed by details of the numerical method of the selected spatial filtering technique.

3.1 Gradient computation methods

The choice of gradient computation scheme for the filtered fields should mimic the ones often used to compute gradients of the velocity fields obtained through experiments. Extensive research on the choice of the appropriate gradient calculation scheme to be used for data obtained through PIV measurements is available in the literature (Foucaut and Stanislas, 2002; Fouras and Soria, 1998). The choice of gradient scheme can have a significant impact upon the velocity gradient tensor, vorticity and the dissipation distribution calculated from experimental measurements as discussed by Fouras and Soria (1998). Foucaut and Stanislas (2002) analyzed the spectral response of various gradient calculation schemes and concluded that a second-order central difference scheme is appropriate for evaluating the derivatives obtained from PIV measurements of velocity fields. They demonstrated that the use of higher order schemes would result in high random error transmission (from measurements); thus no significant gains can be achieved by using higher order schemes. Given that the

second-order central difference scheme is the most common choice of gradient computation method for most experimental data, it will be used to calculate the velocity gradient tensor (hence dissipation) from the filtered velocity fields. To mimic the experimental measurements, the velocity fields obtained are filtered onto a grid with uniform grid-spacing, hence the second-order central difference scheme corresponds to uniform grid spacing and is given by Eq. 3.1.

$$\left. \frac{\partial u_i}{\partial x_i} \right|_x = \frac{u_i(x + \Delta x) - u_i(x - \Delta x)}{2\Delta x} + O(\Delta x^2) \quad (3.1)$$

Here u_i is the velocity along the direction x_i and Δx is the uniform grid spacing along that direction.

3.2 Spatial filtering technique

The quantities measured using different experimental techniques are an average over the size of the measurement volume. Most spatial filtering methods attempt to mimic this volume averaging to study the effect of spatial filtering on turbulent quantities but differ in the method of calculating the averages (Atkinson et al., 2014; Buxton et al., 2011; Philip et al., 2013; Saikrishnan et al., 2006; Segalini et al., 2011; Xu and Chen, 2013). The appropriateness of these methods for the current study was evaluated and is described below.

3.2.1 Study of spatial filtering methods

Saikrishnan et al. (2006) calculated the average velocity inside a filter kernel by taking a simple average of all the DNS grid points that lie inside that kernel. Although this technique is effective when the averaging is performed along the directions where the spacing between DNS grid points is uniform, as can be seen in Fig. 3.1, a simple average (which is calculated by assigning uniform weighing to all the grid points) along the directions having a large variation in grid spacing will give an erroneous result (Atkinson et al., 2014). Thus, for the current case, a simple averaging approach of filtering the velocity fields cannot be performed along the wall-normal direction which has non-uniform DNS grid point spacing. To remove

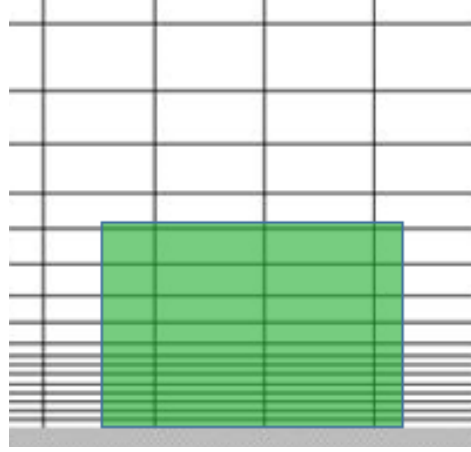


Fig. 3.1 Schematic of clustering of grid points within the filter window (green box) in the near wall region

the bias due to non-uniform grid spacing, Atkinson et al. (2014) computed the filtered velocity fields by applying a volume weighting to the contribution of each cell of DNS velocity field. The averaging operation along a single direction x can be represented schematically by Fig. 3.2. The corresponding mathematical formulation for one-dimension is given by Eq. 3.2, which can be easily extended to three dimensions.

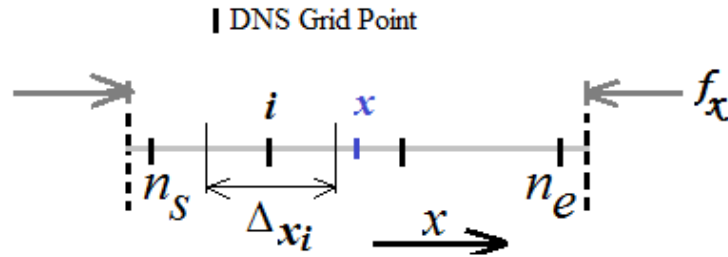


Fig. 3.2 Schematic representation of volume weighted averaging filter

$$\tilde{g}_{VA} = \sum_{i=n_s}^{n_e} W_i g_i \quad (3.2)$$

where \tilde{g}_{VA} is the filtered value of the quantity g calculated using the volume-weighted averaging method (filtered quantities are denoted by a \sim throughout the text), $W(i) = \Delta x_i / f_x$ is the weight corresponding to the DNS grid point i , Δx_i is the length of overlap of DNS cell with the filter of length f_x along the direction of averaging x (Fig. 3.2), while n_s and n_e are the first and last DNS grid points overlapping with the filter centered at x .

The volume weighted averaging method of calculating the mean velocity, as described above, was used to calculate a velocity field filtered along the y - z direction with a filter size of $f_y^+ \times f_z^+ = 8 \times 8$. The resultant mean true turbulent dissipation rate for the filtered velocity field, $\tilde{\epsilon}^+$, is presented in Fig. 3.3. A comparison of distribution of dissipation rate along the channel height for the filtered and unfiltered fields revealed that the volume averaging method of spatial filtering introduces spurious fluctuations in the filtered mean turbulent dissipation rate along the y -direction. These fluctuations were found to be the result of small numerical errors introduced in the filtered velocity field due to the difference in the average calculated by the volume weighted averaging method and the true value; this error is a function of grid spacing, corroborated by the fact that the location of fluctuations was a function of the grid spacing and did not change with the number of samples used to calculate the average.

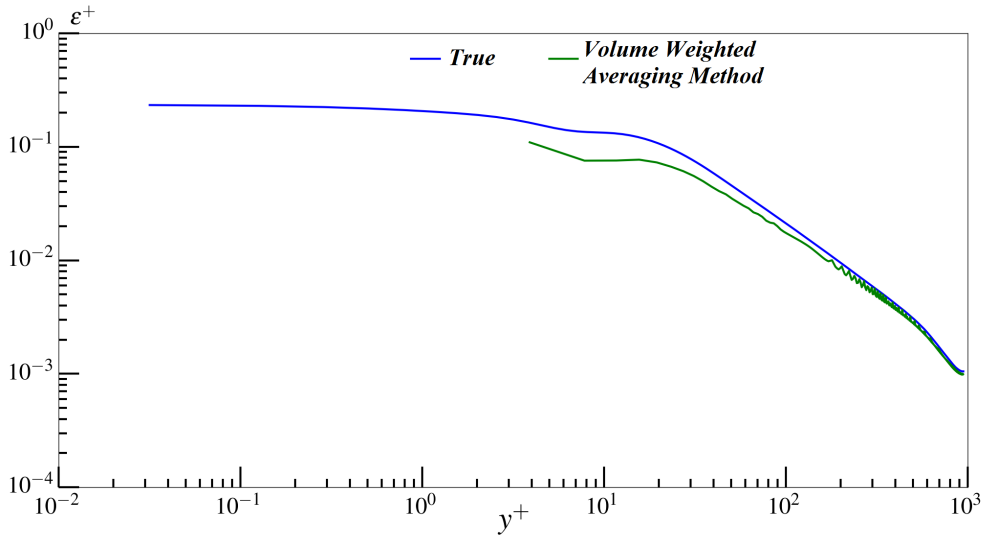


Fig. 3.3 Comparison of the mean turbulent dissipation rate calculated from unfiltered velocity fields with velocity fields spatially filtered using volume weighted averaging method with filter of size $f_x^+ \times f_y^+ \times f_z^+ = 8 \times 8 \times 8$

A different method of averaging was considered, observing that for the canonical case of averaging along a single direction, say along the length of the wire in HWA, the actual averaging operation can be represented by a box filter Eq. 3.3 (Philip et al., 2013)

$$\tilde{g}(x) = \frac{1}{f_x} \int_{-f_x/2}^{f_x/2} g(x+s) ds \quad (3.3)$$

which can be easily extended to 2 and 3 dimensions.

Along the lines of Segalini et al. (2011), the integration operation in Eq. 3.3 was replaced by numerical integration using the Simpson's method. The original Simpson's method requires equidistant grid points and was used for the current analysis. To distribute the grid points equally in the domain, the DNS velocity field had to be interpolated along the y -direction where the DNS grid points have a non-uniform distribution. Since the DNS computations were performed by performing Chebyshev polynomial fits along the wall-normal direction, the interpolation of the data onto a uniform grid was performed using the same method, ensuring that the interpolation is spectrally accurate. Another requirement of Simpson's method is the need of an odd number of grid points along the direction of integration. Five grid points overlapping with the filter window along the y -direction ensured a compromise between the requirement of an adequate number of points in the near-wall region and minimising computational costs of the filtering operation.

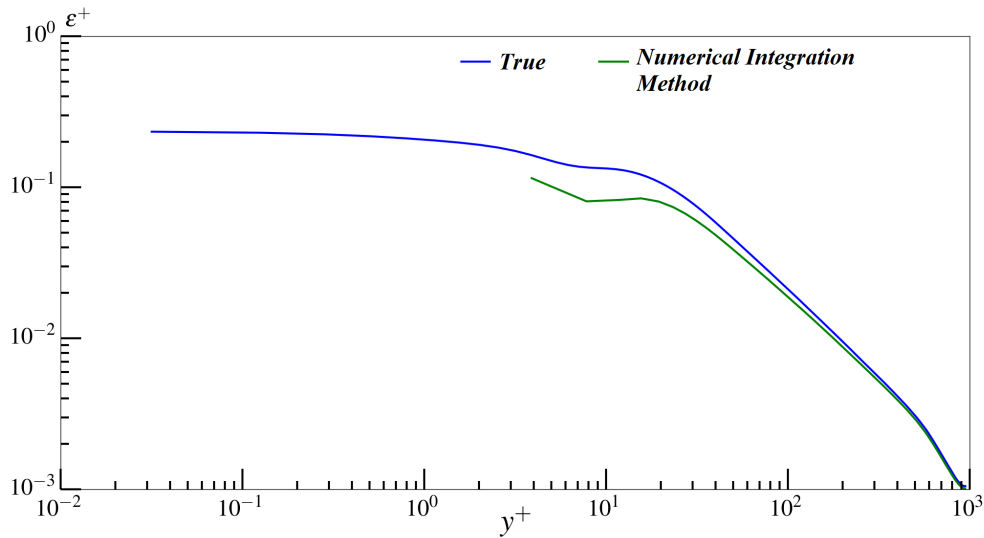


Fig. 3.4 Comparison of the mean turbulent dissipation rate for filtered and unfiltered velocity fields. The filtering operation is performed by applying a box-filter (Eq. 3.3) and using the numerical integration method, the filter size is $f_x^+ \times f_y^+ \times f_z^+ = 8 \times 8 \times 8$

The distribution of the mean turbulent dissipation rate for the filtered velocity fields ($\tilde{\epsilon}^+$) along the wall-normal (y) direction, calculated using the numerical integration filtering method, was smooth with absence of any spurious fluctuations (Fig. 3.4), hence the numerical integration technique was the filtering method adopted for spatial filtering in the remainder of the study. In most experimental measurement techniques like PIV, the adjacent interrogation

windows overlap with the each other as this reduces the grid spacing. A high overlap between adjacent windows has been reported to result in increasing the noise in the gradients due to the resulting large statistical correlation between adjacent grid points for higher overlap fractions. An overlap of 50% of PIV window size is the most common choice of grid resolution for PIV measurements as it is a balance between statistical independence between grid points and grid resolution of the data. The current study mimics this and the grid spacing in the filtered velocity fields corresponds to 50% overlap of windows along the direction of filtering.

Chapter 4

Effect of Spatial Filtering on Dissipation

We have seen in Chapter 1 that velocities obtained from experimental measurements are spatially filtered when the size of the measurement volume is larger than the smallest scales in the flow. To study the effect of spatial filtering on the accuracy of the turbulent dissipation rate calculated from the spatially filtered velocity fields, high-resolution velocity fields obtained from the DNS dataset 2 were spatially filtered using the method described in Chapter 3. The turbulent dissipation rate was calculated from the filtered velocity fields ($\tilde{\epsilon}$) using Eq. 1.4; the second-order central difference scheme was employed to calculate the velocity gradients as discussed in Chapter 3. Velocity gradients calculated using any finite difference method have an associated truncation error which is dependent on the order of accuracy of the scheme and grid spacing. Often, for PIV measurements the grid spacing is a function of the filter size for a fixed overlap ratio, as a result, the truncation error becomes a function of the filter size, thus introducing an additional error along with the error in turbulent dissipation rate due to spatial filtering. A mathematical analysis of the effect of truncation error on dissipation is presented in Section 4.1.

In wall-bounded flows, the distribution of terms contributing to dissipation being anisotropic especially in the near wall region (Chapter 2), the effect of spatial filtering on turbulent dissipation rate is expected to be an anisotropic function of filter size along each of the three Cartesian directions. The current study, therefore involves the analysis of the effect of spatial filtering along each of the wall-normal, span-wise and stream-wise directions separately, which is discussed in Section 4.2, Section 4.3 and Section 4.4 respectively.

4.1 Effect of truncation error on turbulent dissipation rate

Following an approach similar to Foucaut and Stanislas (2002), the velocity gradient calculation is considered to be equivalent to the application of a filter. Thus the calculation of the velocity gradient tensor from spatially filtered velocity fields is the result of the application of the central derivative filter (\mathcal{C}) over the spatial filter (\mathcal{F}).

Ignoring the constant coefficients, each term in the equation for turbulent dissipation rate (Eq. 1.4) can be generically expressed in the form $(\partial u'_i / \partial x_j) (\partial u'_k / \partial x_l)$ (The round brackets around the terms imply that there is no summation over the repeated indices). The corresponding term calculated from the filtered velocity fields can be expressed in the form shown by Eq. 4.1.

$$\left(\frac{\partial \tilde{u}'_i}{\partial x_j} \right) \left(\frac{\partial \tilde{u}'_k}{\partial x_l} \right) = \mathcal{C} [\mathcal{F}(u'_i), x_j] \mathcal{C} [\mathcal{F}(u'_k), x_l] \quad (4.1)$$

Eq. 4.1 is presented in a simplified form in Eq. 4.2, the details of which are provided in appendix A.

$$\left(\frac{\partial \tilde{u}'_i}{\partial x_j} \right) \left(\frac{\partial \tilde{u}'_k}{\partial x_l} \right) = \mathcal{F} \left(\frac{\partial u'_i}{\partial x_j} \right) \mathcal{F} \left(\frac{\partial u'_k}{\partial x_l} \right) + \gamma \quad (4.2)$$

where the first term on the right-hand side of Eq. 4.2 is the result of applying spatial filtering to the true velocity gradient tensor and subsequently calculating the product corresponding to the left-hand side; while γ is the non-linear error term present due to the truncation error introduced by the finite difference scheme and is dependent on the filter size.

Thus using any finite difference scheme for calculating the velocity gradients and hence the turbulent dissipation rate from spatially filtered velocity fields introduces a non-linear truncation error in the turbulent dissipation rate. In absence of any truncation error (i.e. $\gamma \approx 0$), the true filtered mean turbulent dissipation rate ($\tilde{\epsilon}_T$) is given by Eq. 4.3.

$$\begin{aligned}
\tilde{\epsilon}_T = \nu \left\langle 2 \left[\mathcal{F} \left(\frac{\partial u'}{\partial x} \right) \right]^2 + 2 \left[\mathcal{F} \left(\frac{\partial v'}{\partial y} \right) \right]^2 + 2 \left[\mathcal{F} \left(\frac{\partial w'}{\partial z} \right) \right]^2 + \left[\mathcal{F} \left(\frac{\partial u'}{\partial y} \right) \right]^2 \right. \\
+ \left[\mathcal{F} \left(\frac{\partial v'}{\partial x} \right) \right]^2 + \left[\mathcal{F} \left(\frac{\partial w'}{\partial x} \right) \right]^2 + \left[\mathcal{F} \left(\frac{\partial u'}{\partial z} \right) \right]^2 + \left[\mathcal{F} \left(\frac{\partial v'}{\partial z} \right) \right]^2 + \left[\mathcal{F} \left(\frac{\partial w'}{\partial y} \right) \right]^2 \\
\left. + 2 \left[\mathcal{F} \left(\frac{\partial u'}{\partial y} \right) \mathcal{F} \left(\frac{\partial v'}{\partial x} \right) \right] + 2 \left[\mathcal{F} \left(\frac{\partial u'}{\partial z} \right) \mathcal{F} \left(\frac{\partial w'}{\partial x} \right) \right] + 2 \left[\mathcal{F} \left(\frac{\partial v'}{\partial z} \right) \mathcal{F} \left(\frac{\partial w'}{\partial y} \right) \right] \right\rangle
\end{aligned} \tag{4.3}$$

Hence, $\tilde{\epsilon}_T$ is the dissipation calculated when the velocity gradients in the equation of the turbulent dissipation rate (Eq. 1.4) are calculated by spatially filtering the unfiltered velocity gradient fields obtained in Chapter 2, thus having no associated truncation error.

The difference $\tilde{\epsilon} - \tilde{\epsilon}_T$ is the contribution of truncation error to the total error in turbulent dissipation rate due to spatial filtering and Γ (Eq. 4.4) is the truncation error expressed as a fraction of the net error in the turbulent dissipation rate calculated from spatially filtered velocity fields.

$$\Gamma = \frac{\tilde{\epsilon} - \tilde{\epsilon}_T}{\epsilon - \tilde{\epsilon}} \tag{4.4}$$

where $\tilde{\epsilon}$ and ϵ are the turbulent dissipation rate calculated from filtered and unfiltered velocity fields respectively.

Since the truncation error is dependent on the finite difference scheme employed and the filter size, the contribution of truncation error to the total error in turbulent dissipation rate will be taken into consideration when evaluating the effect of spatial filtering.

4.2 Effect of filter size in the wall-normal (y) direction

To study the effect of spatial filtering in the wall-normal direction, the filtered velocity fields were obtained for a range of wall-normal filter sizes (f_y). The grid spacing in the filtered velocity fields corresponds to a 50% overlap in the direction of filtering, unless stated otherwise.

Atkinson et al. (2014) have evaluated the effect of PIV-like filtering on velocity power spectra and demonstrated that the response of power spectra (and hence the turbulent dissipation rate) to spatial filtering along any one direction is affected by the filter size along the other directions. To this end, the effect of filter size along the wall-normal direction (f_y) is evaluated for three different combinations of span-wise (f_z) and stream-wise (f_x) filter sizes. The filter widths (expressed in wall units and rounded off to the nearest integer), are shown in table 4.1. Since the spatial filtering along the wall-normal direction is usually encountered when using PIV techniques, the choice of filter sizes along the three directions are based on the most frequently used interrogation window sizes for typical laboratory scale PIV experiments of turbulent wall-bounded flows.

Table 4.1 Filter size combinations used for study of the effect of spatial filter size in the wall-normal direction (f_y^+), the quantity in brackets is the corresponding grid spacing

$f_x^+(\tilde{\Delta}_x^+)$	$f_y^+(\tilde{\Delta}_y^+)$					$f_z^+(\tilde{\Delta}_z^+)$
0 (8)	8 (4)	12 (6)	16 (8)	20 (10)	24 (12)	0 (4)
16 (8)						12 (6)
16 (8)						20 (10)

where, $\tilde{\Delta}_x^+, \tilde{\Delta}_y^+, \tilde{\Delta}_z^+$ are the grid spacings along the x, y, and z directions respectively. The case with filter width $f_x^+ = 0, f_z^+ = 0$ is the case where no filter is applied along the stream-wise (x) and span-wise(z) directions, hence for this case, the grid spacings along those directions are the same as the reference DNS grids.

Case (i) Study of the effect of filter size in wall-normal direction with no filtering along x and z directions $f_x^+ = 0, f_z^+ = 0$

Fig. 4.1 presents the profiles of the mean turbulent dissipation rate in viscous units (ϵ^+) for various wall-normal filter sizes, the profile of the mean dissipation rate from the unfiltered velocity field from Chapter 2 is included for reference. The difference between the dissipation rate obtained from true and spatially filtered velocity fields is not surprisingly a function of the wall normal distance. To gain a better insight into the effect of wall-normal filter size

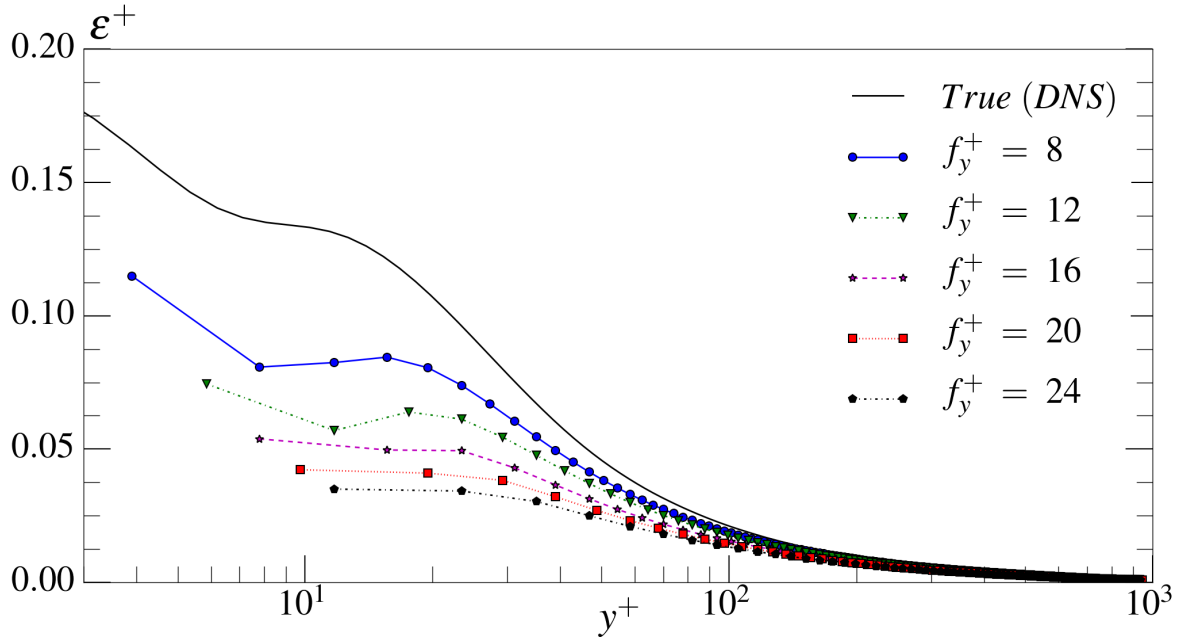


Fig. 4.1 Profiles of the mean turbulent dissipation rate in wall-units ε^+ for the unfiltered case (black) and various wall-normal filter sizes (f_y^+); $f_x^+ = 0$, $f_z^+ = 0$

on turbulent dissipation rate, the change in normalized dissipation rate (r_ε , Eq. 4.5) with increasing wall-normal filter size, is presented at different wall-normal locations, in Fig. 4.2.

$$r_\varepsilon = \frac{\tilde{\varepsilon}}{\varepsilon} \quad (4.5)$$

The largest effect of the filter size in the wall-normal direction on the accuracy of the mean turbulent dissipation rate is in the near wall region, the loss in accuracy of dissipation with increasing the wall-normal filter size decreases with increasing distance from the wall.

The effect of wall-normal filter size on normalized Kolmogorov length scale ($r_\eta = \tilde{\eta}/\eta$), presented in Fig. 4.3, is consistent with the earlier observations. The penalty on the accuracy of η is largest in the near wall region; the overestimation of η at $y^+ = 20$ increases from $\sim 5\%$ of the true value for the wall-normal filter size of $f_y^+ = 8$, to $\sim 30\%$ for $f_y^+ = 24$; the corresponding values at $y^+ = 100$ are $\sim 1\%$ and $\sim 9\%$, respectively.

As described in Section 4.1, the truncation error of gradient calculation scheme affects the accuracy of dissipation calculated from the filtered velocity fields. The fractional contribution of truncation error to the total error in dissipation, Γ (Eq. 4.4), is presented in Fig. 4.4. The negative values of truncation error imply that it leads to an underestimation of dissipation. The

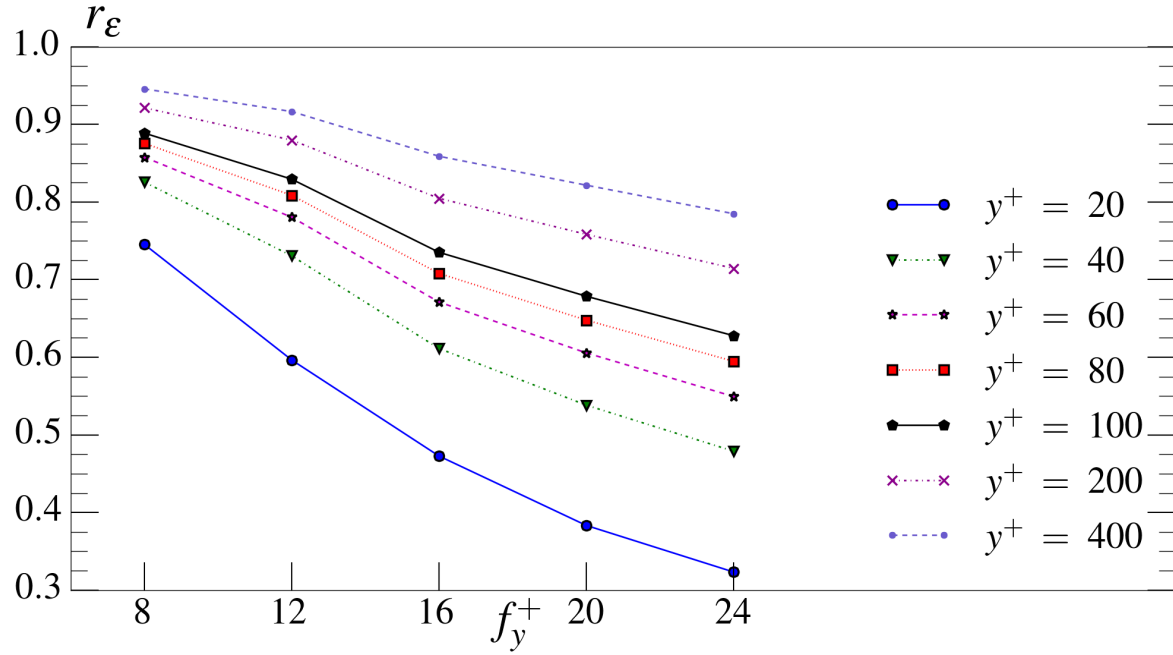


Fig. 4.2 Effect of increasing the filter size in the wall-normal direction (f_y^+) on normalized dissipation (r_ϵ) at various wall-normal locations; $f_x^+ = 0$, $f_z^+ = 0$

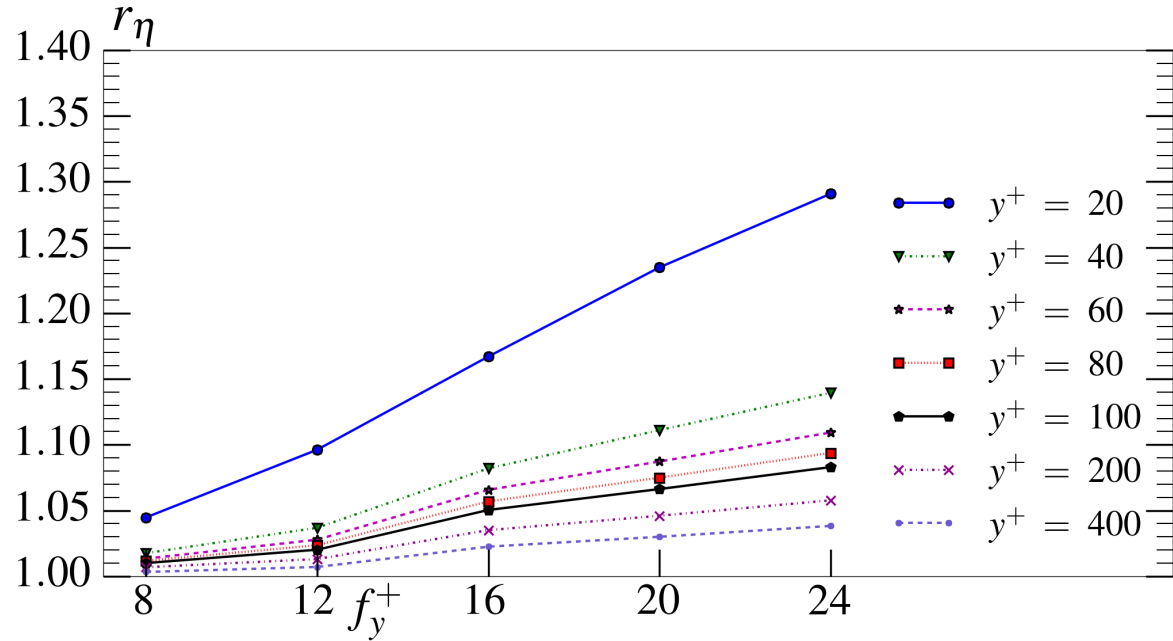


Fig. 4.3 Effect of increasing the filter size in the wall-normal direction (f_y^+) on normalized Kolmogorov length scale (r_η) at various wall-normal heights; $f_x^+ = 0$, $f_z^+ = 0$

fractional contribution of the truncation error to the total error in dissipation is larger in the near wall region, ranging from 15%- 38% of the total error at $y^+ = 20$. The fractional contribution of truncation error to the total error due to spatial filtering clearly shows that spatial filtering is the dominant source of error at most wall-normal locations with the exception of the region very close to the wall where their contributions from spatial filtering and truncation error are similar for large wall-normal filter sizes.

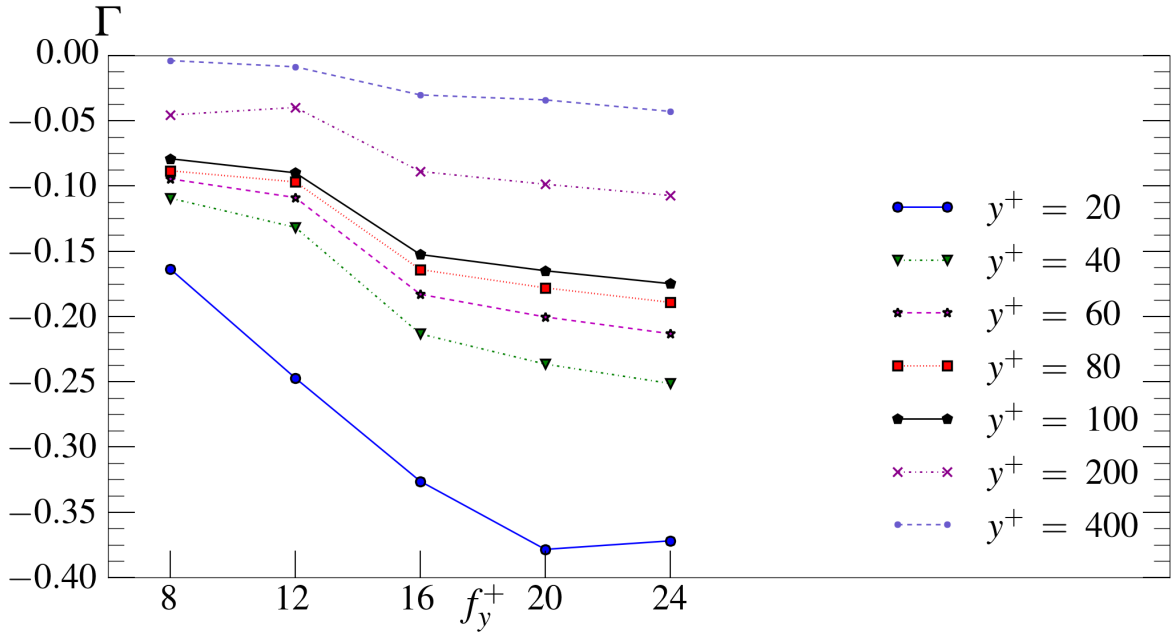


Fig. 4.4 Contribution of truncation error to the total error in dissipation for various wall-normal filter sizes (f_y^+); $f_x^+ = 0$, $f_z^+ = 0$

Often when investigating dissipation, we are concerned not necessarily with local dissipation but total dissipation in the entire flow domain. One way to represent the relative contribution of local error is via the cumulative error from the wall which is expressed as a fraction of the total error in the entire channel by Integral error $\tilde{\xi}(y)$ (Eq. 4.6).

$$\tilde{\xi}(y) = \frac{\int_0^y (\varepsilon - \tilde{\varepsilon}) dy}{\int_0^h (\varepsilon - \tilde{\varepsilon}) dy} \quad (4.6)$$

Profiles of $\tilde{\xi}$ for various wall-normal filter sizes in Fig. 4.5 reveal that the error due to spatial filtering up to the wall-normal height of $y^+ = 200$ is responsible for a substantial proportion (~90%) of the total error in turbulent dissipation in the entire channel. The error

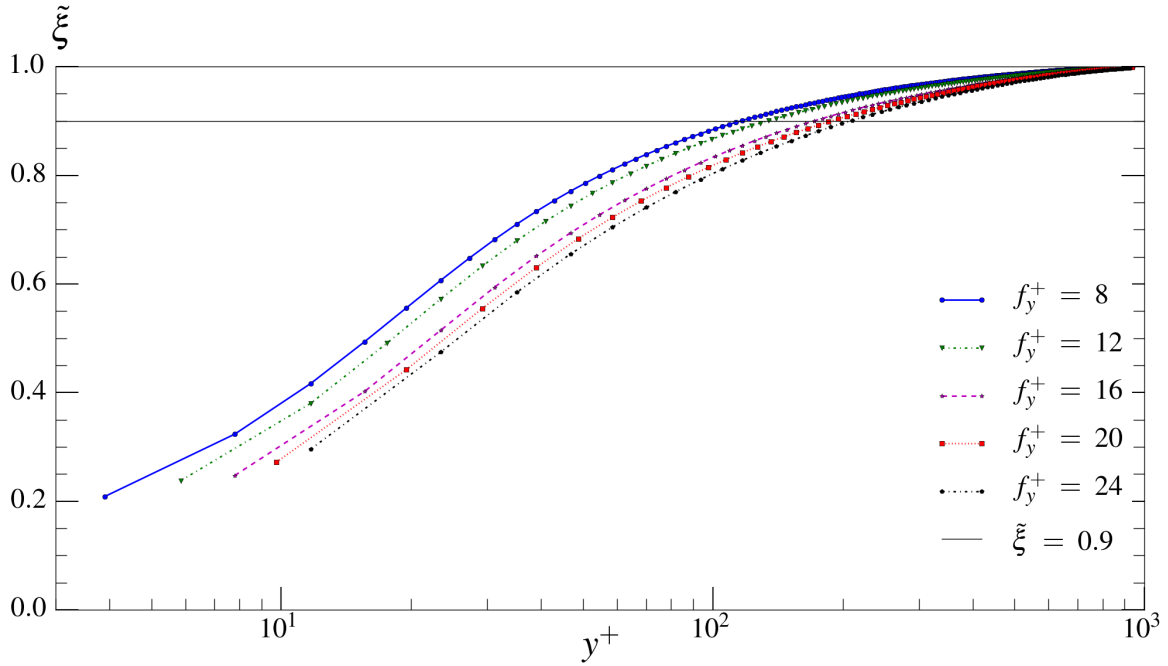


Fig. 4.5 Profiles of integral error ($\tilde{\xi}$) for various wall-normal filter sizes (f_y^+), $f_x^+ = 0$, $f_z^+ = 0$

contributed by filtering in the measurement volume closest to the wall ranges from ~20% to ~30% of the total error for various wall-normal filter sizes. An accurate estimate of the turbulent dissipation rate from experiments clearly warrants the need to maintain small size of the measurement volume in the wall-normal direction, especially in the region responsible for a large fraction of total error in the entire channel ($y^+ < 200$ for the current Reynolds number), or in the region where most of the turbulent kinetic energy is dissipated ($y^+ < 400$ for the current Reynolds number).

To investigate the effect of spatial filtering on various terms in the equation of the mean turbulent dissipation rate (Eq. 2.1) and the corresponding effect on the total dissipation rate in the entire channel, we define r_c as the ratio of filtered value to the true value of each component of dissipation and α_r as the contribution of error in various terms of turbulent dissipation rate to the total error (Eq. 4.7).

$$\begin{aligned} r_c &= \frac{\tilde{c}}{c} \\ \alpha_r &= \frac{\tilde{c} - c}{\tilde{\varepsilon} - \varepsilon} \end{aligned} \quad c = D_{ij}, C_{ij}, M_{ij} \quad (4.7)$$

Fig. 4.6 presents the distribution of α_r for $f_y^+ = 8$ and $f_y^+ = 24$. The profiles in Fig. 4.6 are restricted to $y^+ \leq 300$ since the largest error in turbulent dissipation rate occurs in

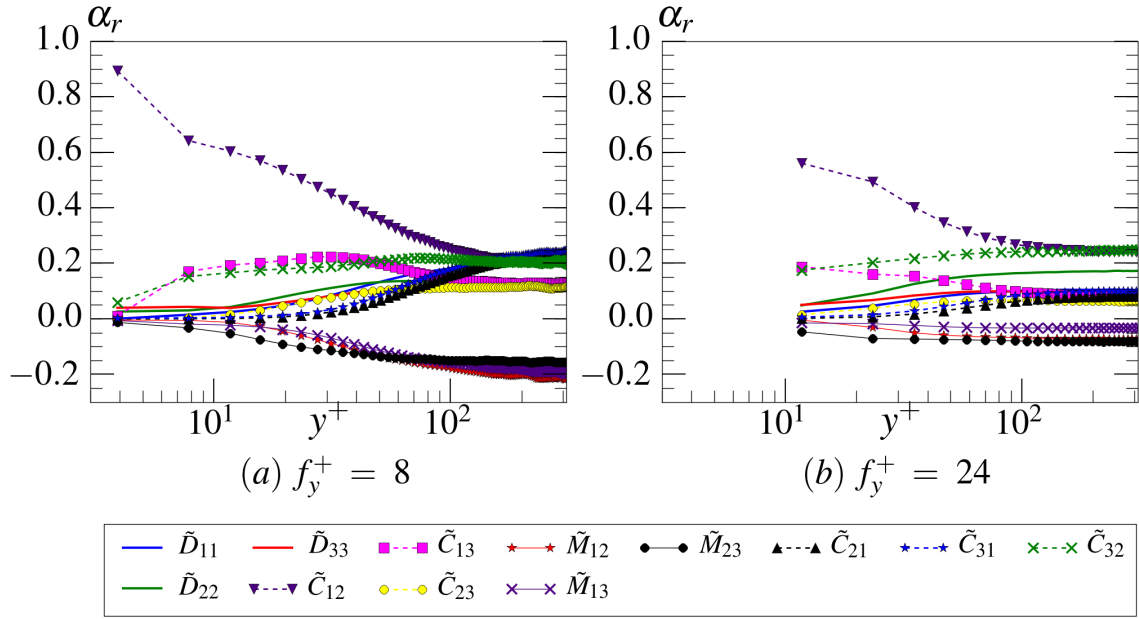


Fig. 4.6 Contribution of error in various gradient terms to the error in dissipation (α_r) for different wall-normal filter sizes ($f_y^+ = 8$); $f_x^+ = 0, f_z^+ = 0$

this region. In regions away from the wall $y^+ > 50$, the fractional contribution of error in the wall-normal derivative terms ($(\partial u'/\partial y)^2 (C_{12})$, $(\partial w'/\partial y)^2 (C_{32})$ and $(\partial v'/\partial y)^2 (D_{22})$) increases with the filter size in the wall-normal direction, while the contribution from the remaining terms decreases.

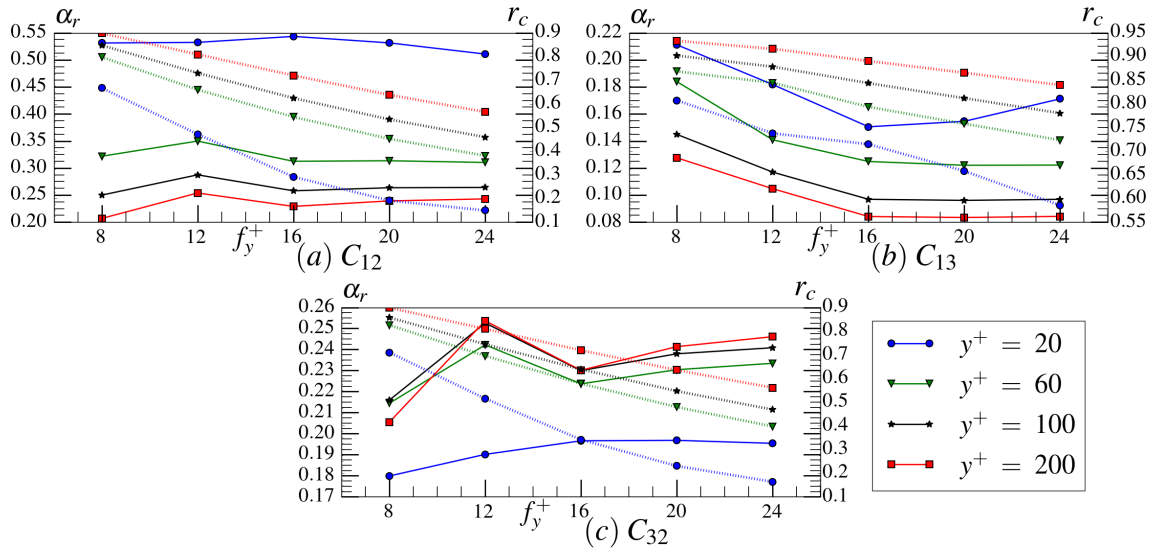


Fig. 4.7 Effect of increasing the filter size in the wall-normal direction (f_y^+) on α_r (solid lines) and r_c (dashed)

The plots of r_c and α_r are presented in Fig. 4.7 for the top three contributors to the error in the near wall region ($(\partial u'/\partial y)^2$ (C_{12}), $(\partial w'/\partial y)^2$ (C_{32}) and $(\partial u'/\partial z)^2$ (C_{31})); the corresponding plots of the remaining terms are provided in Appendix B, Fig. B.1. The plots of C_{12} and C_{32} reveal that the wall-normal derivative terms have the largest penalty to their accuracy ($\sim 55\%$ of the true value at $y^+ = 20$), while their contribution to the total error either remains the same or increases. The effect of filter size in the wall-normal direction on the terms containing velocity derivatives along the span-wise and stream-wise directions was similar to that of C_{13} ; a relatively small rise in the error with increasing filter size in the wall-normal direction, while their fractional contribution to the total error in dissipation reduced. This demonstrates that the net response of error in the turbulent dissipation rate to wall-normal filter size is primarily dictated by the behavior of wall-normal derivative terms.

Case (ii) Study of the effect of filter size in wall-normal direction with spatial filtering along x and z directions $f_x^+, f_z^+ = 16, 12$ and $f_x^+, f_z^+ = 16, 20$

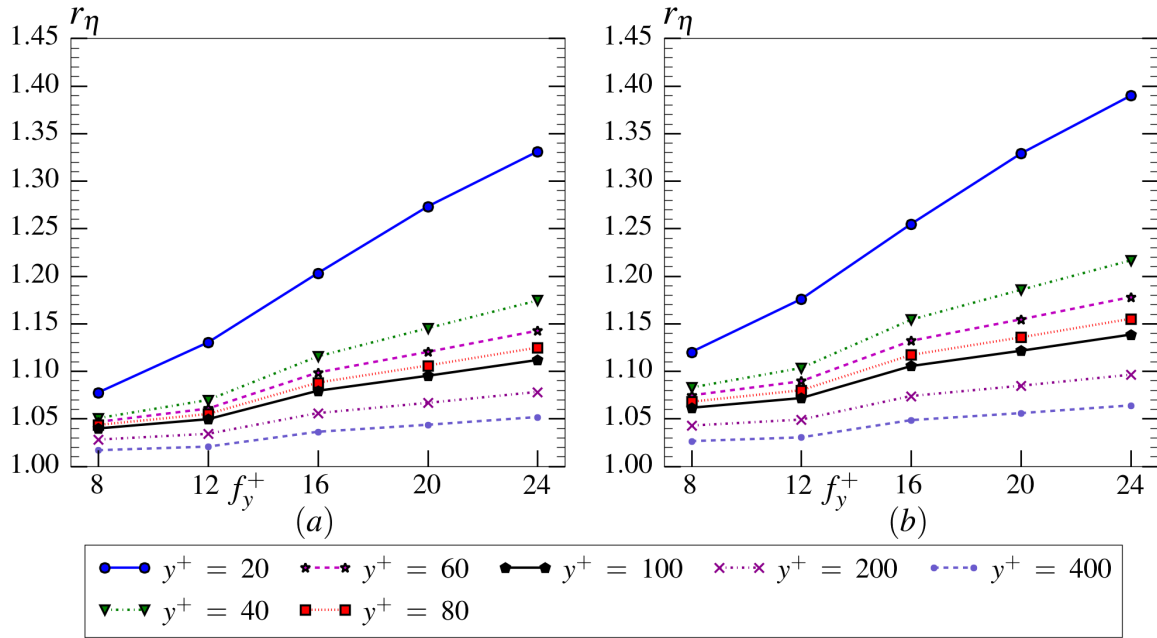


Fig. 4.8 Effect of increasing the filter size in the wall-normal direction on normalized Kolmogorov length scale (r_η) at various wall-normal heights: (a) $f_x^+ = 16$, $f_z^+ = 12$, (b) $f_x^+ = 16$, $f_z^+ = 20$

The effect of only filter size in the wall-normal direction on the mean turbulent dissipation rate (and on the corresponding variables), as seen in Section 4.2, shows little change in trend with the introduction of filtering along the stream-wise and span-wise directions. Fig 4.8 shows the effect of filter size in wall-normal direction on the normalized Kolmogorov length scale when the velocity data is spatially filtered along both stream-wise and span-wise directions. Comparison with the plots of r_η for the case of spatial filtering along wall-normal direction alone (Fig. 4.3), reveals that there is an increase in error in the Kolmogorov length scale due to the introduction of spatial filtering along the stream-wise and span-wise directions, the reduction in the accuracy of the Kolmogorov length scale being larger in the near-wall region for large wall-normal filter sizes.

To gain an insight into the overall effect of spatial filtering on dissipation, we define integral ratio (Eq. 4.8).

$$\tilde{\beta}(y) = \frac{\int_0^y \tilde{\varepsilon} dy}{\int_0^y \varepsilon dy} \quad (4.8)$$

The integral ratio at channel mid-height is the total dissipation in the entire channel for the spatially filtered fields expressed as a fraction of the true value and is presented in Fig. 4.9. The smallest length scale in the flow, which is in the range of minimum Kolmogorov length scale (η_{min}) in the flow domain is often a quantity of interest in turbulence research. For wall bounded flows, the minimum Kolmogorov length scale is on the wall, where the dissipation is maximum. The minimum Kolmogorov length scale in the channel calculated from the filtered velocity fields expressed as the corresponding value calculated from the un-filtered fields ($\tilde{\eta}_{min}/\eta_{min}$) is presented in Fig. 4.9.

The effect of wall-normal filtering shows little difference in the trends with the introduction of filtering along the other two directions. However, the error in minimum Kolmogorov length scale and the total turbulent dissipation rate in the entire channel increases with the introduction of filtering along the stream-wise and span-wise directions.

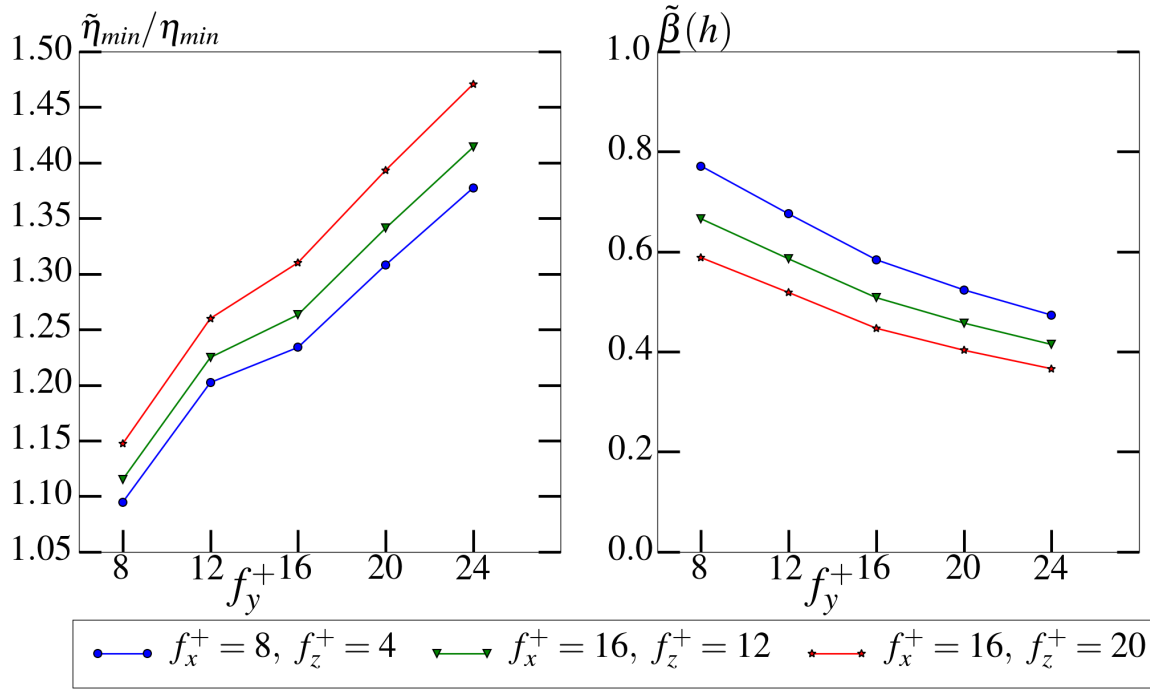


Fig. 4.9 Consolidated results of the effect of filtering along wall-normal direction on the error in total dissipation in the channel ($\tilde{\beta}(h)$) and minimum Kolmogorov length scale ($\tilde{\eta}_{min}/\eta_{min}$)

4.3 Effect of filter size in the span-wise (z) direction

Following an approach similar to the study of the effect of filter-size in the wall-normal direction, the effect of varying the span-wise filter sizes was studied for three combinations of stream-wise (x) and wall-normal (y) filter sizes, the filter size combinations used in this study are listed in table 4.2.

Table 4.2 Filter size combinations used to study the effect of filter size along the span-wise direction (f_z^+) direction, the quantities in brackets are the corresponding grid spacings

$f_x^+(\tilde{\Delta}_x^+)$	$f_y^+(\tilde{\Delta}_y^+)$	$f_z^+(\tilde{\Delta}_z^+)$				
0(8)	0(4)	0 (4)	8 (4)	12 (6)	16 (8)	20 (10)
0 (8)	8 (4)					
24 (12)	24 (12)					

The $f_y^+ = 0$ is a special case when data is filtered along the span-wise and stream-wise directions. Since the original DNS grid in the wall-normal direction is non-uniform, the DNS data was interpolated onto a uniform grid using Chebyshev interpolation (since such an interpolation in the wall-normal direction would be spectrally accurate as is demonstrated in

Chapter 2). The grid spacing in the wall-normal direction, for this particular case is $\tilde{\Delta}_y^+ = 4$ (the smallest grid-size in the wall-normal direction in the previous case).

Case (i) Study of the effect of filter size in span-wise direction with no spatial filtering along x and y directions $f_x^+ = 0, f_y^+ = 0$

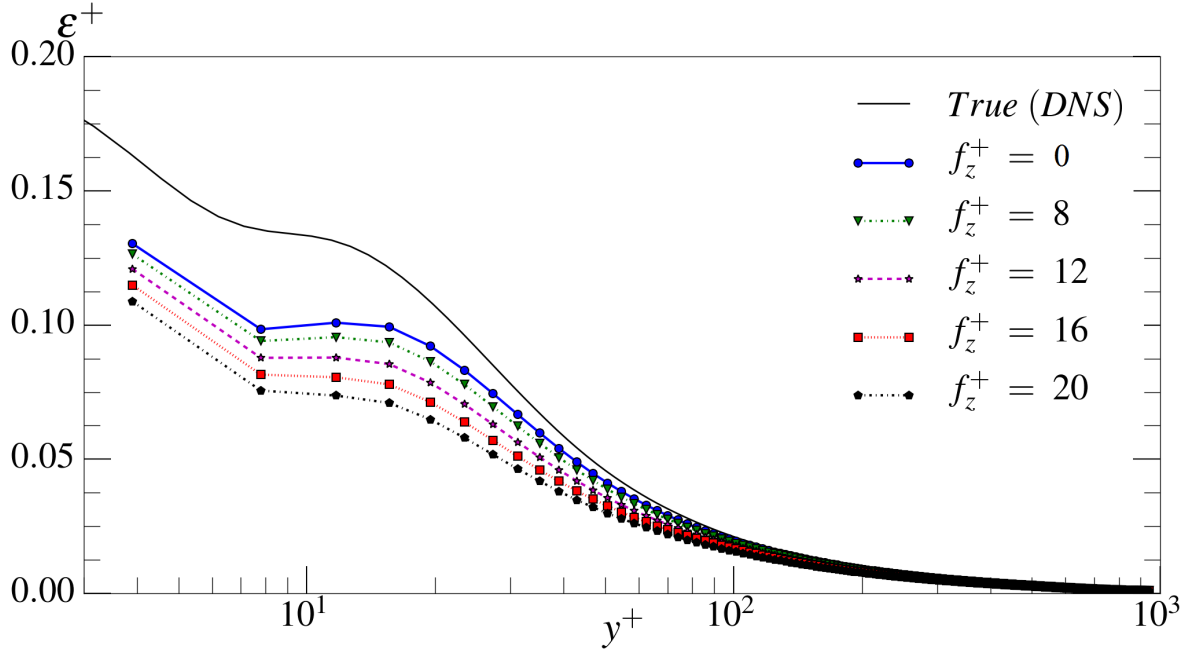


Fig. 4.10 Profiles of the mean turbulent dissipation rate in wall-units ε^+ for the unfiltered case (black) and various span-wise filter sizes (f_z^+), $f_x^+ = 0, f_y^+ = 0$.

The profiles of the mean turbulent dissipation rate (ε^+) (Fig. 4.10) do not show any significant difference in the trend with increasing span-wise filter size (f_z^+). The plots of r_ε v/s f_z^+ (Fig. 4.11) indicate that the loss in accuracy of turbulent dissipation rate with increasing span-wise filter size (f_z^+) is more severe in the near wall region ($y^+ \leq 100$), most likely due to the small Kolmogorov length scale in that region leading to larger filtering of the relevant scales (Fig. 2.3).

The fractional contribution of truncation error to the total error in dissipation (Γ) is largest in the near wall region (Fig. 4.12). Unlike the case of increasing wall-normal filter size, there seems to be a very small variation in the fractional contribution of truncation error with increasing span-wise filter size.

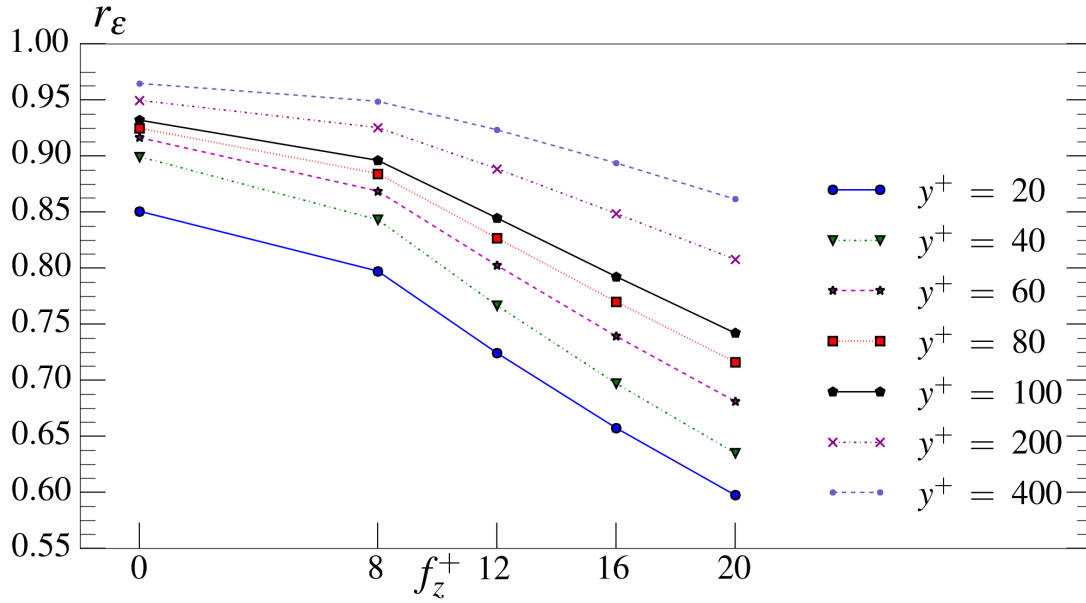


Fig. 4.11 Effect of increasing the filter size in the span-wise direction (f_z^+) on normalized dissipation (r_ϵ) at various wall-normal locations; $f_x^+ = 0$, $f_y^+ = 0$

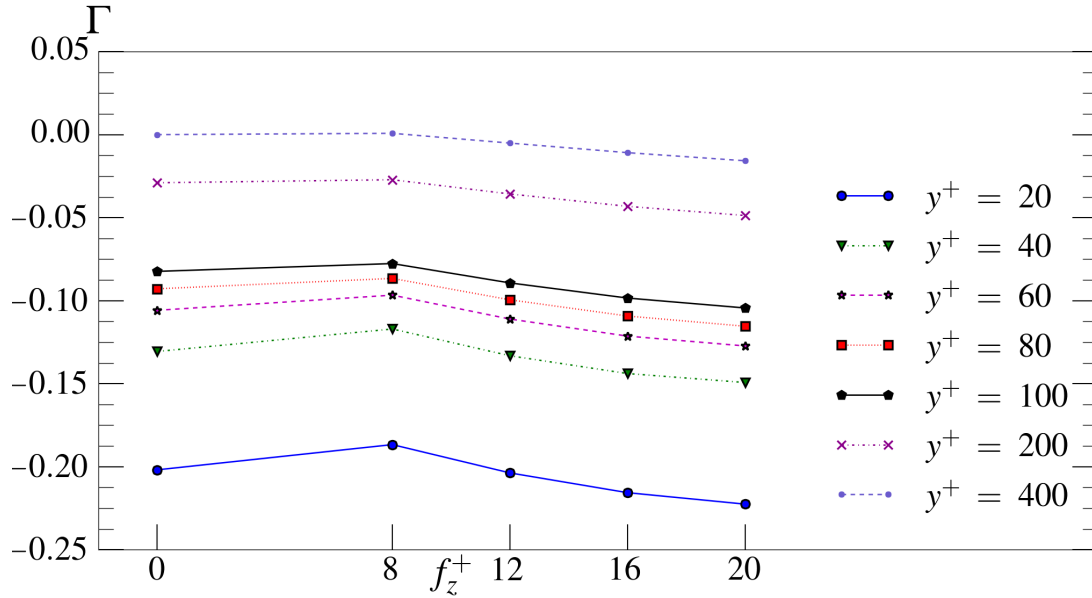


Fig. 4.12 Contribution of truncation error to the total error in dissipation for various span-wise filter sizes(f_z^+); $f_x^+ = 0$, $f_y^+ = 0$

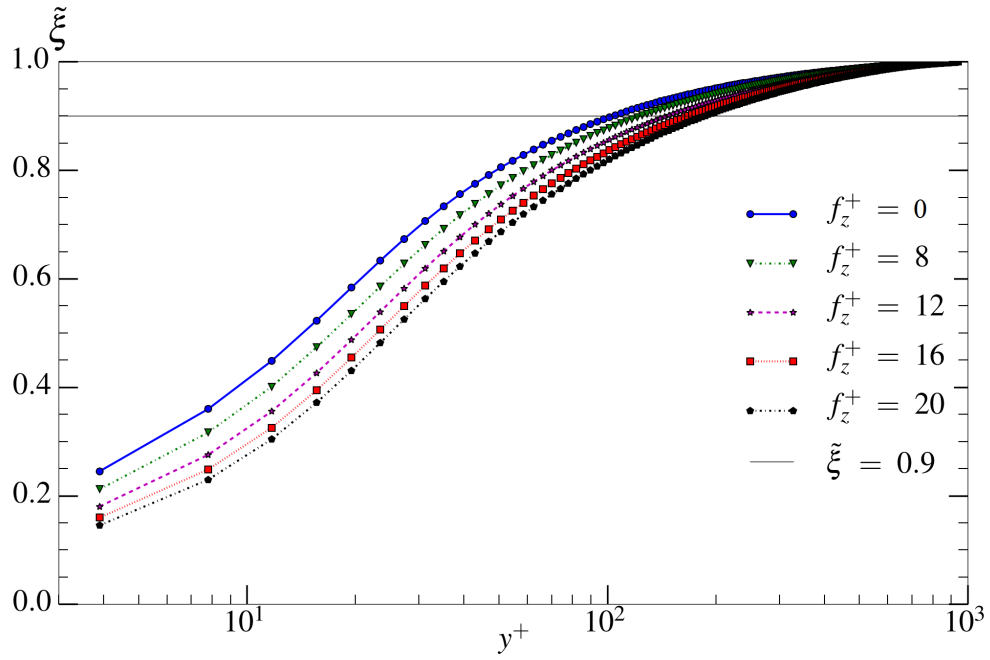


Fig. 4.13 Profiles of Integral error ($\tilde{\xi}$) for various span-wise filter sizes (f_z^+); $f_x^+ = 0$, $f_y^+ = 0$

The profiles of integral error ($\tilde{\xi}$) for various span-wise filter sizes (4.13), show that a large proportion of the total error in turbulent dissipation rate in the entire channel ($\sim 90\%$) comes from spatial filtering in the span-wise direction below wall-normal distances of $y^+ = 100$ to $y^+ = 200$ for all span-wise filter sizes.

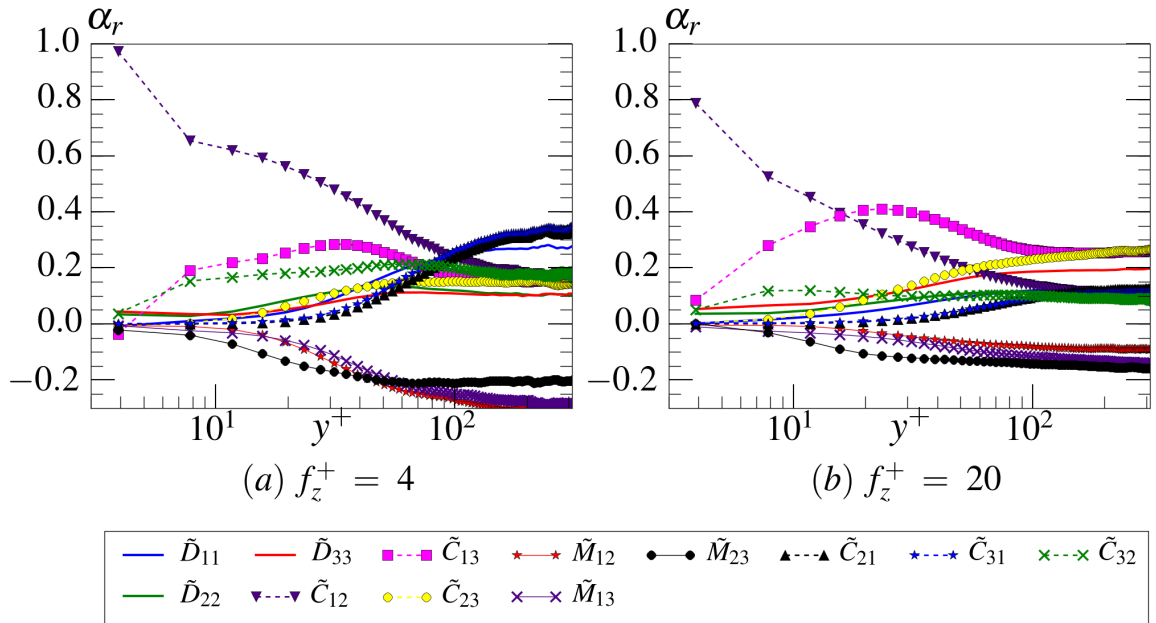


Fig. 4.14 Contribution of error in various terms to the error in dissipation (α_r) for different span-wise filter sizes (f_z^+); $f_x^+ = 0$, $f_y^+ = 0$

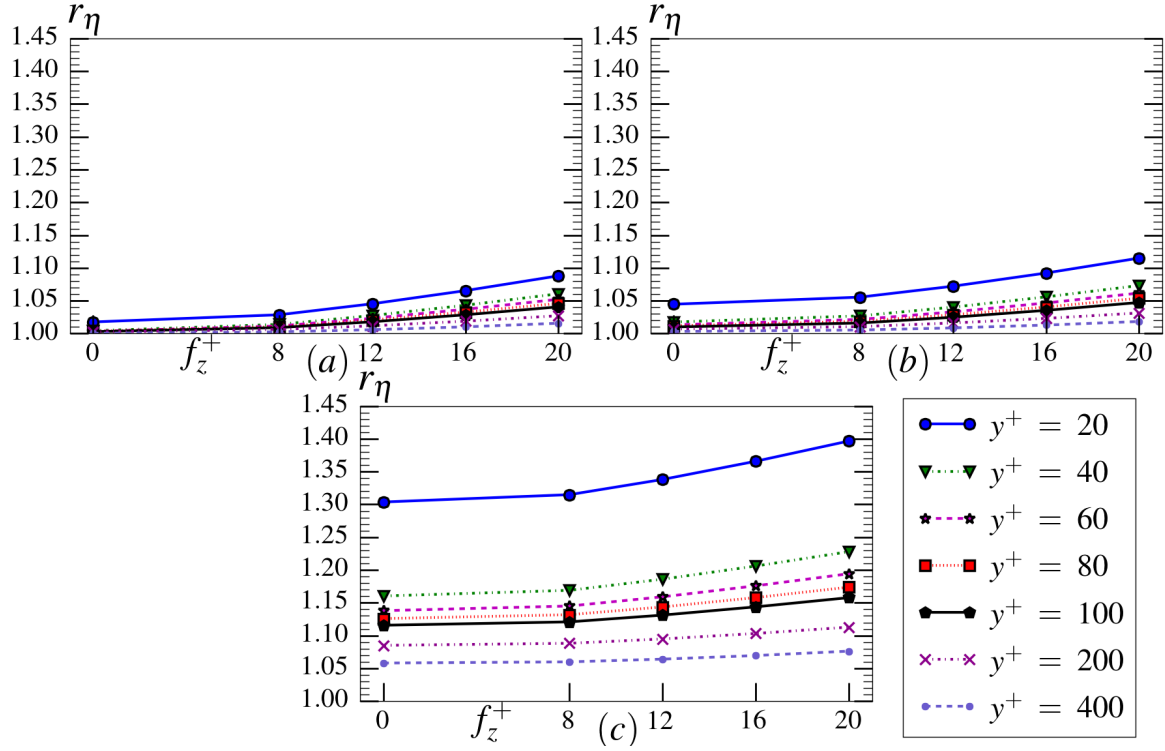


Fig. 4.15 Effect of spatial filter size in the span-wise direction (f_z^+) on normalized Kolmogorov length scale (r_η) at various wall-normal heights: (a) $f_x^+ = 0, f_y^+ = 0$, (b) $f_x^+ = 0, f_y^+ = 8$, (c) $f_x^+ = 24, f_y^+ = 24$

The contribution of error in various terms in the equation of turbulent dissipation rate to the total error in the turbulent dissipation rate due to spatial filtering (α_r) are presented in Fig. 4.14 for span-wise filter sizes of $f_z^+ = 4$ and $f_z^+ = 20$. The terms involving derivatives in the direction of filtering ($(\partial u' / \partial z)^2$ (C_{13}), $(\partial v' / \partial z)^2$ (C_{23}) and $(\partial w' / \partial z)^2$ (D_{33})) have a drastic rise in contribution to the total error in dissipation, a result similar to the observation in the case of wall-normal filtering. At the wall-normal height of $y^+ \approx 200$ for the filter size of $f_z^+ = 20$, the net contribution of error in the span-wise derivative terms is $\approx 70\%$ of the total error in dissipation due to filtering in the span-wise direction.

Case (ii) Study of the effect of filter size in span-wise direction with spatial filtering along x and y directions $f_x^+, f_y^+ = 0, 8$ and $f_x^+, f_y^+ = 24, 24$

The effect of span-wise filter size on Kolmogorov length scale (r_η) for various stream-wise and wall-normal filter sizes is shown in Fig. 4.15. The Kolmogorov length scale shows greater sensitivity to span-wise filtering in the near wall region as compared to the regions away from

the wall, although the penalty of increasing span-wise filter size is less severe as compared to the effect of increasing the wall-normal filter size. The increase in error in the Kolmogorov length scale (Fig. 4.15) due to spatial filtering in the span-wise direction is still largest in the near-wall region. The trends do not change drastically with the introduction of filtering in the wall-normal and stream-wise directions, however there is a drastic increase in the overestimation of the Kolmogorov length scale with increase in the filter size in wall-normal (f_y^+) and stream-wise directions (f_x^+), an observation reiterated from consolidated plots of the integral ratio at channel half width ($\tilde{\beta}(h)$) and the ratio of minimum Kolmogorov length scales for filtered and unfiltered fields (Fig. 4.16).

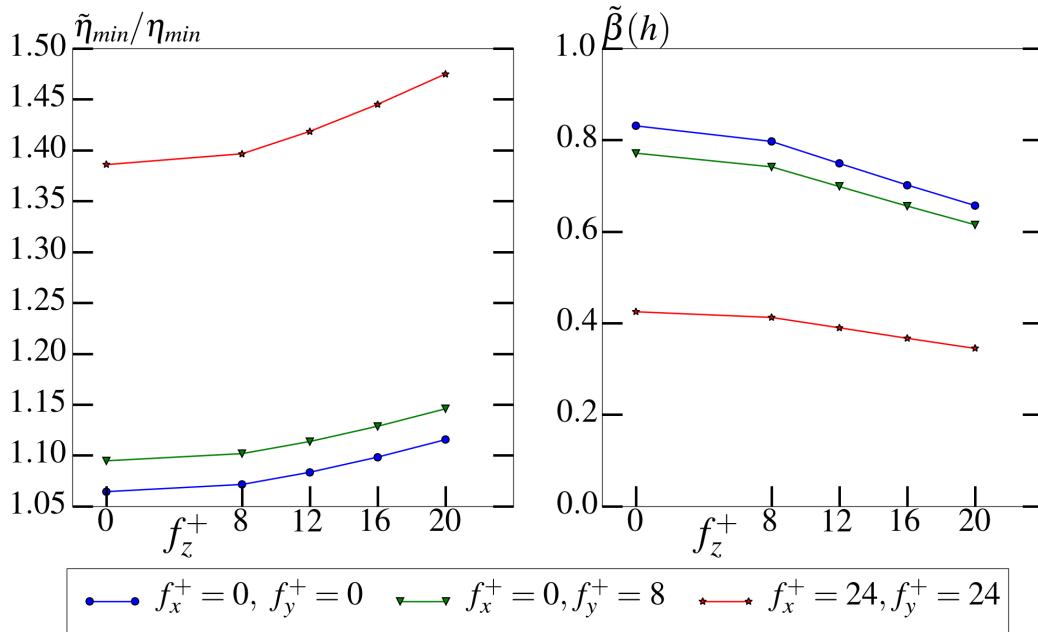


Fig. 4.16 Consolidated results of the effect of filtering along span-wise direction on the error in total dissipation in the channel ($\tilde{\beta}(h)$) and minimum Kolmogorov length scale ($\tilde{\eta}_{min}/\eta_{min}$)

4.4 Effect of filter size in the stream-wise (x) direction

The filter sizes used for studying the effect of stream-wise filter size are shown in table 4.3. It was observed during the studies that the error in dissipation is a relatively weak function of the filter size along the stream-wise direction (f_x^+) as compared to filter sizes along the other two directions, hence the filter sizes are increased in steps of 8^+ units for this study.

Table 4.3 Filter size combinations used for study of the effect of filter size in the stream-wise direction (f_x^+) direction, the quantities in brackets are the corresponding grid spacings

$f_x^+(\tilde{\Delta}_x^+)$				$f_y^+(\tilde{\Delta}_y^+)$	$f_z^+(\tilde{\Delta}_z^+)$
0 (8)	16 (8)	24 (12)	32 (16)	0 (4)	0 (4)
				8 (4)	8 (4)
				24 (12)	16 (8)

Case (i) Study of the effect of filter size in stream-wise direction with no spatial filtering along y and z directions $f_y^+ = 0, f_z^+ = 0$

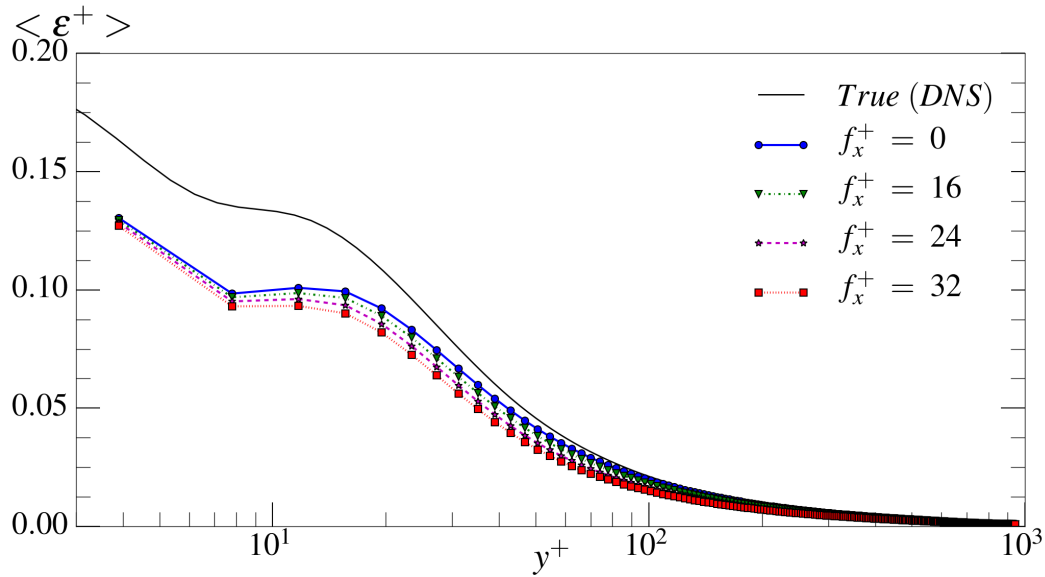


Fig. 4.17 Profiles of the mean turbulent dissipation rate in wall-units ε^+ for the unfiltered case (black) and various stream-wise filter sizes (f_x^+), $f_y^+ = 0, f_z^+ = 0$.

Profiles of the mean turbulent dissipation rate in wall-units (ε^+) for various stream-wise filter sizes are presented in Fig. 4.17. Since the case of $f_y^+ = 0$ corresponds to the velocity fields interpolated along the wall-normal direction on to a uniform grid with grid spacing $\tilde{\Delta}_y^+ = 4$ and use of central difference scheme, the profile of ε^+ for this case indicates that almost all the underestimation of dissipation in the near-wall region is due to the coarse grid interpolation and the corresponding truncation error.

As compared to the case of wall-normal filtering (Fig. 4.2), the magnitude of decrease in the values of normalized dissipation rate (r_ε) with increasing stream-wise filter size (Fig.

4.18) indicates that the error in the turbulent dissipation rate is a relatively weak function of the stream-wise filter size.

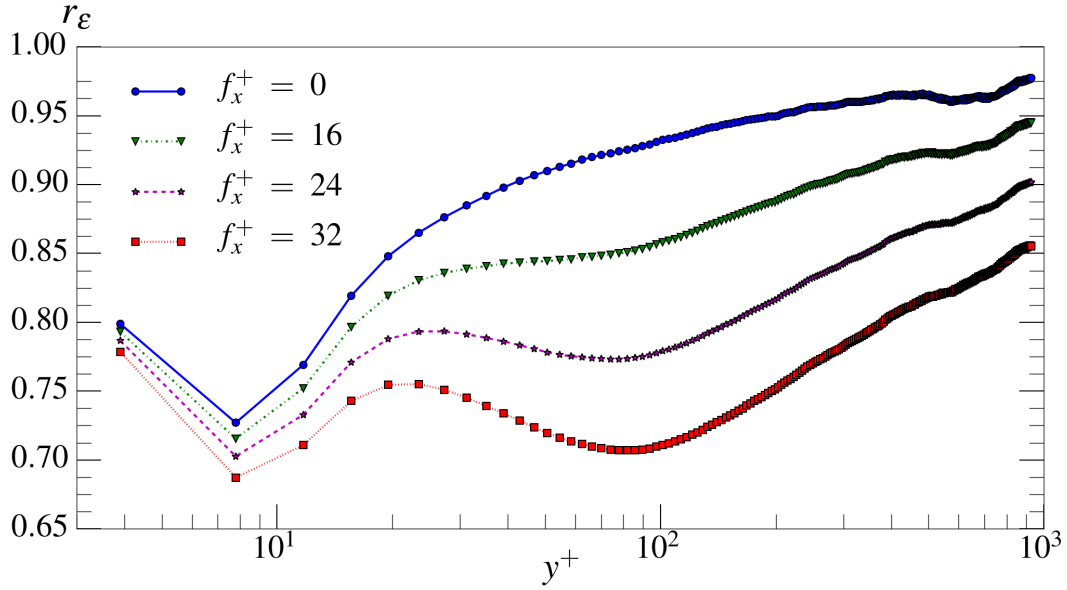


Fig. 4.18 Effect of increasing the filter size in the stream-wise direction (f_x^+) on normalized dissipation rate (r_ϵ); $f_y^+ = 0$, $f_z^+ = 0$

Increasing the stream-wise filter size has a peculiar effect on the normalized turbulent dissipation rate as observed in Fig. 4.18. With the introduction of filtering along the stream-wise direction, the underestimation of the turbulent dissipation rate does not continuously decrease with increasing wall-normal distance.

To isolate the contribution of spatial filtering alone, we compare the profiles of the normalized true dissipation rate ($r_{\epsilon_T} = \tilde{\epsilon}_T/\epsilon$, Fig. 4.19) with the corresponding profiles of the normalized dissipation rate (r_ϵ , 4.18). The underestimation of the turbulent dissipation rate due to only spatial filtering increases with the wall-normal distance (Fig. 4.19), peaks around $y^+ \approx 100$ and then starts decreasing again. The increase in underestimation of the turbulent dissipation rate due to spatial filtering in the stream-wise direction alone is most likely caused by spatial filtering of the relevant length scales and the peculiar behavior seen in the normalized dissipation rate in Fig. 4.18 is a combination of the filtering of length scales and the truncation error, which is maximum close to the wall (Fig. 4.20).

The profiles of integral error ($\tilde{\xi}$) for various stream-wise filter sizes (Fig. 4.21) show that the contribution of error in dissipation in the regions away from the wall to the total error in the turbulent dissipation rate increases with increasing stream-wise filter size.

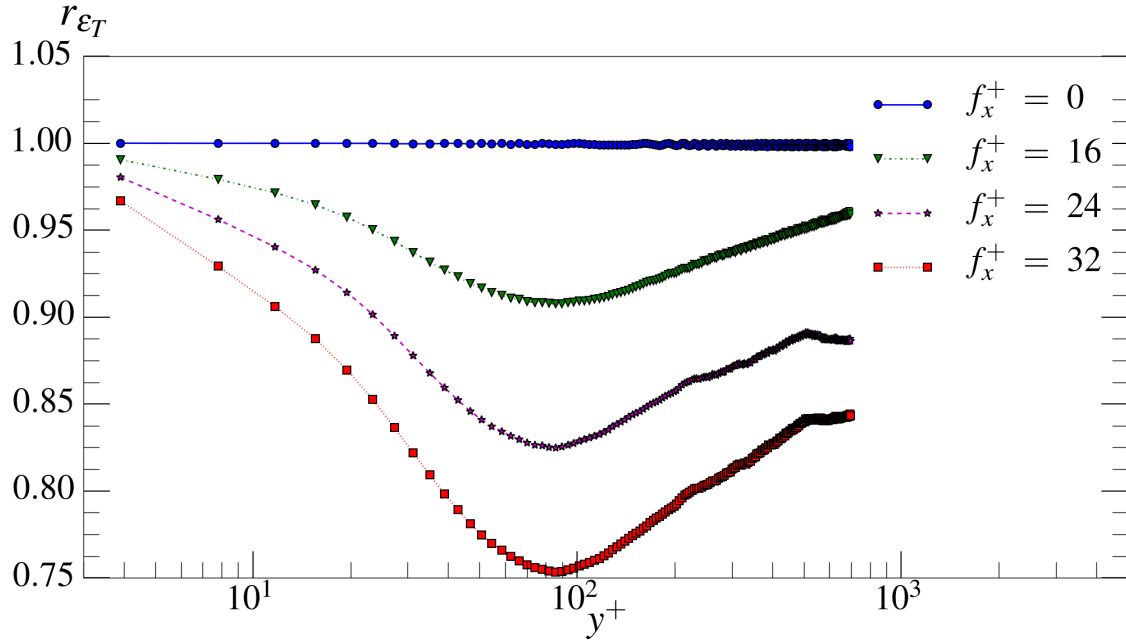


Fig. 4.19 Effect of spatial filtering alone on normalized turbulent dissipation rate (r_{ϵ_T}) for various stream-wise filter sizes (f_x^+), $f_y^+ = 0$, $f_z^+ = 0$.

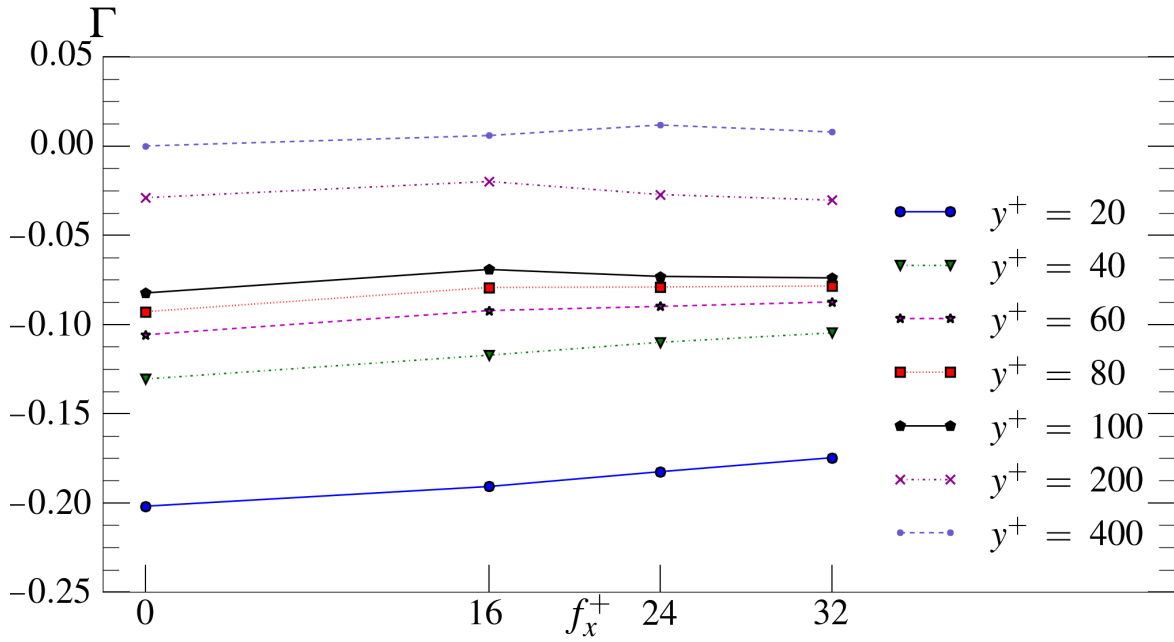


Fig. 4.20 Contribution of truncation error to total error for various stream-wise filter sizes (f_x^+), $f_y^+ = 0$, $f_z^+ = 0$

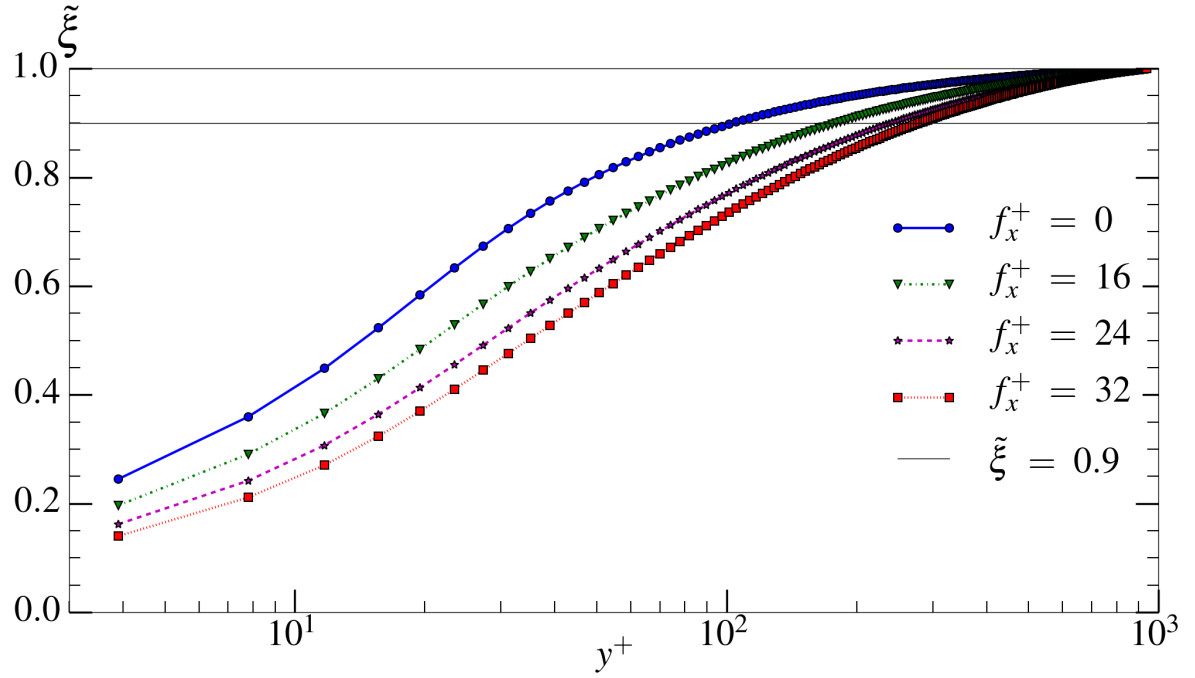


Fig. 4.21 Profiles of integral error ($\tilde{\xi}$) for various stream-wise filter sizes (f_x^+), $f_y^+ = 0$, $f_z^+ = 0$

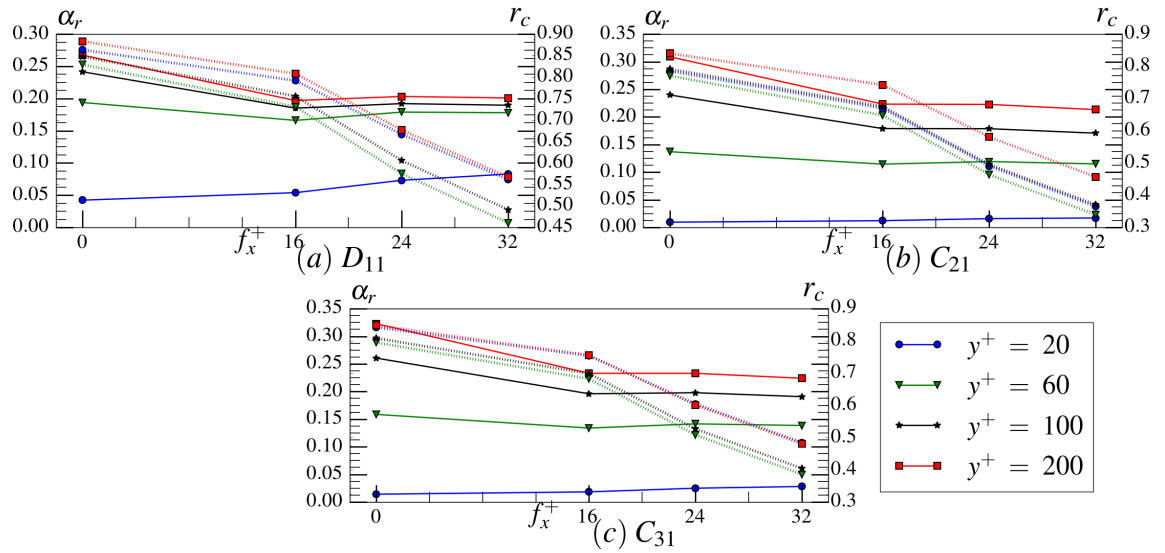


Fig. 4.22 Effect of increasing the filter size in the stream-wise direction (f_x^+) on α_r (solid lines) and r_c (dashed)

Similar to the observations in previous sections, a substantial proportion of increase in total error in the turbulent dissipation rate (Fig. 4.22) is due to increase in the error in terms involving velocity derivatives in the direction of filtering ($(\partial u'/\partial x)^2 (D_{11})$, $(\partial v'/\partial x)^2 (C_{21})$ and $(\partial w'/\partial x)^2 (C_{31})$).

Case (ii) Study of the effect of filter size in stream-wise direction with spatial filtering along y and z directions, $f_y^+, f_z^+ = 8, 8$ and $f_y^+, f_z^+ = 24, 16$

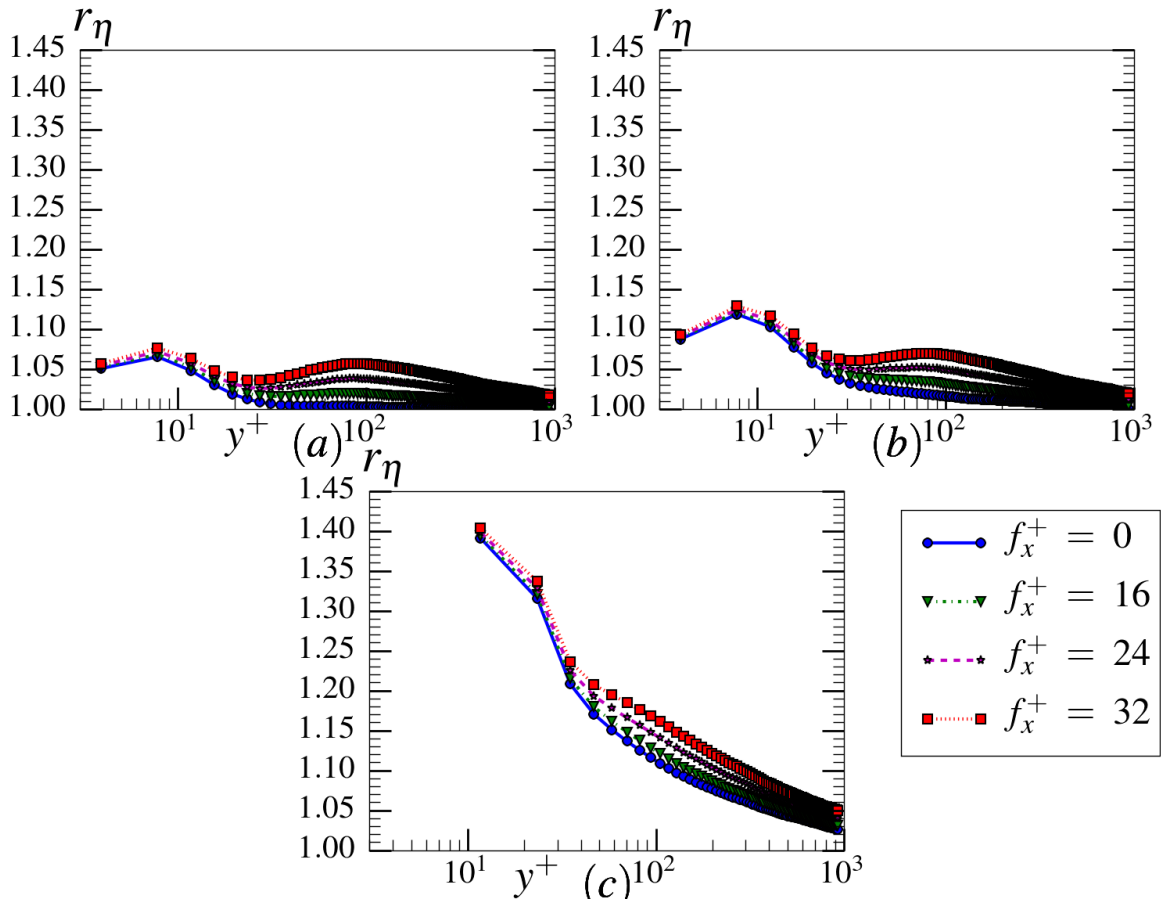


Fig. 4.23 Effect of increasing the filter size in the stream-wise direction (f_x^+) on normalized Kolmogorov length scale (r_η) at various wall-normal heights : (a) $f_y^+ = 0, f_z^+ = 0$, (b) $f_y^+ = 8, f_z^+ = 8$, (c) $f_y^+ = 16, f_z^+ = 24$

The trend of increase in the error in Kolmogorov length scale with increasing stream-wise filter size (f_x^+) changes drastically for large wall-normal and span-wise filter sizes as seen from profiles of normalized Kolmogorov length scale (r_η) presented in Fig. 4.23. While for small wall-normal filter size of $f_y^+ = 8$ the increase in error with increasing distance from

the wall is still observed in the buffer layer along with a slight increase in the error at each wall-normal location, the increase in error with wall-normal distance is not observed for the filter size of $f_y^+ \times f_z^+ = 24 \times 16$.

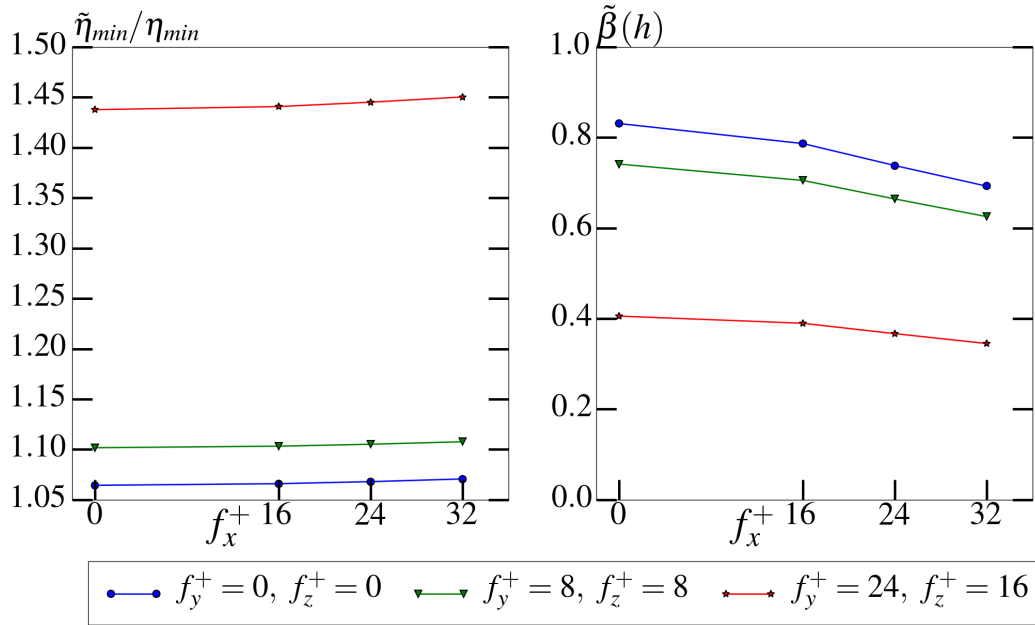


Fig. 4.24 Consolidated results of the effect of filtering along stream-wise direction on the error in total dissipation in the channel ($\tilde{\beta}(h)$) and minimum Kolmogorov length scale ($\tilde{\eta}_{min}/\eta_{min}$)

The consolidated plots of $\tilde{\beta}(h)$ and $\tilde{\eta}_{min}/\eta_{min}$ (Fig. 4.24) reiterate the observations from consolidated plots for wall-normal (Fig. 4.9) and span-wise filtering (Fig. 4.16). When velocity data is spatially filtered along all the three directions, the wall-normal filter size has the largest impact on the accuracy of the turbulent dissipation rate. Any technique targeted at estimating the effect of spatial filtering on the turbulent dissipation rate for wall-bounded flows should take into consideration this anisotropic impact of filter size dissipation.

Chapter 5

Effect of Dimensionally Limited Data on Dissipation

We have seen in Chapter 1 that most measurement techniques provide dimensionally limited velocity fields data which is either 1C-1D, 2C-2D or 3C-2D; only a few components of the velocity gradient tensor can be calculated from such measurements. In the absence of some of the components of the velocity gradient tensor, various models are employed to calculate the turbulent dissipation rate. This chapter discusses the effectiveness of various models in accurately calculating the turbulent dissipation rate in wall-bounded flows.

In the current chapter, high accuracy velocity gradients of unfiltered DNS velocity fields from Chapter 2 have been employed to evaluate the accuracy of various models. Attempts at improving the existing 2C-2D velocity field formulations have been presented in Section 5.1 along with the derivations of the 3C-2D velocity field formulations based on the existing models. A new model with improved near wall performance has been developed in Section 5.2 with a demonstration of its effectiveness in accurately calculating dissipation in wall-bounded flows.

5.1 Existing models

5.1.1 Local axisymmetry model

The 2C-2D formulation of dissipation for turbulence which is axisymmetric about the x_1 direction was presented Chapter 1 (Eq. 1.8). The existing formulation of dissipation based on

the local axisymmetry assumption generally assumes turbulence to be axisymmetric about the stream-wise (x) direction (Antonia et al., 1991). Substituting $x_1 = x$, $x_2 = y$ and $x_3 = z$ in Eq. 1.8 we get the 2C-2D formulation of dissipation for the current domain orientation (Eq. 5.1)

$$\varepsilon_{LA-2x} = \nu \left\langle \left(\frac{\partial u'}{\partial x} \right)^2 + 8 \left(\frac{\partial v'}{\partial y} \right)^2 + 2 \left(\frac{\partial u'}{\partial y} \right)^2 + 2 \left(\frac{\partial v'}{\partial x} \right)^2 + 4 \left(\frac{\partial u'}{\partial y} \frac{\partial v'}{\partial x} \right) \right\rangle \quad (5.1)$$

where ε_{LA-2x} is the formulation of dissipation for 2C-2D velocity fields calculated by assuming axisymmetry of turbulence about the stream-wise (x) direction.

As we have seen in Chapter 2, the wall-normal distribution of various terms in the equation for turbulent dissipation rate (Fig. 2.2) indicates that the near-wall turbulence is highly anisotropic. Since the wall-normal gradients of the velocity components are one of the largest contributors to dissipation in the near-wall region, dissipation in the near-wall region is over-estimated by the existing formulation based on the assumption of axisymmetry about the stream-wise (x) direction (Antonia et al., 1991) (Fig. 5.1). This assumption fails in the near-wall region probably due to the presence of the wall, as the impermeability and no-slip condition at the wall results in large wall-normal gradients of velocity components as compared to their gradients along other directions; thus leading to failure of the assumption of axisymmetry of turbulence about the x direction.

Due to the absence of the wall in the wall-parallel x - z plane, a more suitable assumption could be that of axisymmetry of turbulence about the wall-normal (y) direction. The derivative equivalence relations to be satisfied when assuming axisymmetry of turbulence about wall-normal (y) direction (Eq. 5.2) are obtained by substituting $x_1 = y$, $x_2 = z$, $x_3 = x$ and $u_1 = v$, $u_2 = w$, $u_3 = u$ in the derivative equivalence relations for turbulence which is axisymmetric about the x_1 direction (Eq. 1.7).

$$\begin{aligned}
\left\langle \left(\frac{\partial v'}{\partial z} \right)^2 \right\rangle &= \left\langle \left(\frac{\partial v'}{\partial x} \right)^2 \right\rangle \\
\left\langle \left(\frac{\partial w'}{\partial y} \right)^2 \right\rangle &= \left\langle \left(\frac{\partial u'}{\partial y} \right)^2 \right\rangle \\
\left\langle \left(\frac{\partial w'}{\partial z} \right)^2 \right\rangle &= \left\langle \left(\frac{\partial u'}{\partial x} \right)^2 \right\rangle \\
\left\langle \left(\frac{\partial w'}{\partial x} \right)^2 \right\rangle &= \left\langle \left(\frac{\partial u'}{\partial z} \right)^2 \right\rangle \\
\left\langle \left(\frac{\partial w'}{\partial z} \right)^2 \right\rangle &= \frac{1}{3} \left\langle \left(\frac{\partial v'}{\partial y} \right)^2 \right\rangle + \frac{1}{3} \left\langle \left(\frac{\partial w'}{\partial x} \right)^2 \right\rangle \\
\left\langle \frac{\partial w'}{\partial x} \frac{\partial u'}{\partial z} \right\rangle &= \frac{1}{6} \left\langle \left(\frac{\partial v'}{\partial y} \right)^2 \right\rangle - \frac{1}{3} \left\langle \left(\frac{\partial w'}{\partial x} \right)^2 \right\rangle \\
\left\langle \frac{\partial v'}{\partial z} \frac{\partial w'}{\partial y} \right\rangle &= \left\langle \frac{\partial v'}{\partial x} \frac{\partial u'}{\partial y} \right\rangle = -\frac{1}{2} \left\langle \left(\frac{\partial v'}{\partial y} \right)^2 \right\rangle
\end{aligned} \tag{5.2}$$

The missing terms in an $x-y$ plane, 2C-2D measurement are $(\partial u'/\partial z)^2$, $(\partial v'/\partial z)^2$, $(\partial w'/\partial z)^2$, $(\partial w'/\partial x)^2$, $(\partial w'/\partial y)^2$, $(\partial u'/\partial z)(\partial w'/\partial x)$ and $(\partial v'/\partial z)(\partial w'/\partial y)$. Modelling the missing terms by using Eq. 5.2, the 2C-2D formulation of dissipation, based on the assumption of axisymmetry of turbulence about the wall-normal (y) direction (ϵ_{LA-2y}) is obtained (Eq. 5.3).

$$\epsilon_{LA-2y} = \nu \left\langle 8 \left(\frac{\partial u'}{\partial x} \right)^2 + \left(\frac{\partial v'}{\partial y} \right)^2 + 2 \left(\frac{\partial u'}{\partial y} \right)^2 + 2 \left(\frac{\partial v'}{\partial x} \right)^2 + 4 \left(\frac{\partial u'}{\partial y} \frac{\partial v'}{\partial x} \right) \right\rangle \tag{5.3}$$

When 2C-2D measurements are available, the x - y (stream-wise - wall-normal) plane is the most appropriate choice of measurement plane as it enables direct determination of $(\partial u'/\partial y)^2$, the largest contributor to dissipation in the near wall region (Fig. 2.2). In case of 3C-2D measurements, all the three velocity components can be measured in a planar 2D field, thus the gradients of every velocity component can be obtained along two directions by using this technique. For any wall-normal measurement plane (x - y or y - z), all the wall-normal gradients can be directly determined from measurements. As a result of this, the choice of measurement plane expands to both the wall-normal x - y and y - z planes for 3C-2D measurements.

The missing terms are modelled in a manner similar to the 2C-2D case. A 3C-2D measurement in the y - z plane cannot determine the terms $(\partial v'/\partial x)^2$ and $(\partial w'/\partial x)^2$ in the equation of the turbulent dissipation rate (Eq. 1.4). When assuming axisymmetry of turbulence about the x -axis, the corresponding derivative equivalence relations (Eq. 1.8) have only one equation relating the above-mentioned terms. As a result, it is not possible to derive the formulation of dissipation for y - z plane measurements by assuming axisymmetry of turbulence about the x -axis. The formulations for the remaining three possible combinations are given by Eq. 5.4-Eq. 5.6.

$$\begin{aligned} \varepsilon_{LA-3x-xy} = \nu \left\langle \left(\frac{\partial u'}{\partial x} \right)^2 + 5 \left(\frac{\partial v'}{\partial y} \right)^2 + 2 \left(\frac{\partial u'}{\partial y} \right)^2 + \left(\frac{\partial v'}{\partial x} \right)^2 + \left(\frac{\partial w'}{\partial x} \right)^2 \right. \\ \left. + \left(\frac{\partial w'}{\partial y} \right)^2 + 2 \left(\frac{\partial u'}{\partial y} \frac{\partial v'}{\partial x} \right) \right\rangle \end{aligned} \quad (5.4)$$

$$\begin{aligned} \varepsilon_{LA-3y-xy} = \nu \left\langle 5 \left(\frac{\partial u'}{\partial x} \right)^2 + \left(\frac{\partial v'}{\partial y} \right)^2 + \left(\frac{\partial u'}{\partial y} \right)^2 + 2 \left(\frac{\partial v'}{\partial x} \right)^2 + \left(\frac{\partial w'}{\partial x} \right)^2 \right. \\ \left. + \left(\frac{\partial w'}{\partial y} \right)^2 + 2 \left(\frac{\partial u'}{\partial y} \frac{\partial v'}{\partial x} \right) \right\rangle \end{aligned} \quad (5.5)$$

$$\begin{aligned} \varepsilon_{LA-3y-yz} = \nu \left\langle \left(\frac{\partial v'}{\partial y} \right)^2 + 5 \left(\frac{\partial w'}{\partial z} \right)^2 + \left(\frac{\partial u'}{\partial y} \right)^2 + 2 \left(\frac{\partial v'}{\partial z} \right)^2 + \left(\frac{\partial u'}{\partial z} \right)^2 \right. \\ \left. + \left(\frac{\partial w'}{\partial y} \right)^2 + 4 \left(\frac{\partial u'}{\partial y} \frac{\partial v'}{\partial x} \right) \right\rangle \end{aligned} \quad (5.6)$$

where, $\varepsilon_{LA-3X-xy}$ and $\varepsilon_{LA-3Y-xy}$ are the x - y plane, 3C-2D velocity field formulations of dissipation based on the assumption of local axisymmetry of turbulence about x and y axis respectively. Similarly, $\varepsilon_{LA-3Y-yz}$ is formulation when turbulence is assumed to be axisymmetric about the y -axis and the measurements are performed in the y - z plane.

5.1.2 Weak local isotropy model

The 2C-2D formulation of dissipation based on the weak local isotropy model (ϵ_{WI-2xy}) was presented in Eq. 1.10 in Chapter 1. Similar to the case of the local axisymmetry model, the 3C-2D velocity field formulations for the current model has been derived for both the wall-normal x - y and y - z measurement planes. The unknown terms, in either case, are derived by modelling them by assuming weak local isotropy of turbulence which is based on the simple assumption that the out-of-plane cross gradient terms are equal to the average of the in-plane cross gradient terms (Eq. 1.9). The 3C-2D formulations of dissipation for measurements in x - y (ϵ_{WI-3xy}) and y - z (ϵ_{WI-3yz}) planes are given by Eq. 5.7a and Eq. 5.7b respectively.

$$\epsilon_{WI-3XY} = \nu \left\langle 4 \left(\frac{\partial u'}{\partial x} \right)^2 + 4 \left(\frac{\partial v'}{\partial y} \right)^2 + 2 \left(\frac{\partial u'}{\partial y} \right)^2 + 2 \left(\frac{\partial v'}{\partial x} \right)^2 + \left(\frac{\partial w'}{\partial x} \right)^2 + \left(\frac{\partial w'}{\partial y} \right)^2 + 6 \left(\frac{\partial u'}{\partial y} \frac{\partial v'}{\partial x} \right) + 4 \left(\frac{\partial u'}{\partial x} \frac{\partial v'}{\partial y} \right) \right\rangle \quad (5.7a)$$

$$\epsilon_{WI-3YZ} = \nu \left\langle 4 \left(\frac{\partial v'}{\partial y} \right)^2 + 4 \left(\frac{\partial w'}{\partial z} \right)^2 + \left(\frac{\partial u'}{\partial y} \right)^2 + 2 \left(\frac{\partial v'}{\partial z} \right)^2 + \left(\frac{\partial u'}{\partial z} \right)^2 + 2 \left(\frac{\partial w'}{\partial y} \right)^2 + 6 \left(\frac{\partial u'}{\partial y} \frac{\partial v'}{\partial x} \right) + 4 \left(\frac{\partial u'}{\partial x} \frac{\partial v'}{\partial y} \right) \right\rangle \quad (5.7b)$$

5.1.3 Evaluation of performance of the existing models

Similar to Chapter 4, Eq. 4.5, normalized turbulent dissipation rate calculated by using the models is defined as $r_\epsilon^m = \epsilon^m / \epsilon$, where the superscript m signifies that the quantity is estimated using a model. Profiles of r_ϵ^m are presented in Fig. 5.1 for 1C-1D (local isotropy assumption) and 2C-2D (local axisymmetry assumption and weak local isotropy assumption) velocity field formulations of the existing models.

The local axisymmetry assumption based model provides a slightly better estimate of dissipation when the turbulence is assumed to be axisymmetric about the wall-normal (y) direction as compared to the estimate of dissipation calculated by assuming axisymmetry

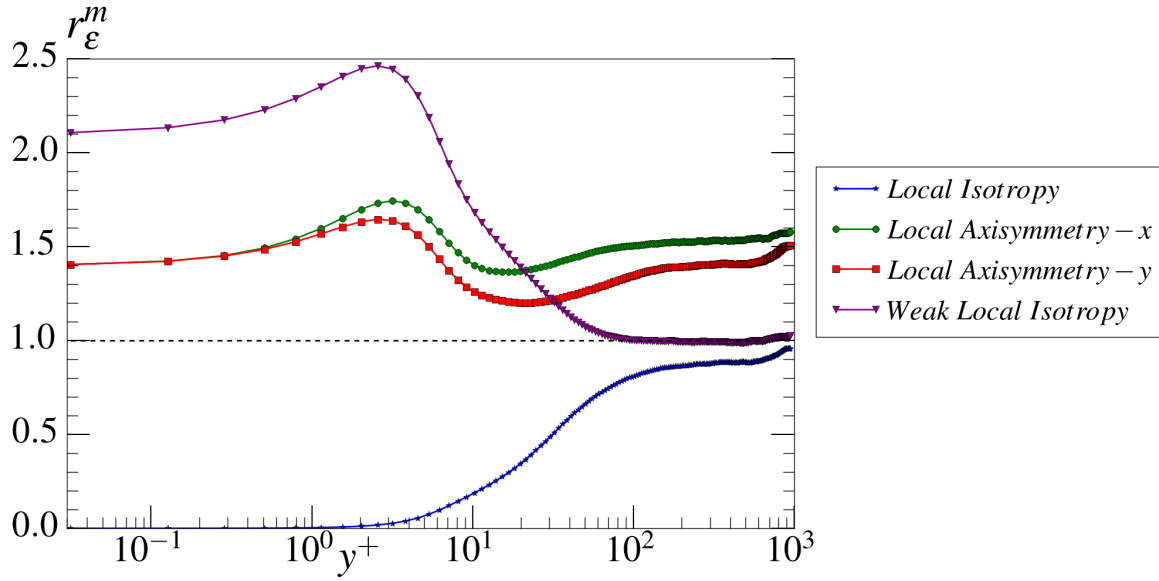


Fig. 5.1 Distribution of the normalized turbulent dissipation rate (r_{ϵ}^m) along the channel height for 1C-1D and 2C-2D velocity field formulations based on local isotropy, local axisymmetry and weak local isotropy assumptions; $r_{\epsilon}^m = 1$ (black dash)

of turbulence about the stream-wise (x) direction. The weak local isotropy model, although more erroneous than the local axisymmetry model in the near wall region ($y^+ < 30$), gives an almost perfect estimate of dissipation above $y^+ \approx 80$ for the 2C-2D formulation.

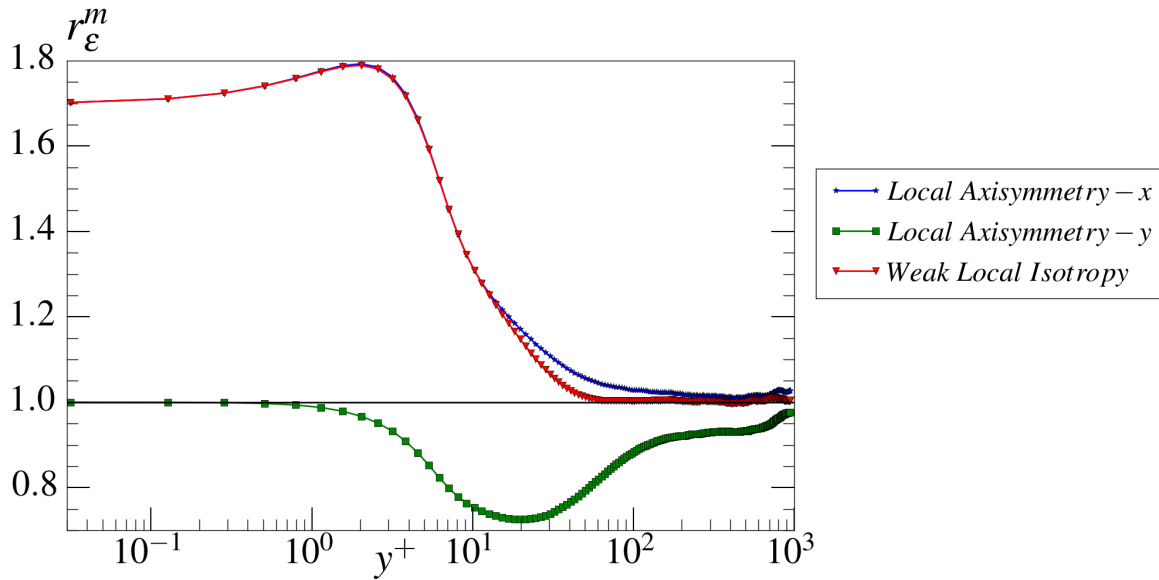


Fig. 5.2 Distribution of the normalized turbulent dissipation rate (r_{ϵ}^m) along the channel height for 3C-2D velocity field formulations based on local axisymmetry and weak local isotropy assumptions; x - y plane formulation

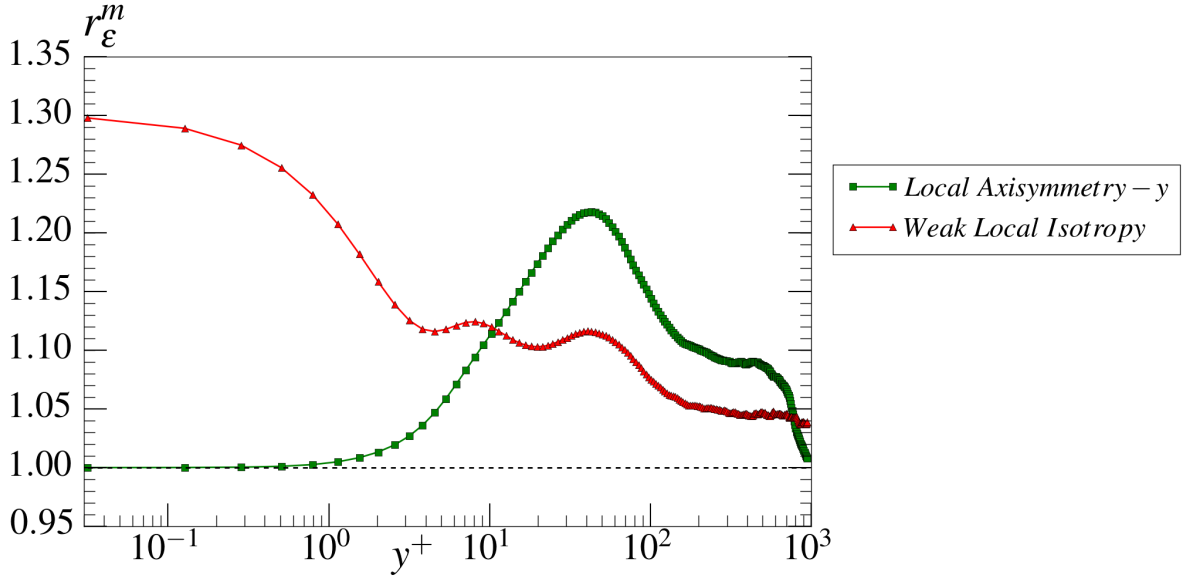


Fig. 5.3 Distribution of the normalized turbulent dissipation rate (r_{ϵ}^m) along the channel height for 3C-2D velocity field formulations based on local axisymmetry and weak local isotropy assumptions; y - z plane formulation

The dissipation estimated by 3C-2D formulations of local axisymmetry and weak local isotropy models for x - y and y - z measurement planes are given in Fig. 5.2 and Fig. 5.3 respectively. The y - z plane formulation of the weak local isotropy model gives a better estimate of dissipation than the corresponding x - y plane formulation in the near wall region. The estimate of dissipation based on the assumption of local axisymmetry of turbulence about y -axis has a smaller maximum error as compared to the corresponding value based on the assumption of axisymmetry about the x -axis (Fig. 5.3). Consistent with observations from the comparison of 2C-2D velocity formulations, the weak local isotropy formulation gives an accurate estimation of dissipation above a distance of $y^+ \sim 50$ from the wall for 3C-2D velocity field formulations.

5.2 Local homogeneity model

The existing models clearly fail to provide an accurate estimate of dissipation in the near-wall region, especially for the 2C-2D case. We have seen in Chapter 2 (Fig. 2.4) that a substantial proportion of dissipation in the channel ($\sim 50\%$) takes place in the near wall region, hence the near-wall poor performance of the local axisymmetry assumption and weak

local isotropy assumption based models is not desired as it leads to a larger error in the minimum Kolmogorov length scale (which is on the wall) and the total turbulent dissipation rate in the entire channel.

A new model was derived to improve the estimate of dissipation, especially in the near-wall region by noting that the estimation of dissipation by the weak local isotropy assumption based formulations is inaccurate mainly in the near wall region while providing an accurate estimate in regions away from the wall. As seen in Chapter 2, the near wall anisotropy of dissipation is a result of the relatively large magnitude of wall-normal gradients of fluctuating velocity components as compared to the magnitude of their gradients along the stream-wise and span-wise directions. The anisotropy of velocity gradients leads to failure of the weak local isotropy model in the near-wall region since it assumes homogeneity between x - z , y - z and x - y planes, as seen from the weak local isotropy model assumptions (Eq. 1.9). The x - z plane being a wall-parallel plane, the assumption of homogeneity in this plane can be assumed to be independent of the homogeneity in the wall-normal x - y and y - z planes. Thus the new formulation was derived by assuming local homogeneity in the x - z plane independently of the homogeneity in the wall-normal x - y and y - z planes (i.e. by assuming equality of only the x - z plane cross-derivative terms) while maintaining the other assumptions of weak local isotropy model (Eq. 5.8).

$$\begin{aligned}
 \left\langle \left(\frac{\partial u'}{\partial z} \right)^2 \right\rangle &= \left\langle \left(\frac{\partial v'}{\partial z} \right)^2 \right\rangle = \left\langle \left(\frac{\partial w'}{\partial x} \right)^2 \right\rangle = \left\langle \left(\frac{\partial v'}{\partial x} \right)^2 \right\rangle \\
 \left\langle \left(\frac{\partial w'}{\partial y} \right)^2 \right\rangle &= \frac{1}{2} \left\langle \left(\frac{\partial u'}{\partial y} \right)^2 + \left(\frac{\partial v'}{\partial x} \right)^2 \right\rangle \\
 \left\langle \frac{\partial u'}{\partial z} \frac{\partial w'}{\partial x} \right\rangle &= \left\langle \frac{\partial u'}{\partial y} \frac{\partial v'}{\partial x} \right\rangle = \left\langle \frac{\partial v'}{\partial z} \frac{\partial w'}{\partial y} \right\rangle
 \end{aligned} \tag{5.8}$$

The 2C-2D and 3C-2D formulations of dissipation derived based on the new local homogeneity model are given by Eq. 5.9 and Eq. 5.10 respectively.

$$\epsilon_{LH-2xy} = \nu \left\langle 4 \left(\frac{\partial u'}{\partial x} \right)^2 + 4 \left(\frac{\partial v'}{\partial y} \right)^2 + 1.5 \left(\frac{\partial u'}{\partial y} \right)^2 + 4.5 \left(\frac{\partial v'}{\partial x} \right)^2 + 4 \left(\frac{\partial u'}{\partial x} \frac{\partial v'}{\partial y} \right) + 6 \left(\frac{\partial u'}{\partial y} \frac{\partial v'}{\partial x} \right) \right\rangle \quad (5.9)$$

$$\epsilon_{LH-3xy} = \nu \left\langle 4 \left(\frac{\partial u'}{\partial x} \right)^2 + 4 \left(\frac{\partial v'}{\partial y} \right)^2 + \left(\frac{\partial u'}{\partial y} \right)^2 + 3 \left(\frac{\partial v'}{\partial x} \right)^2 + \left(\frac{\partial w'}{\partial x} \right)^2 + \left(\frac{\partial w'}{\partial y} \right)^2 + 6 \left(\frac{\partial u'}{\partial y} \frac{\partial v'}{\partial x} \right) + 4 \left(\frac{\partial u'}{\partial x} \frac{\partial v'}{\partial y} \right) \right\rangle \quad (5.10a)$$

$$\epsilon_{LH-3yz} = \nu \left\langle 4 \left(\frac{\partial v'}{\partial y} \right)^2 + 4 \left(\frac{\partial w'}{\partial z} \right)^2 + \left(\frac{\partial u'}{\partial y} \right)^2 + 3 \left(\frac{\partial v'}{\partial z} \right)^2 + \left(\frac{\partial u'}{\partial z} \right)^2 + \left(\frac{\partial w'}{\partial y} \right)^2 + 6 \left(\frac{\partial u'}{\partial y} \frac{\partial v'}{\partial x} \right) + 4 \left(\frac{\partial u'}{\partial x} \frac{\partial v'}{\partial y} \right) \right\rangle \quad (5.10b)$$

where, ϵ_{LH-2xy} is the 2C-2D velocity field formulation while ϵ_{LH-3xy} and ϵ_{LH-3yz} are respectively, the x - y and y - z plane, 3C-2D velocity field formulations of dissipation based on the assumption of local homogeneity.

The normalized turbulent dissipation rate, normalized Kolmogorov length scale and integral ratio calculated using the 2C-2D and 3C-2D formulations of local homogeneity assumption based model are compared with the corresponding quantities for the weak-local isotropy model in Fig. 5.4 and Fig. 5.5 respectively. The local homogeneity model provides an improved estimate of dissipation at the wall as compared to the local axisymmetry and weak local isotropy models, while the weak local isotropy model is still more accurate in regions away from the wall ($y^+ > 100$).

Since the local homogeneity model performs well in the viscous sub-layer and the weak local isotropy model in the region $y^+ > 100$, an improved estimate of dissipation can be obtained by calculating a weighted sum of the local homogeneity and the weak local isotropy formulations as given by Eq. 5.11.

$$\varepsilon_{Bl} = b \cdot \varepsilon_{LH} + (1 - b) \cdot \varepsilon_{WI} \quad (5.11)$$

where b is the blend function given by Eq. 5.12

$$\begin{aligned} b(y^+) &= 1 & y^+ < 2 \\ b(y^+) &= (50 - y^+)/48 & 2 \leq y^+ \leq 50 \\ b(y^+) &= 0 & y^+ > 50 \end{aligned} \quad (5.12)$$

The maximum error in dissipation estimated using the new blend formulation is $\sim 25\%$ for 2C-2D velocity fields (Fig. 5.4) while it is $\sim 11\%$ and $\sim 13\%$ respectively for the 3C-2D velocity field x - y and y - z plane formulations (Fig. 5.5).

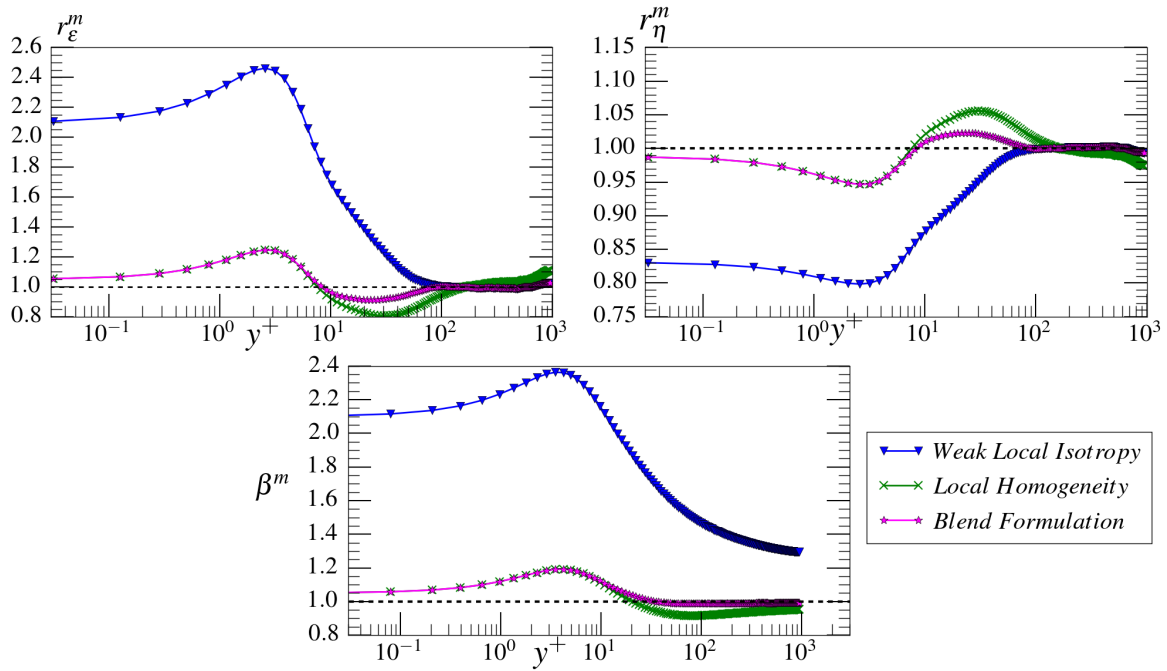


Fig. 5.4 Profiles of the normalized turbulent dissipation rate (r_ε^m), normalized Kolmogorov length scale (r_η^m) and Integral ratio (β^m) calculated using 2C-2D velocity field formulations of local homogeneity assumption, weak local isotropy assumption and blend formulation

The current choice of the blend function giving 100% weighting to the local homogeneity model near the wall ($y^+ < 2$) and to weak local isotropy model in the region $y^+ > 50$ is the simplest choice as it varies linearly from 1 at $y^+ = 2$ to 0 at $y^+ = 40$. As can be seen from

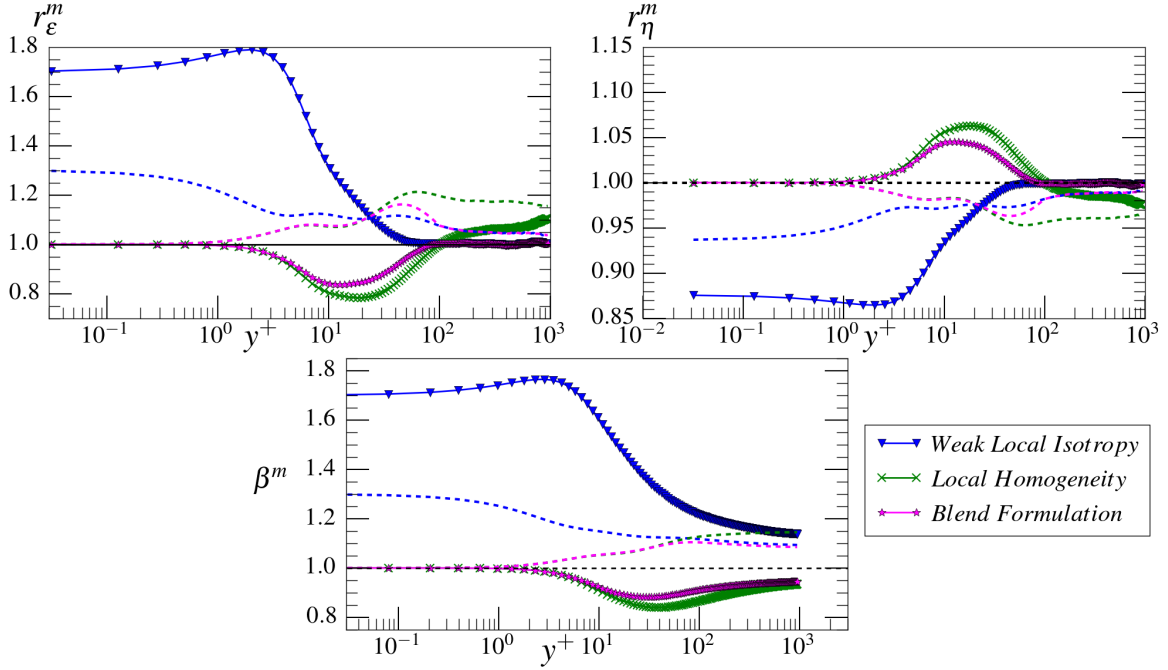


Fig. 5.5 Profiles of the normalized turbulent dissipation rate (r_ϵ^m), normalized Kolmogorov length scale (r_η^m) and Integral ratio (β^m) calculated using 3C-2D velocity field formulations of weak local isotropy assumption, local homogeneity assumption and blend formulation; solid lines (x-y plane formulation), dashed (y-z plane formulation)

Fig. 5.4 and Fig. 5.5, a more complex non-linear weighing function would give a better estimate of dissipation for the present case, but such a function would require choosing an additional co-efficient in the non-linear function which would depend on the flow. Since the success of such a choice cannot be determined apriori in experiments, only results for the simple linear blend function have been presented here, even though more complex choices are possible.

We have seen in Chapter 4, that the total error in dissipation for the entire channel is given by the value of the integral ratio (Eq. 4.8) at channel mid-height ($\beta^m(h)$). The total error in dissipation calculated by the blend formulation for 2C-2D velocity fields is $\sim 0.8\%$ of the total dissipation in the channel (Fig. 5.4), while it is $\sim 5.5\%$ and $\sim 8.5\%$ respectively for the 3C-2D velocity field x-y and y-z plane formulations (Fig. 5.5).

The Kolmogorov length scale estimated by the blend formulation has a maximum error of 5.35% of the true value for the 2C-2D velocity fields while it is 2.96% and 3.05% respectively for 3C-2D velocity field x-y and y-z formulations (Fig. 5.5).

Chapter 6

Combined Effect of Spatial Filtering and Limited Dimensionality on Turbulent Dissipation Rate

We have discussed in Chapter 1 how spatial filtering and limited dimensionality are characteristic to velocities obtained from most experimental measurements. This chapter quantifies the combined error in turbulent dissipation rate due to spatial filtering and limited dimensionality.

The net error in the turbulent dissipation rate calculated from data provided by most experimental measurements is affected by both spatial filtering and limited dimensionality. We have seen in chapter 4 that the error in each term in the equation of the turbulent dissipation rate (Eq. 1.4) depends on the size of the filter in each direction. Taking into consideration the fact that the formulations of dissipation based on different models are developed by assuming equivalence of various products of velocity gradients (chapter 5), we can conclude that the ability of various models to accurately estimate the dissipation calculated from 3C-3D data is dependent on the accuracy of the equivalence relations. Due to the anisotropic response of the error in various terms of the fluctuating velocity gradient tensor to the filter size along each direction, the pre-defined equivalence relations will not hold true in filtered fields. As a result, the accuracy of the turbulent dissipation rate calculated by the models will depend on the size of the measurement volume (length of the wire in case hot-wire anemometry and the interrogation window volume in case of PIV measurement techniques).

In order to evaluate the net error in turbulent dissipation rate, velocity fields were spatially filtered at resolutions equivalent to the typical measurement volume size in experiments and the dissipation was calculated using the various models described in Chapter 5. The sections below present the accuracy of the turbulent dissipation rate and Kolmogorov length scales for various spatial filter sizes and formulations based on 1C-1D, 2C-2D and 3C-2D formulations based on different models.

6.1 1C-1D Velocity Fields

In hot-wire anemometry, the most common orientation of the wire is employed along the span-wise direction since it allows the measurement of the stream-wise derivative of the stream-wise velocity from its temporal gradient by applying Taylor's hypothesis (Atkinson et al., 2014). Additionally, we have seen in Chapter 4 that the error introduced in the turbulent dissipation rate due to spatial filtering is most sensitive to the filter size wall-normal direction; hence when one component of velocity can be measured using a single hot-wire, the span-wise orientation of the wire is the most appropriate choice. Thus, in order to evaluate the net error in turbulent dissipation rate and Kolmogorov length scale due to spatial filtering and limited dimensionality when 1C-1D data is available from measurements from techniques like HWA, velocity fields were spatially filtered in the span-wise direction to mimic the effect of increasing the wire length.

The effect of increasing the wire length ranging from 4^+ to 20^+ wall units has been studied. Since the data is assumed to be present in the form of 1C-1D velocity fields, the normalised dissipation rate $r_{\epsilon}^m = \tilde{\epsilon}^m / \epsilon$ and normalised Kolmogorov length scale, $r_{\eta}^m = \tilde{\eta}^m / \eta$ are calculated using the local isotropy model (Eq. 1.6) and presented in Fig. 6.1; the superscript m denotes that the dissipation has been calculated using a model and the \sim indicates that the velocity fields were spatially filtered.

Since the DNS grid has a spacing of ($\Delta x^+ = 4$), the cases corresponding to ($l^+ = 4$) do not involve any spatial filtering in the span-wise direction. The difference between Unfiltered ($l^+ = 4$) and ($l^+ = 4$) case is the use of accurate derivatives from Chapter 2 in the former and central difference scheme for the gradient calculation in the latter case. The spatial filtering

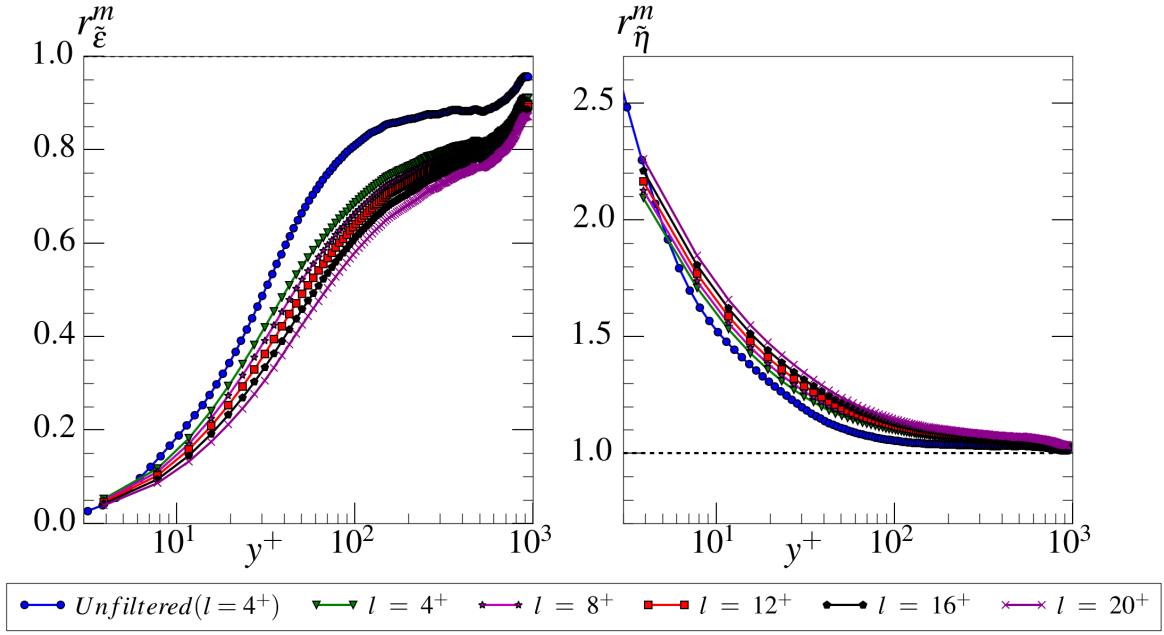


Fig. 6.1 Effect of span-wise wire length(l) on normalised dissipation rate (r_{ϵ}^m) and normalised Kolmogorov length scale (r_{η}^m) calculated using the local isotropy formulation

in span-wise direction due to finite wire length has the largest effect on the accuracy of the turbulent dissipation rate and the Kolmogorov length scale in the near wall region. The largest impact of wire-length on dissipation is seen in the region above $y^+ \sim 30$. The inaccuracy of both, the turbulent dissipation rate and the Kolmogorov length scale in the near wall region is due to the inaccuracy of the local isotropy model which is demonstrated by the values of both these quantities for the Unfiltered ($l^+ = 4$) case.

When using data obtained from experiments, it is useful to get an estimate of the error in dissipation and minimum Kolmogorov length scale calculated from experimental data. These errors are calculated assuming that the error in velocity due to end conduction effects in the hot-wire anemometer is negligible, which requires the length to diameter ratio of the wire to be greater than 200 (Philip et al., 2013). Table 6.1 presents effect of wire length on $\tilde{\beta}_m$ (Eq. 4.8), the integral ratio of dissipation at channel mid-height, calculated for spatially filtered fields using the local isotropy model and $\tilde{\eta}_{min}^m/\eta_{min}$, the ratio of the corresponding minimum Kolmogorov length scale to the true value; the corresponding 3C-3D velocity field data is provided for reference. A large proportion of the error in the estimated Kolmogorov length scale can be attributed to the truncation error in the central difference scheme which is

proved by the fact that the effect of wire length on Kolmogorov length scale is negligible in the near-wall region and the entire error in the Unfiltered case is the truncation error.

Due to the inadequacy of local isotropy model to accurately estimate the dissipation calculated using 3C-3D velocity fields, especially in the near wall region, the minimum Kolmogorov length scale estimated by local isotropy model is almost twice the true minimum Kolmogorov length scale. The net error in dissipation for the entire channel is $\sim 50\%$ of the true value.

Table 6.1 Consolidated results of net effect of wire length and use of the 1C-1D velocity field, Local Isotropy Formulation (ISO) formulation

l^+	$\tilde{\beta}_m$		$\tilde{\eta}_{min}^m/\eta_{min}$	
	3C-3D	1C-1D	3C-3D	1C-1D
4	0.896	0.542	1.058	2.092
8	0.859	0.524	1.066	2.126
12	0.807	0.504	1.078	2.164
16	0.756	0.482	1.092	2.209
20	0.708	0.459	1.107	2.261

An alternative approach to get an approximate estimate of the Kolmogorov length scale near the wall can be obtained by noting that the gradients of all the fluctuating velocity components in the stream-wise (x) and span-wise (z) directions are zero at the wall due to the no-slip condition. Since $\partial u'/\partial x = 0$ and $\partial w'/\partial z = 0$ are zero at the wall, continuity equation leads to $\partial v'/\partial y = 0$ at the wall. Thus, the only terms contributing to dissipation at the wall are $(\partial u'/\partial y)^2$ and $(\partial w'/\partial y)^2$. We can see from plots of the Kolmogorov length scale for the unfiltered fields (Fig 2.2) that in the near-wall region ($y^+ < 10$), the Kolmogorov length scale is almost constant and the largest contributors to dissipation in that region are the non-zero terms at the wall, viz $(\partial u'/\partial y)^2$ and $(\partial w'/\partial y)^2$. Applying the local homogeneity assumption (Eq. 5.8) to model the term $(\partial w'/\partial y)^2$, we get a 1D local homogeneity approximation for dissipation in the viscous sub-layer as

$$\epsilon_{1D-LH} = 1.5 \left\langle \left(\frac{\partial u'}{\partial y} \right)^2 \right\rangle \quad (6.1)$$

Since a measurement at $y^+ = 8$ using a hot-wire anemometer would lead to spatial-filtering only along the span-wise direction, the error due to spatial filtering along the wall-normal direction would be eliminated by such a measurement. Not considering the effect of measurement noise and under the assumption of negligible end-conduction effects, the minimum Kolmogorov length scale estimated by such a measurement and application of Eq. 6.1 is given in table 6.2 for a range of wire lengths. Thus, if one can get an accurate estimate of the viscous length scale, an accurate estimate of minimum Kolmogorov length scale η_{min} can be potentially obtained in the near-wall region.

Table 6.2 Estimate of minimum Kolmogorov length scale expressed as a fraction of the true value calculated using Eq. 6.1, the stream-wise velocity is assumed to be measured using a hot-wire anemometer at $y^+ = 8$ and the wall-normal derivative is calculated using the second-order central difference scheme

l^+	$\tilde{\eta}_{min}^m / \eta_{min}$
4	1.035
8	1.040
12	1.047
16	1.056
20	1.066

6.2 2C-2D Velocity Fields

For 2C-2D and 3C-2D velocity fields, the net effect of spatial filtering and limited dimensionality is presented for select spatial resolutions typical to PIV measurements and are given in table 6.3.

Profiles of normalised dissipation ($r_{\tilde{\epsilon}}^m$) and normalised Kolmogorov length scale ($r_{\tilde{\eta}}^m$) for the different models discussed in Chapter 5 is presented in Fig. 6.2-Fig. 6.5 for various sizes of the measurement volume.

Due to underestimation of the turbulent dissipation rate due to spatial filtering, the models which overestimate the dissipation and underestimate the Kolmogorov length scale in the unfiltered fields (viz. local axisymmetry and weak local isotropy models) counter the effect of spatial filtering and seemingly perform better near the wall as compared to the Blend formulation. The near wall values of $r_{\tilde{\eta}}^m = \tilde{\eta}^m / \eta$ show that even with the use of models, the

Table 6.3 Interrogation window/spatial filter sizes and grid spacing of the velocity fields used to evaluate net error in the turbulent dissipation rate due to limited dimensionality and spatial filtering in experimental measurements using PIV

f_x^+, f_y^+, f_z^+	$\Delta_x^+, \Delta_y^+, \Delta_z^+$	$F^+ = \sqrt[3]{f_x^+ \cdot f_y^+ \cdot f_z^+}$
8, 8, 8	8, 4, 4	8
16, 8, 20	8, 4, 10	14
16, 16, 12	8, 8, 6	15
24, 24, 8	12, 12, 4	17
16, 24, 20	8, 12, 10	20
24, 24, 20	12, 12, 10	23
32, 24, 16	16, 12, 8	23

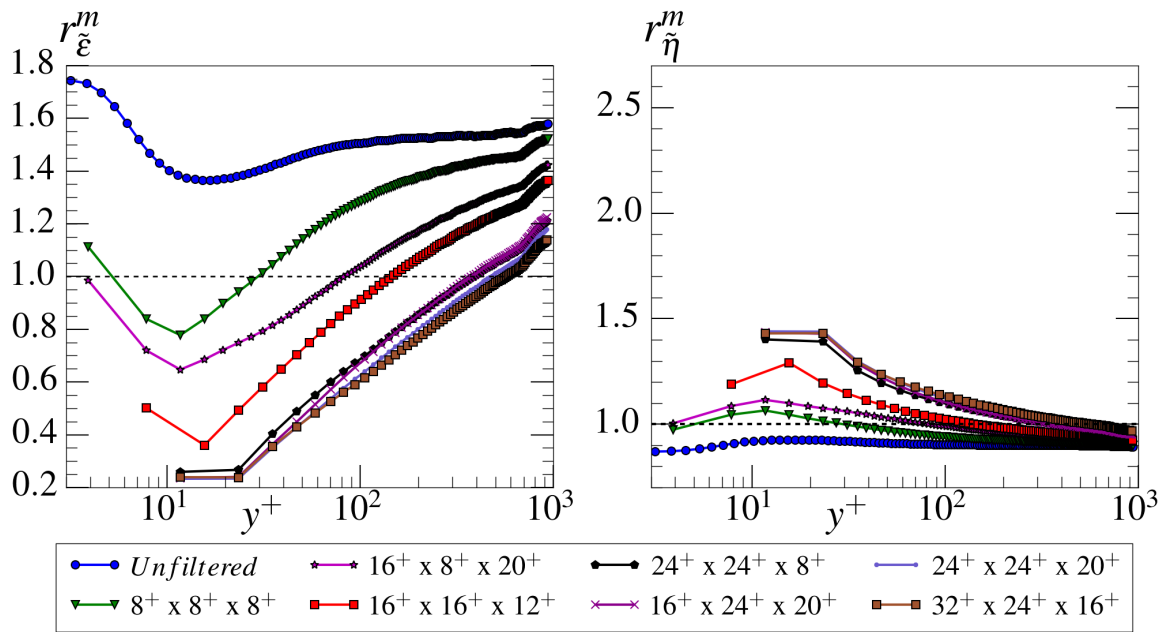


Fig. 6.2 Profiles of the normalised turbulent dissipation rate (r_{ϵ}^m) and normalised Kolmogorov length scale (r_{η}^m) for various measurement volume sizes calculated using 2C-2D velocity field Local axisymmetry- x formulation for various measurement volume sizes

error in Kolmogorov length scale is more sensitive to wall-normal filter size. The reduction in accuracy of the Kolmogorov length due to increasing the stream-wise and span-wise filter sizes is small at small wall-normal filter sizes, thus the wall-normal filter size should be restricted to small values in order to minimize the error in Kolmogorov length scale.

Table 6.4 presents the consolidated results of net error in turbulent dissipation rate for 2C-2D velocity fields. The values of normalised minimum Kolmogorov length scale ($\tilde{\eta}_{min}^m/\eta_{min}$)

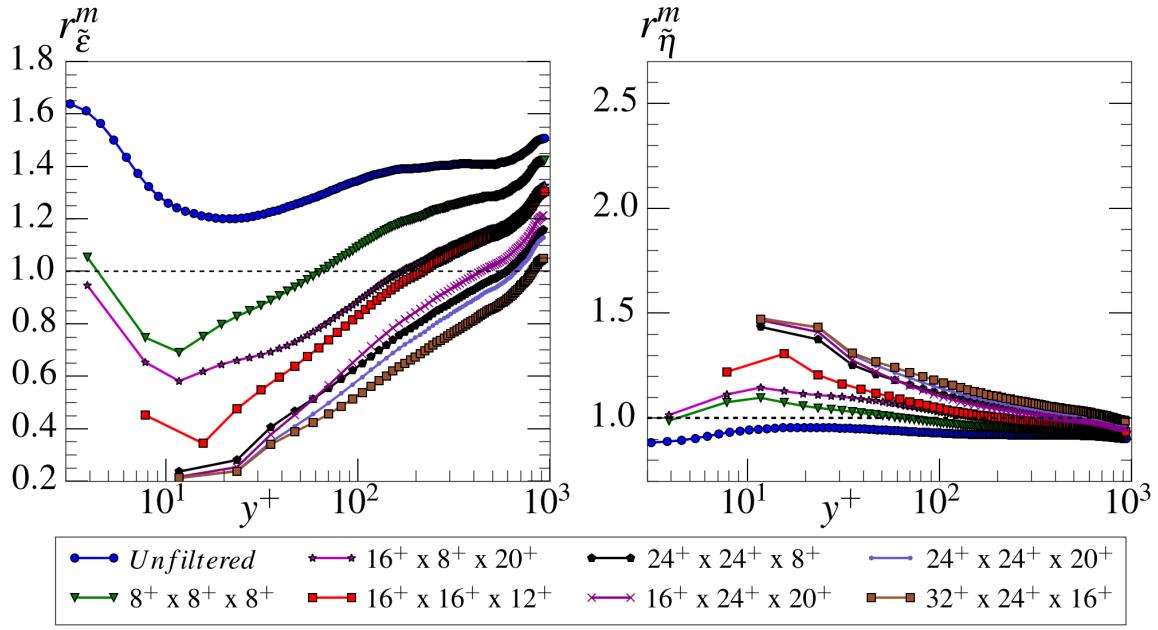


Fig. 6.3 Profiles of the normalised turbulent dissipation rate ($r_{\tilde{\epsilon}}^m$) and normalised Kolmogorov length scale ($r_{\tilde{\eta}}^m$) for various measurement volume sizes calculated using 2C-2D velocity field Local axisymmetry-y formulation for various measurement volume sizes

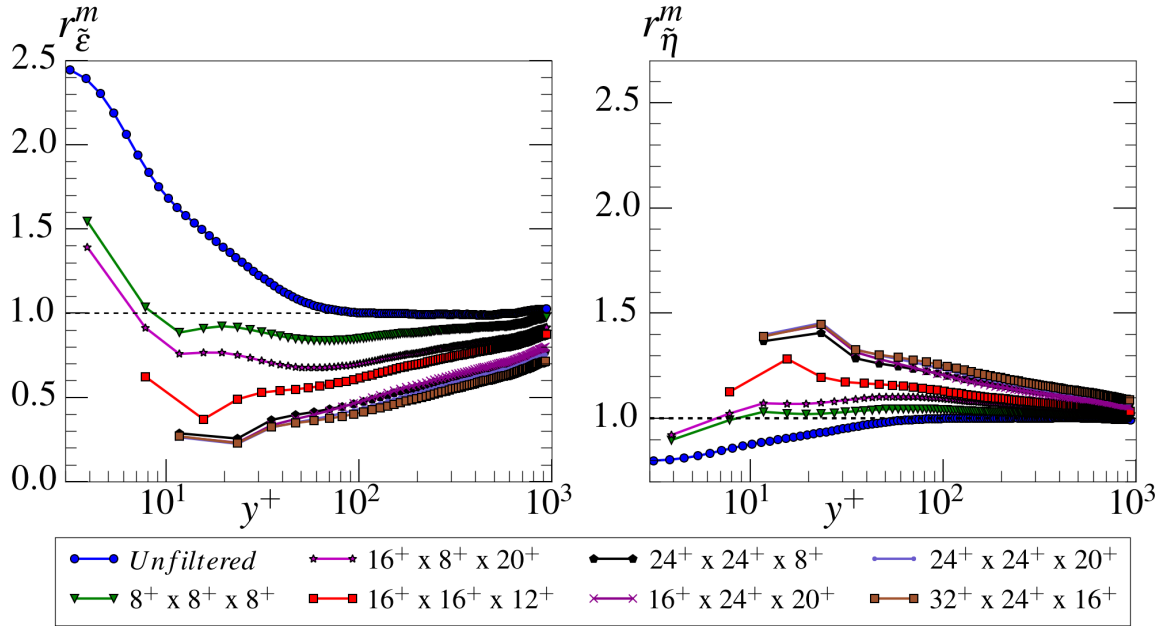


Fig. 6.4 Profiles of the normalised turbulent dissipation rate ($r_{\tilde{\epsilon}}^m$) and normalised Kolmogorov length scale ($r_{\tilde{\eta}}^m$) for various measurement volume sizes calculated using 2C-2D velocity field Weak local isotropy formulation for various measurement volume sizes

and the integral ratio ($\tilde{\beta}_m$) as calculated using different models are presented; the corresponding values for 3C-3D fields have been included for reference.

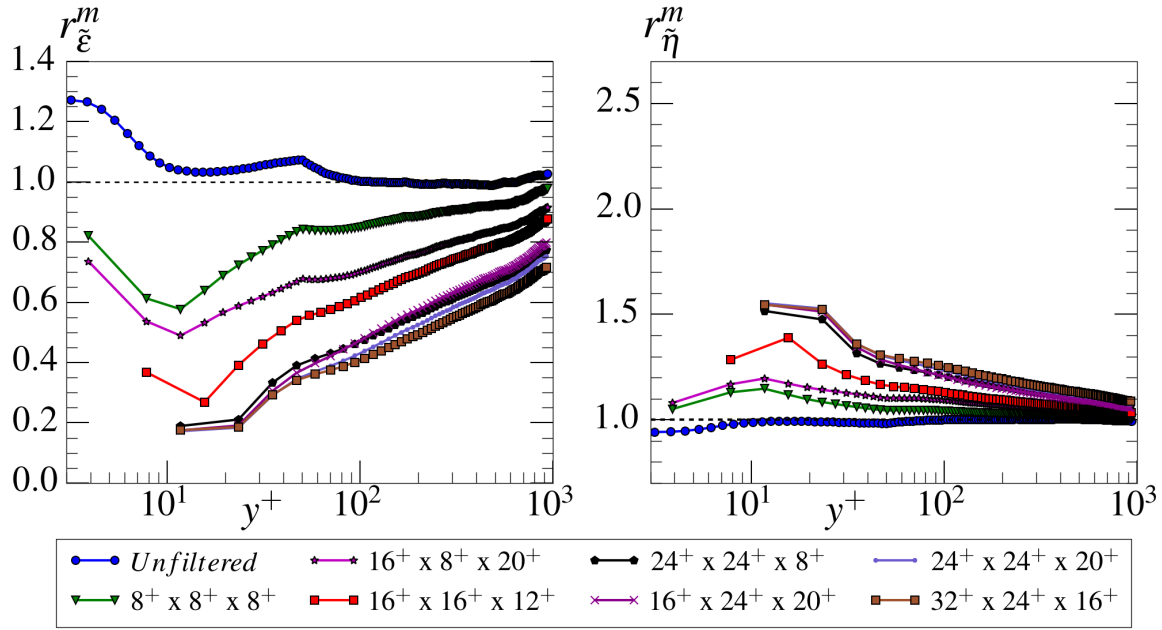


Fig. 6.5 Profiles of the normalised turbulent dissipation rate (r_{ϵ}^m) and normalised Kolmogorov length scale (r_{η}^m) for various measurement volume sizes calculated using 2C-2D velocity field Blend formulation for various measurement volume sizes

Table 6.4 Consolidated results of 2C-2D velocity field formulations of various models: LA-x, LA-y: Local Axisymmetry about x, Local Axisymmetry about y; WLI : Weak Local Isotropy; Bl : Blend

f_x^+, f_y^+, f_z^+	$\tilde{\beta}_m$					$\tilde{\eta}_{min}^m / \eta_{min}$				
	3C-3D	LA-x	LA-y	WLI	Bl	3C-3D	LA-x	LA-y	WLI	Bl
8,8,8	0.799	1.167	1.020	0.916	0.807	1.100	0.974	0.987	0.897	1.051
16,8,20	0.634	0.976	0.856	0.780	0.684	1.142	1.004	1.014	0.921	1.080
16,16,12	0.583	0.822	0.759	0.608	0.567	1.297	1.189	1.220	1.126	1.284
24,24,8	0.502	0.642	0.604	0.461	0.443	1.419	1.402	1.435	1.367	1.516
16,24,20	0.446	0.626	0.619	0.457	0.441	1.523	1.435	1.467	1.393	1.547
24,24,20	0.420	0.593	0.558	0.427	0.410	1.527	1.440	1.476	1.396	1.553
32,24,16	0.420	0.578	0.516	0.411	0.394	1.495	1.430	1.471	1.389	1.545

A comparison of values of integral ratio ($\tilde{\beta}_m$) for various formulations with the 3C-3D velocity field values show that the performance of models is dependent on the interrogation window size. The weak local isotropy and blend formulations underestimate the minimum Kolmogorov length scale at small interrogation window sizes as compared to the corresponding 3C-3D values while overestimating it at larger sizes. The use of models on spatially filtered fields thus introduces an uncertainty in the turbulent dissipation rate as the use of

models cause a change in magnitude and sign of the error with the filter size. The error in dissipation and Kolmogorov length scale due to limited dimensionality increases with spatial filtering, thus increasing the net error.

6.3 3C-2D Velocity Fields

The plots of normalised dissipation and Kolmogorov length scale calculated using the x - y plane, 3C-2D formulations of different models are presented in Fig. 6.6-Fig. 6.9 for various filter sizes, while the corresponding plots for y - z plane are presented in Fig 6.10-Fig 6.12. As compared to the corresponding 2C-2D formulations, the errors introduced by the 3C-2D formulations are larger atleast in the near wall region. The larger near wall error of 3C-2D formulations can be attributed to the fact that 3C-2D formulations provide a more accurate estimate of turbulent dissipation rate, indicated by the values for unfiltered cases, the overestimation of dissipation in the near-wall region by the 2C-2D formulations counters the underestimation of dissipation due to spatial filtering, thus leading to smaller near-wall error.

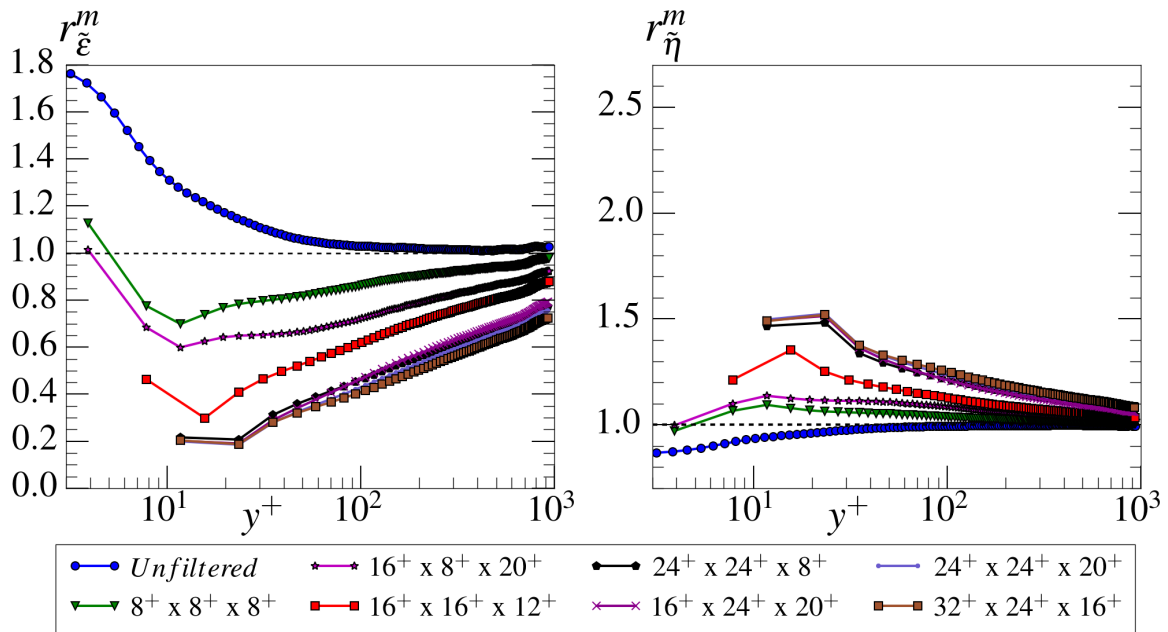


Fig. 6.6 Profiles of the normalised turbulent dissipation rate ($r_{\tilde{\epsilon}}^m$) and normalised Kolmogorov length scale ($r_{\tilde{\eta}}^m$) for various measurement volume sizes calculated using x - y plane Local axisymmetry- x formulation: 3C-2D velocity fields

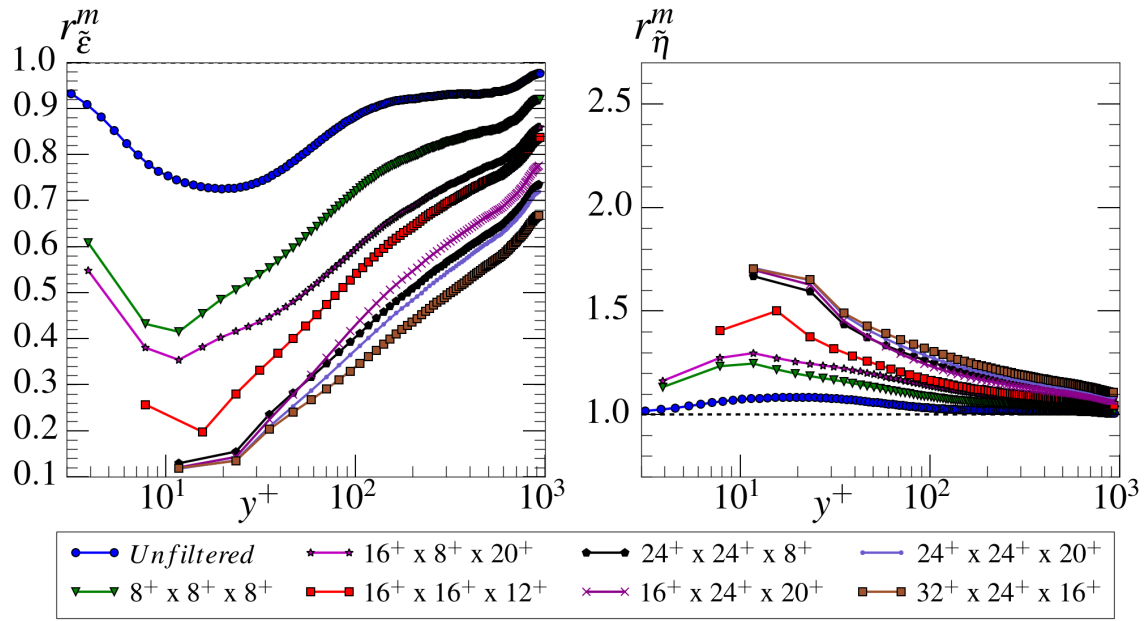


Fig. 6.7 Profiles of the normalised turbulent dissipation rate ($r_{\tilde{\epsilon}}^m$) and normalised Kolmogorov length scale ($r_{\tilde{\eta}}^m$) for various measurement volume sizes calculated using x - y plane Local axisymmetry- y formulation: 3C-2D velocity fields

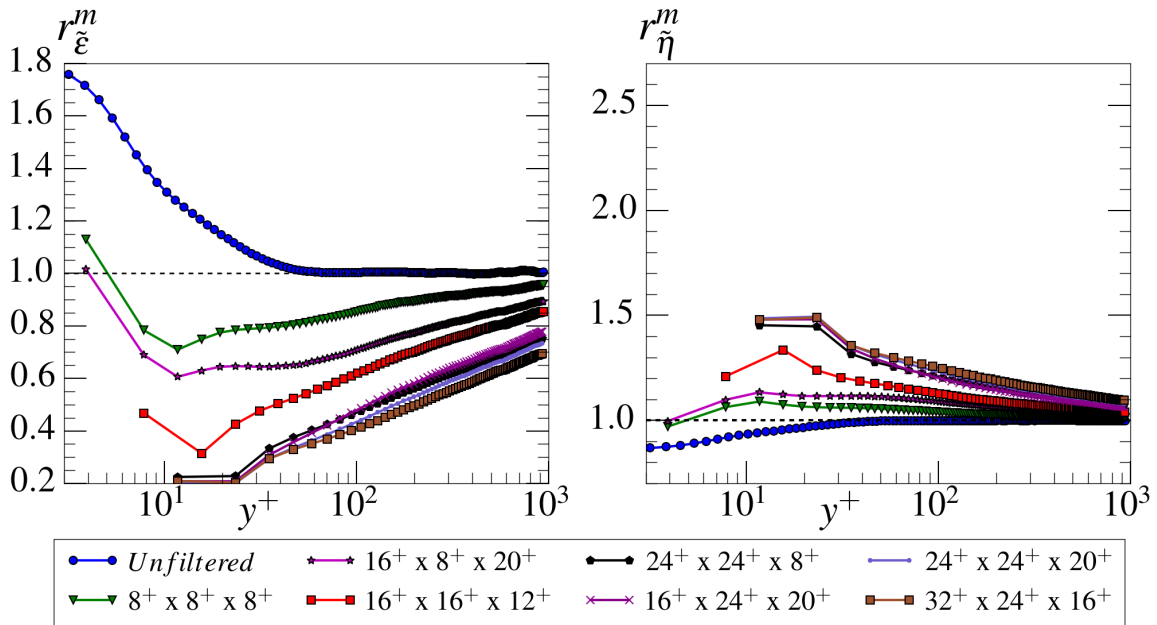


Fig. 6.8 Profiles of the normalised turbulent dissipation rate ($r_{\tilde{\epsilon}}^m$) and normalised Kolmogorov length scale ($r_{\tilde{\eta}}^m$) for various measurement volume sizes calculated using x - y plane Weak local isotropy formulation: 3C-2D velocity fields

The y - z plane 3C-2D formulations (table 6.6) consistently overestimate the minimum Kolmogorov length scale and underestimate the total dissipation in the channel as compared to the 3C-3D values, resulting in a reduced net error in both the quantities. Additionally,

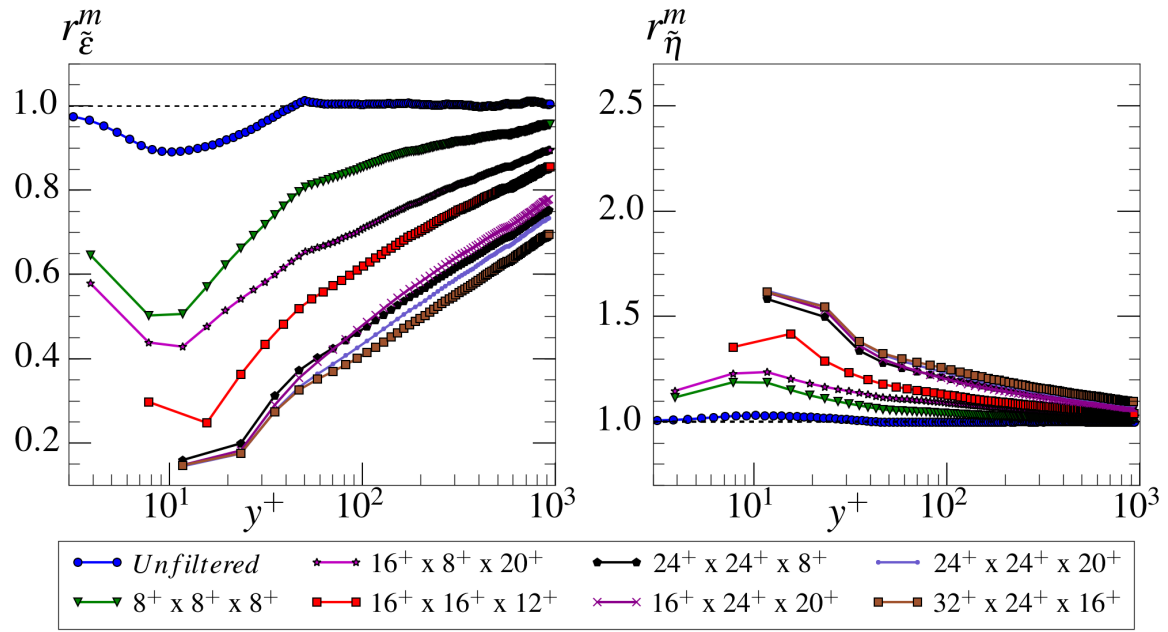


Fig. 6.9 Profiles of the normalised turbulent dissipation rate ($r_{\tilde{\epsilon}}^m$) and normalised Kolmogorov length scale ($r_{\tilde{\eta}}^m$) for various measurement volume sizes calculated using x - y plane Blend formulation: 3C-2D velocity fields

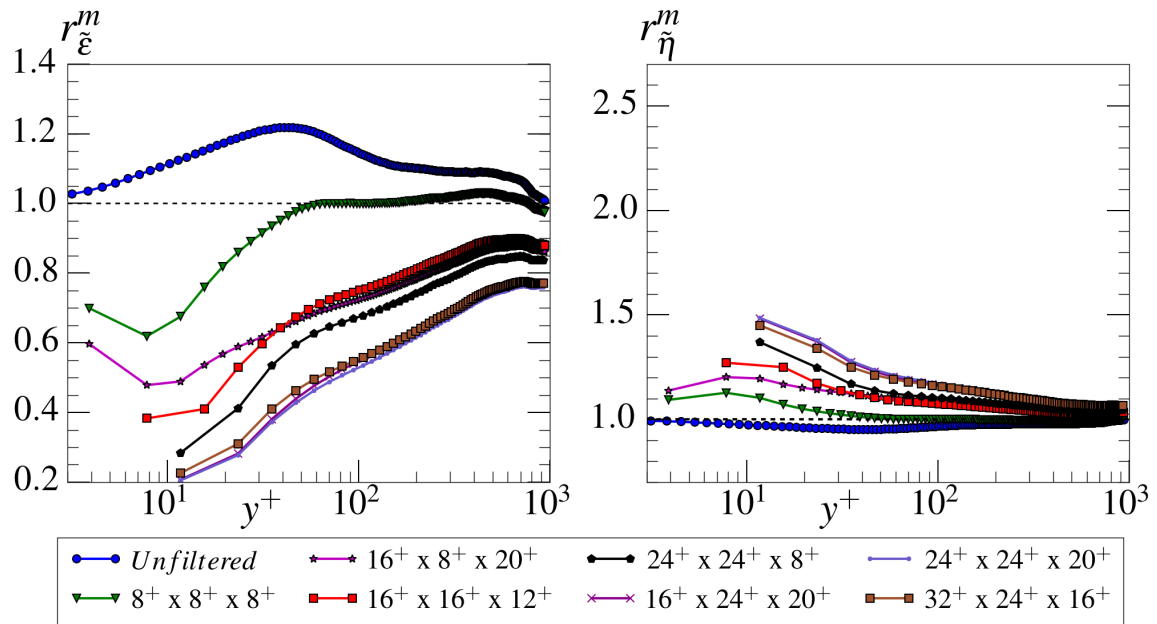


Fig. 6.10 Profiles of the normalised turbulent dissipation rate ($r_{\tilde{\epsilon}}^m$) and normalised Kolmogorov length scale ($r_{\tilde{\eta}}^m$) for various measurement volume sizes calculated using y - z plane Local axisymmetry- y formulation: 3C-2D velocity fields

error in dissipation calculated using the y - z plane formulations show reduced sensitivity to filter size as compared to the error in dissipation calculated using the corresponding x - y plane formulation.

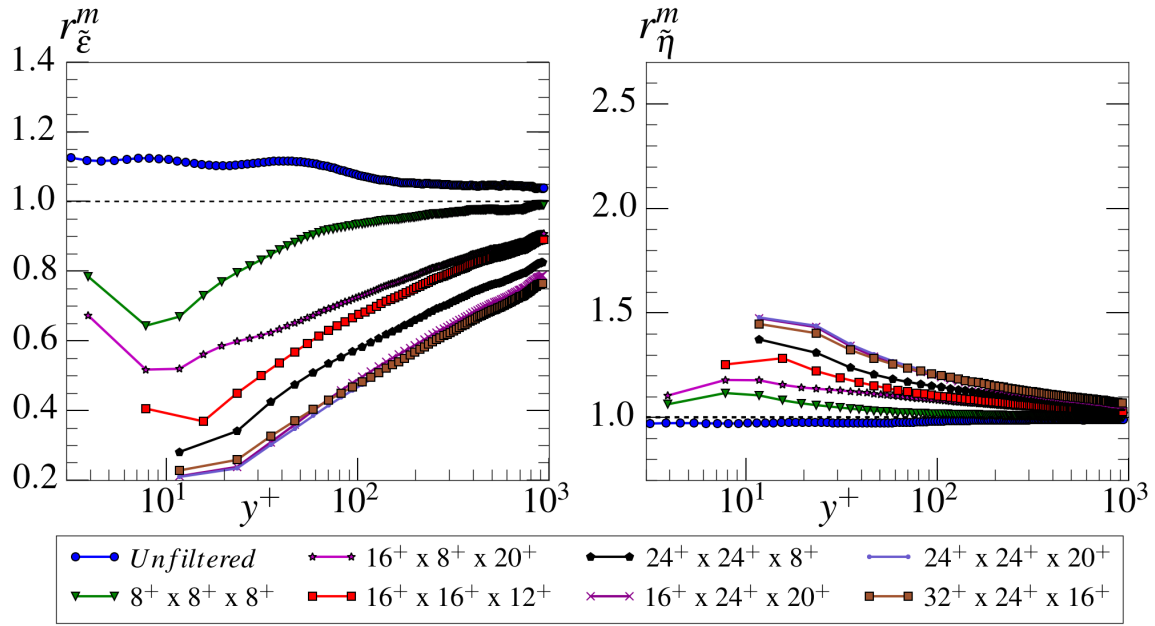


Fig. 6.11 Profiles of the normalised turbulent dissipation rate ($r_{\tilde{\epsilon}}^m$) and normalised Kolmogorov length scale ($r_{\tilde{\eta}}^m$) for various measurement volume sizes calculated using y-z plane Weak local isotropy formulation: 3C-2D velocity fields

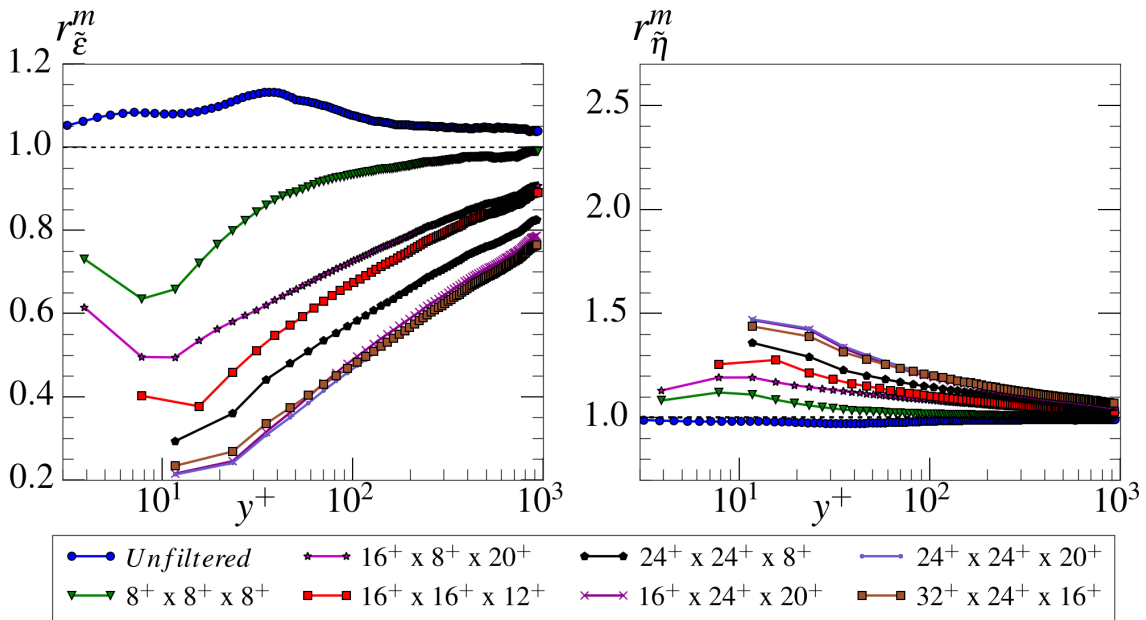


Fig. 6.12 Profiles of the normalised turbulent dissipation rate ($r_{\tilde{\epsilon}}^m$) and normalised Kolmogorov length scale ($r_{\tilde{\eta}}^m$) for various measurement volume sizes calculated using y-z plane Blend formulation: 3C-2D velocity fields

Table 6.5 Consolidated results for x - y plane 3C-2D velocity field formulations of various models

f_x^+, f_y^+, f_z^+	$\tilde{\beta}_m$					$\tilde{\eta}_{min}^m/\eta_{min}$				
	3C-3D	LA- x	LA- y	WLI	BI	3C-3D	LA- x	LA- y	WLI	BI
8,8,8	0.799	0.851	0.652	0.847	0.775	1.100	0.971	1.132	0.970	1.116
16,8,20	0.634	0.732	0.557	0.723	0.660	1.142	0.997	1.162	0.996	1.147
16,16,12	0.583	0.580	0.483	0.582	0.556	1.297	1.212	1.405	1.209	1.354
24,24,8	0.502	0.438	0.377	0.447	0.435	1.419	1.467	1.668	1.453	1.583
16,24,20	0.446	0.436	0.392	0.448	0.437	1.523	1.493	1.699	1.481	1.614
24,24,20	0.420	0.411	0.354	0.416	0.405	1.527	1.497	1.708	1.486	1.622
32,24,16	0.420	0.397	0.327	0.398	0.386	1.495	1.490	1.703	1.479	1.615

Table 6.6 Consolidated results for y - z plane 3C-2D velocity field formulations of various models

f_x^+, f_y^+, f_z^+	$\tilde{\beta}_m$				$\tilde{\eta}_{min}^m/\eta_{min}$			
	3C-3D	LA- y	WLI	BI	3C-3D	LA- y	WLI	BI
8,8,8	0.799	0.919	0.870	0.875	1.100	1.094	1.063	1.082
16,8,20	0.634	0.686	0.694	0.685	1.142	1.138	1.104	1.130
16,16,12	0.583	0.685	0.620	0.630	1.297	1.271	1.253	1.256
24,24,8	0.502	0.623	0.542	0.557	1.419	1.370	1.374	1.357
16,24,20	0.446	0.506	0.457	0.464	1.523	1.482	1.475	1.467
24,24,20	0.420	0.493	0.442	0.448	1.527	1.486	1.478	1.471
32,24,16	0.420	0.518	0.459	0.463	1.495	1.451	1.447	1.437

Chapter 7

Discussion and Conclusions

Most flows of importance encountered in industry and nature are in the high Reynolds number regime. As a result, a substantial proportion of turbulent flow research is aimed at understanding the behaviour of turbulence in the high Reynolds number regime. We have seen in Chapter 1 that the turbulent dissipation rate is determined in high Reynolds number flows by employing experimental measurements. The accurate determination of the turbulent dissipation rate from experimental measurements is a challenging task due to the inherent spatial filtering and the limited dimensionality of the velocity fields provided by them. Any experimental measurement technique inherently involves spatial filtering of the smallest scales in the flow when the finite size of the measurement volume is much larger than the smallest length scales in the flow (of the order of Kolmogorov length scale), which is often the case for high Reynolds number flows where the Kolmogorov length scales are much smaller than the size of measurement volume for most laboratory scale experiments. Due to the spatial filtering of the length scales smaller than the measurement volume, in absence of measurement noise, the dissipation calculated from experimental measurements is underestimated and the corresponding Kolmogorov length scale is overestimated. The inability of most experimental measurement techniques to provide all the components of the velocity gradient tensor makes the application of simplifying assumptions necessary, most of which are often not suitable for every flow configuration. Thus when dissipation and the corresponding quantities are determined from experiments, they have an inherent bias error. In absence of an estimate of this bias error, experimentalists cannot determine the appropriate size of measurement volume needed to maintain the error levels within certain limits.

As discussed in Chapter 1, the existing research on determining the error in turbulent dissipation rate and Kolmogorov length scale is limited to free-shear flows. The anisotropy of near-wall turbulence makes the dynamics of turbulence in wall-bounded flows different from free-shear flows, especially in the near-wall region; the extension of existing results based on free-shear flows to wall-bounded flows is not straightforward. An estimate of the bias errors in dissipation and Kolmogorov length scale, as well as the validation of the capability of existing models to determine dissipation in wall-bounded turbulent flows was needed.

The present analysis has revealed that the spatial filtering due to the finite size of the measurement volume results in a greater underestimation of dissipation close to the wall as compared to the region away from it. The minimum Kolmogorov length scale in the flow can be overestimated by as much as 50% of the true value for moderate sizes of measurement volume ($< 12^+$ units). Unsurprisingly, the gradients of velocity components along the direction of filtering are most affected by spatial filtering, as a result, the error in turbulent dissipation rate due to spatial filtering depends on the size and orientation of the measurement volume. A substantial proportion of dissipation in wall-bounded flows is found to be anisotropic (Chapter 3), the largest contribution to dissipation in the near wall region coming from wall-normal derivatives of fluctuating velocity components. The anisotropic nature of dissipation, combined with the effect of spatial filtering on various velocity components, makes the error in dissipation due to spatial filtering a stronger function of the size of the measurement volume along the wall-normal direction as compared to its size along the other directions. An increase in the filter size in the wall-normal direction beyond $y^+ \approx 12$, is found to result in a large error in the minimum Kolmogorov length scale ($\sim 30\%$) and the total turbulent dissipation rate in the channel ($\sim 60\%$). The underestimation of dissipation due to spatial filtering along the span-wise and wall-normal directions is largest at the wall and decreases with the wall-normal distance while peaking in the log-layer for stream-wise filtering (Fig. 4.19, Chapter 4).

The truncation error in the finite difference schemes used to calculate the derivatives is found to be another major source of error in the near wall region which further increases the underestimation of the turbulent dissipation rate. Its fractional contribution to the total error in dissipation is found to increase with the size of measurement volume (if a constant window

overlap is maintained), and in the near wall region, this contribution can be as large as 50% of the total error for large filter sizes in the wall-normal direction. A reduction in truncation error warrants the reduction of the spacing of velocity vectors in experiments by either reducing the size of the measurement volume or increasing the fractional overlap between adjacent measurement volumes, the latter reduces the statistical independence of each measurement.

Various existing models that are employed to estimate the turbulent dissipation rate when dimensionally limited data from experiments is available, overestimate the dissipation in the near-wall region in most cases. A new model to estimate dissipation when only 2C-2D and 3C-2D data is available has been developed (Section 5.2). This model is based on the assumption of local homogeneity and is demonstrated to be an improvement over the existing models in accurately estimating the dissipation in the entire channel for unfiltered velocity fields.

The investigation into the total error in turbulent dissipation rate due to spatial filtering and limited dimensionality in Chapter 6 revealed that spatial filtering is a major source of error in both the turbulent dissipation rate and the Kolmogorov length scale. Given the fact that the accuracy of various models is dependent on the correctness of derivative equivalence relations which are the basis of the models, and the anisotropic nature of error introduced into the velocity gradient tensor due to spatial filtering skews the derivative equivalence relations; the accuracy of the dissipation calculated by the models as compared to the 3C-3D value, varies with the size of the measurement volume along each direction. Apriori tests on the accuracy of models at a different Reynolds number and measurement volume size may not provide an accurate estimate of the error introduced by these models. In general, the models which locally overestimate the turbulent dissipation rate act to reduce the local underestimation of dissipation due to spatial filtering, although this is usually not enough to eliminate the entire underestimation of dissipation due to spatial filtering.

Challenges in the determination of dissipation from high Reynolds number flow measurements

The turbulent dissipation rate (in wall-units) and the corresponding integral fraction (χ , Eq. 2.3) calculated from DNS of the channel flows for friction Reynolds number in the range $Re_\tau \approx 180 - 5200$ (Lee and Moser, 2015) are presented in Fig. 7.1. The profiles of dissipation for various Reynolds numbers indicate that the dissipation in the near-wall region is a strong function of Reynolds number at low Reynolds numbers, indicated by the large jump in dissipation ($\sim 50\%$) at the wall upon increase in friction Reynolds number from $Re_\tau = 180$ to $Re_\tau = 950$ as compared to corresponding value ($\sim 16\%$) when Reynolds number increases by a similar factor from $Re_\tau = 950$ to $Re_\tau = 5200$. An increase in Reynolds number leads to an increase in the wall-normal gradient of dissipation, especially in the near-wall region. As seen in Chapter 4, the large wall-normal gradient of dissipation is responsible for large near wall error due to spatial filtering in the wall-normal direction. Thus, an increase in the wall-normal gradient of dissipation due to an increase in the friction Reynolds number will lead to a rise in the error in dissipation due to spatial filtering in wall-normal direction for the same filter size in wall units.

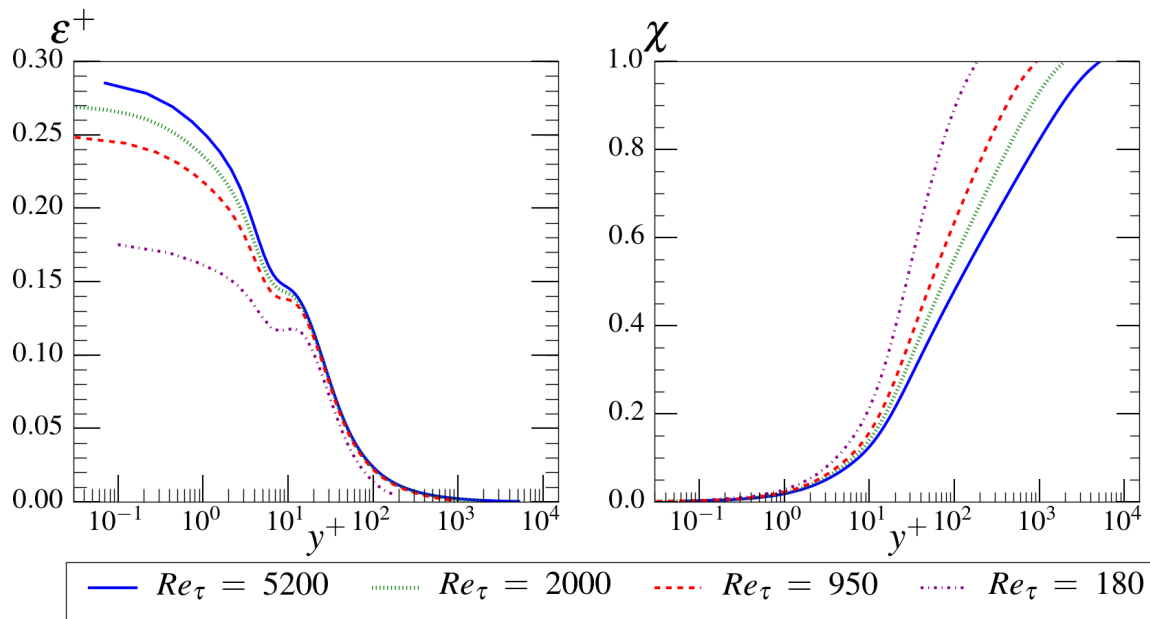


Fig. 7.1 Turbulent dissipation rate in wall units and integral fraction (χ) for a range of Reynolds number obtained from channel flow DNS of Lee and Moser (2015)

An estimate of the effect of increased near wall error in dissipation on the total error in dissipation can be obtained for different Reynolds numbers by observing the plots of integral fraction (χ) for various Reynolds numbers from Fig. 7.1; selected values of χ are presented in table 7.1. The profiles of χ show that the fractional contribution of the near-wall dissipation ($y^+ < 50$) to the total dissipation in the channel decreases with increasing Reynolds number.

Table 7.1 Distribution of dissipation in channel flow for various Reynolds number

Re_τ	$\chi@y^+ = 50$	$y^+@ \chi = 0.9$	$y^+/h^+@ \chi = 0.9$
180	0.71	104	0.58
950	0.49	415	0.44
2000	0.42	800	0.40
5200	0.39	1800	0.35

The values in table 7.1 indicate that with an increase in Reynolds number, the contribution of dissipation in the viscous region ($y^+ \leq 50$) to the total dissipation does not reduce drastically at large Reynolds numbers. The distance from the wall (in viscous units) up to which 90% of turbulent kinetic energy is dissipated, increases with Reynolds number, although it decreases in terms of the fraction of the channel height. Hence, if the physical size of the channel is not changed, an increase in Reynolds number would result in most of the dissipation in the channel occurring closer to the wall. Although the trend of increase in error in turbulent dissipation rate with an increase in size of measurement volume is expected to remain the same with increasing Reynolds number, the redistribution of dissipation along the wall-normal direction might change the distribution and the magnitude of the error due to spatial filtering in the turbulent dissipation rate and Kolmogorov length scale obtained from experimental measurements at different Reynolds number. We have seen in Chapter 6 that the accuracy of dissipation estimated by the models is dependent on the degree of spatial filtering, hence it is expected to decrease with increasing Reynolds number, thus increasing the overall error is the turbulent dissipation rate due to both spatial filtering and limited dimensionality.

Conclusions

The turbulent dissipation rate and Kolmogorov length scale determined from experimental measurements inherently involve a bias error which is introduced due to the finite size of the measurement volume and limited dimensionality of the velocity fields. An estimate of the magnitude and the nature of this bias error in wall-bounded flows was needed, which was the aim of the current research work.

The error introduced in dissipation and the corresponding derived quantities due to spatial filtering is dependent on the size and orientation of the measurement volume. The accuracy of these quantities is most affected by the size of the measurement volume in the wall-normal direction. There is a large jump in the error when the wall-normal size of measurement volume is increased beyond $y^+ \approx 12$ units and it is advised to limit the wall-normal size of the measurement volume within this value. The spatial filtering in the wall-normal direction is due to both, the filtering of the small length scales of the flow and the averaging of the anisotropic part of the dissipation rate tensor, hence any method that estimates the effect of spatial filtering on dissipation should take this fact into consideration. Any other wall-bounded flow which has similar anisotropy along other (stream-wise and span-wise) directions, will exhibit a similar behaviour of error and this anisotropy of the velocity gradient tensor (hence the dissipation rate tensor) will differ from that presented in this thesis.

The various existing models available in the literature, which are used when dimensionally limited data is available, provide an inaccurate estimate of dissipation and Kolmogorov length scale in the near-wall region, often overestimating the turbulent dissipation rate. The maximum error introduced in dissipation due to the use of various existing models alone ranges from $\approx 80\%$ to $\approx 150\%$ of the true value. A new model has been developed which provides an improved estimate of dissipation, the maximum error in dissipation estimated by this model for the unfiltered velocity fields is limited to $\approx 10\%$ of the true value, while the error in total dissipation in the entire channel is within 9% of the true value.

The local isotropy model, which used when 1C-1D data is available from measurement techniques like hot-wire anemometry, presents a poor estimate of the minimum Kolmogorov length scale in the flow (at the wall), over-predicting the value by 120% for wire length of

20^+ units in the absence of measurement noise. A modification of the local homogeneity assumption based model, combined with the measurement of wall-normal gradient of stream-wise velocity close to the wall (at $y^+ = 4$) and span-wise orientation of the wire (which results in spatial filtering only in the span-wise direction) can estimate the minimum Kolmogorov length scale within 7% of the true value for the same wire length, providing a quick estimation of the smallest length scales in a flow for 1C-1D velocity measurements. The underestimation of dissipation due to spatial filtering is reduced when using models like local axisymmetry and weak-local isotropy which overestimate the dissipation in the near-wall region for the unfiltered case for unfiltered 2C-2D and 3C-2D velocity fields. The degree of reduction of underestimation of dissipation due to spatial filtering, due to the use of these models depends on the size of measurement volume along each direction. The overestimate of minimum Kolmogorov length scale when calculated using the new blend formulation can be maintained within 20% by limiting the wall-normal filter size below 16^+ units.

An analysis of error in dissipation and Kolmogorov length scale for various sizes of measurement volumes and different models suggests that, for current Reynolds number, a 2C-2D PIV measurement obtained by restricting the wall-normal measurement volume size to $f_y^+ < 12$ and application of the newly-derived blend formulation would lead to an error within 10% of the true value in Kolmogorov length scale and within 30% of the true value in the total dissipation in the channel. The corresponding values for the 3C-2D formulation are 35% and 15% while they are 20% and 12% respectively, for the 3C-3D velocity fields.

With an increase in Reynolds number, the error due to spatial filtering is expected to increase due to increase in the near-wall gradients. Maintaining the error in dissipation due to spatial filtering within the same limits as low Reynolds number flow experiments is expected to become an increasingly challenging task with increasing Reynolds number. This fact must be taken into consideration when employing the guidelines from the current work for different Reynolds number and flow configurations.

Appendix A

Formulation of True Error in Dissipation due to Spatial Filtering

Ignoring the constant coefficients, each term in the equation for turbulent dissipation rate (Eq. 1.4) can be expressed in the form $(\partial u'_i / \partial x_j) (\partial u'_k / \partial x_l)$. If the spatial filter is denoted by the operator \mathcal{F} , the filtered fluctuating velocity components can be expressed as $\mathcal{F}(u'_i)$.

The calculation of spatial derivatives from the velocity field can be considered as application of the derivative filter (Foucaut and Stanislas, 2002). Let \mathcal{C} be the central derivative operator. The calculation of velocity gradient tensor of the filtered velocity field using the central derivative scheme can thus be represented by the successive application of the spatial filter \mathcal{F} and the central derivative filter \mathcal{C} on the unfiltered velocity field. The term $(\partial \tilde{u}'_i / \partial x_j) (\partial \tilde{u}'_k / \partial x_l)$ can then be expressed as in Eq. A.1.

$$\left(\frac{\partial \tilde{u}'_i}{\partial x_j} \right) \left(\frac{\partial \tilde{u}'_k}{\partial x_l} \right) = \mathcal{C} [\mathcal{F}(u'_i), \Delta \tilde{x}_j] \mathcal{C} [\mathcal{F}(u'_k), \Delta \tilde{x}_l] \quad (\text{A.1})$$

where $\Delta \tilde{x}_j$ is the grid spacing of the filtered velocity field along the direction x_j .

Since both the central derivative filter and spatial filter are linear operators, their order of application can be interchanged and was verified mathematically. Eq. A.1 thus becomes

$$\left(\frac{\partial \tilde{u}'_i}{\partial x_j} \right) \left(\frac{\partial \tilde{u}'_k}{\partial x_l} \right) = \mathcal{F} [\mathcal{C}(u'_i, \Delta x_j)] \mathcal{F} [\mathcal{C}(u'_k, \Delta x_l)] \quad (\text{A.2})$$

The central difference formula for calculation of derivatives can be expressed in the form given by Eq. A.3

$$\mathcal{C}(u'_i, \Delta x_j) = \frac{\partial u'_i}{\partial x_j} + \epsilon_t(u'_i, \Delta x_j) \quad (\text{A.3})$$

where ϵ_t is the operator denoting the truncation error associated with the truncation of the Taylor series expansion of velocity component u'_i along the direction x_j .

Combining Eq. A.2 and Eq. A.3 we get Eq. A.4

$$\left(\frac{\partial \tilde{u}'_i}{\partial x_j}\right) \left(\frac{\partial \tilde{u}'_k}{\partial x_l}\right) = \mathcal{F} \left[\frac{\partial u'_i}{\partial x_j} + \epsilon_t(u'_i, \Delta x_j) \right] \mathcal{F} \left[\frac{\partial u'_k}{\partial x_l} + \epsilon_t(u'_k, \Delta x_l) \right] \quad (\text{A.4})$$

Eq. A.5 is obtained by resolving the terms in brackets in Eq. A.4 by applying the additivity property of linear operators.

$$\left(\frac{\partial \tilde{u}'_i}{\partial x_j}\right) \left(\frac{\partial \tilde{u}'_k}{\partial x_l}\right) = \left\{ \mathcal{F} \left[\frac{\partial u'_i}{\partial x_j} \right] + \mathcal{F} [\epsilon_t(u'_i, \Delta x_j)] \right\} \left\{ \mathcal{F} \left[\frac{\partial u'_k}{\partial x_l} \right] + \mathcal{F} [\epsilon_t(u'_k, \Delta x_l)] \right\} \quad (\text{A.5})$$

Upon further simplification, we arrive at Eq. A.6.

$$\begin{aligned} \left(\frac{\partial \tilde{u}'_i}{\partial x_j}\right) \left(\frac{\partial \tilde{u}'_k}{\partial x_l}\right) &= \mathcal{F} \left(\frac{\partial u'_i}{\partial x_j} \right) \mathcal{F} \left(\frac{\partial u'_k}{\partial x_l} \right) + \mathcal{F} [\epsilon_t(u'_i, \Delta x_j)] \mathcal{F} \left(\frac{\partial u'_k}{\partial x_l} \right) \\ &+ \mathcal{F} \left(\frac{\partial u'_i}{\partial x_j} \right) \mathcal{F} [\epsilon_t(u'_k, \Delta x_l)] + \mathcal{F} [\epsilon_t(u'_i, \Delta x_j)] \mathcal{F} [\epsilon_t(u'_k, \Delta x_l)] \end{aligned} \quad (\text{A.6})$$

Thus we can see from Eq. A.6 that, truncation error of the finite difference scheme introduces a non-linear error in each term of dissipation equation, which is dependent on both, the spatial filtering operation and truncation error in the finite difference scheme. To simplify Eq. A.6, all the terms associated with truncation error are consolidated into a single term γ_{cd-nl} (Eq.A.7)

$$\begin{aligned} \gamma_{cd-nl} &= \mathcal{F} [\epsilon_t(u'_i, \Delta x_j)] \mathcal{F} \left(\frac{\partial u'_k}{\partial x_l} \right) + \mathcal{F} \left(\frac{\partial u'_i}{\partial x_j} \right) \mathcal{F} [\epsilon_t(u'_k, \Delta x_l)] \\ &+ \mathcal{F} [\epsilon_t(u'_i, \Delta x_j)] \mathcal{F} [\epsilon_t(u'_k, \Delta x_l)] \end{aligned} \quad (\text{A.7})$$

where γ_{cd-nl} is the error introduced purely due to truncation error in individual velocity gradients and $\gamma = 0$ when there is no truncation error associated with the gradient calculation.

Thus every term in Eq. 1.4 can be presented in the simplified form given by Eq. A.8

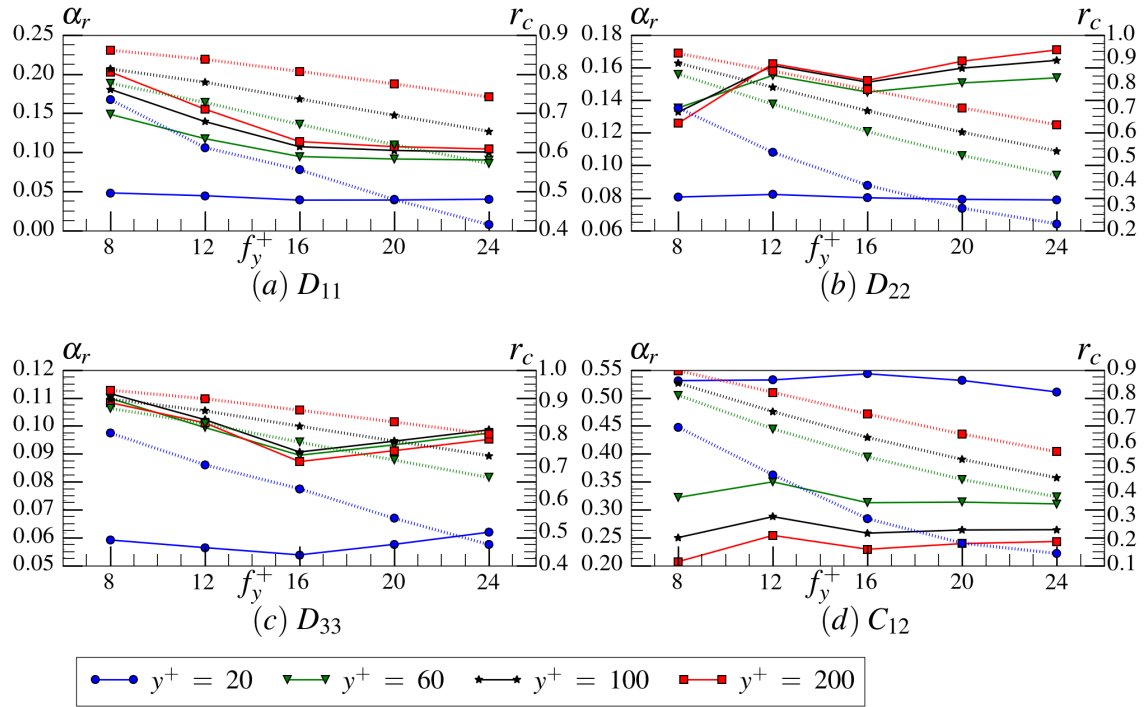
$$\left(\frac{\partial \tilde{u}'_i}{\partial x_j}\right) \left(\frac{\partial \tilde{u}'_k}{\partial x_l}\right) = \mathcal{F} \left(\frac{\partial u'_i}{\partial x_j}\right) \mathcal{F} \left(\frac{\partial u'_k}{\partial x_l}\right) + \gamma \quad (\text{A.8})$$

Appendix B

Results

B.1 Effect of Spatial Filtering: Contribution of error from various components

B.1.1 Effect of filter size in the wall-normal direction



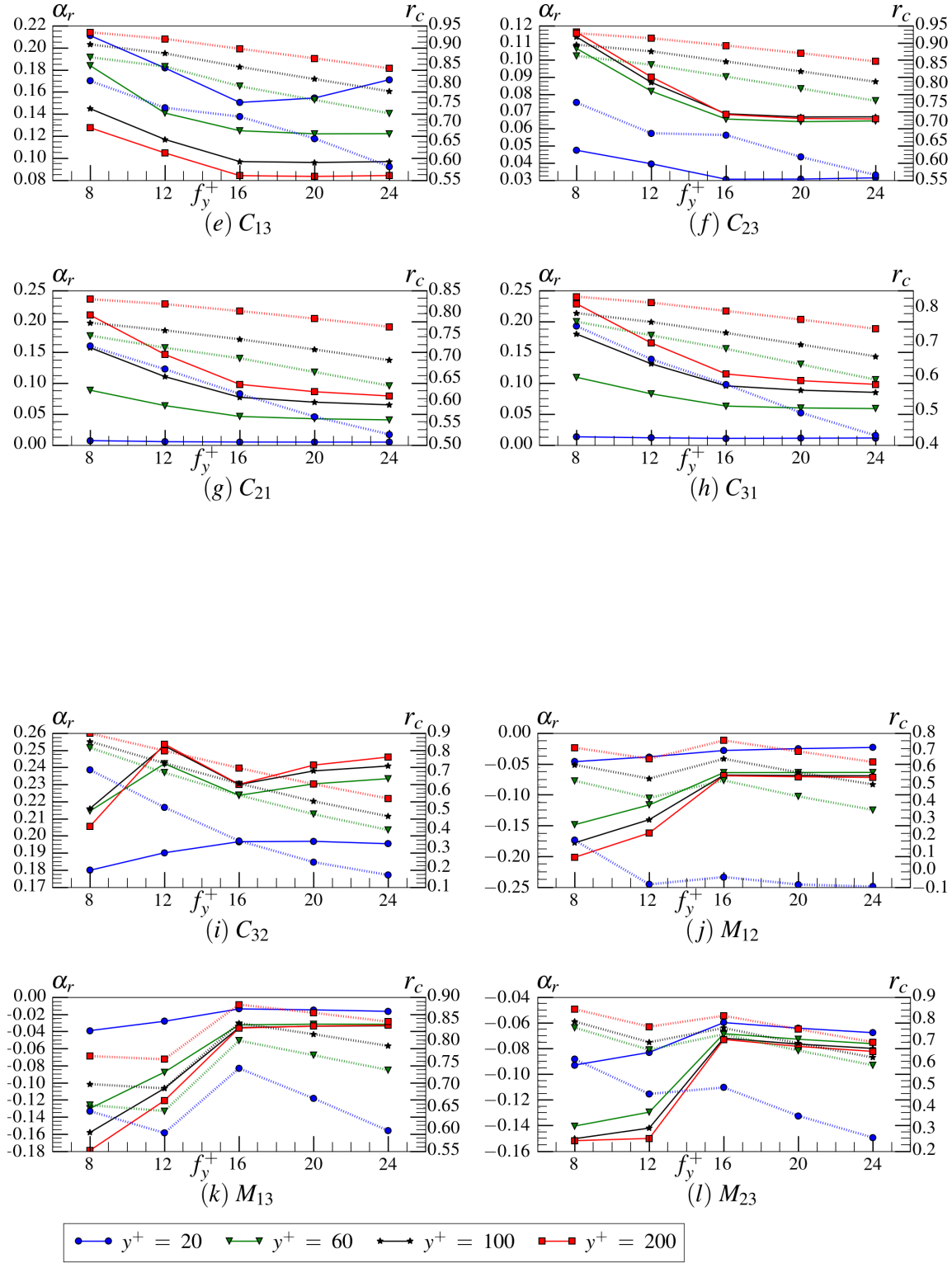
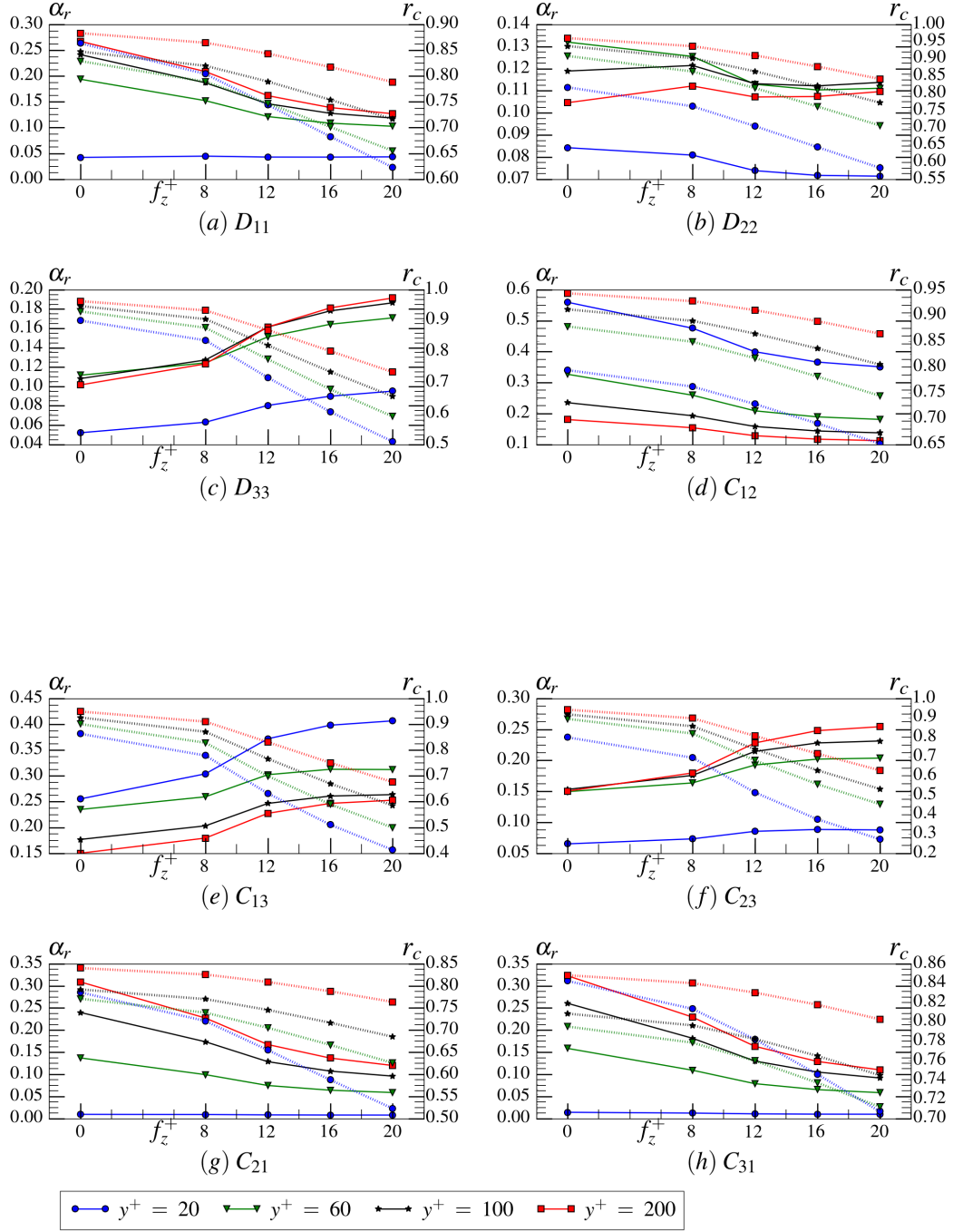


Fig. B.1 Effect of increasing the filter size in the wall-normal direction (f_y^+) on α_r (solid lines) and r_c (dashed)

B.1.2 Effect of filter size in the span-wise direction



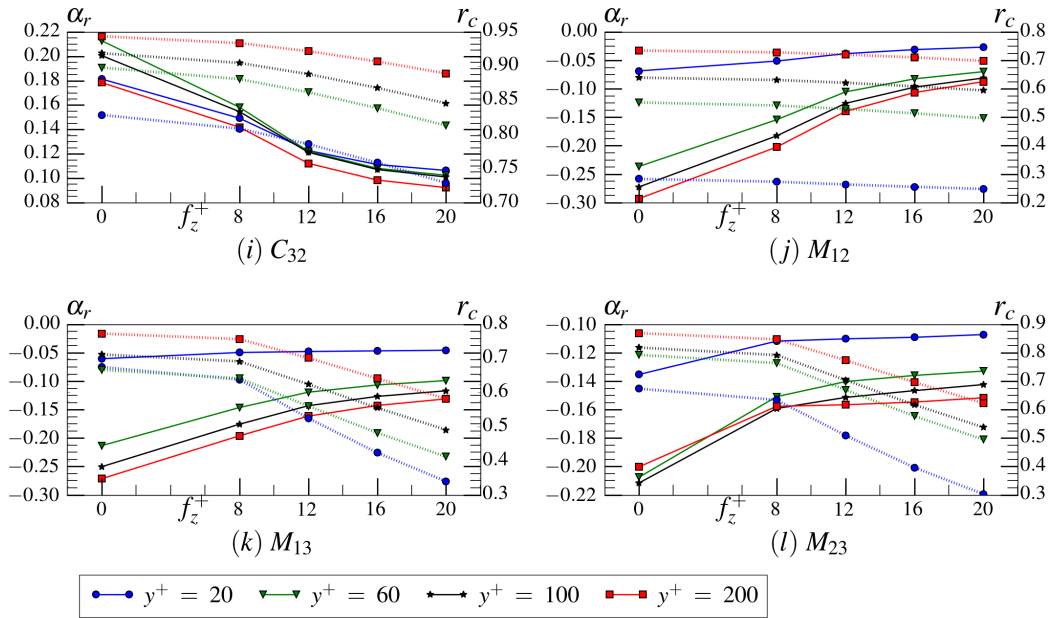
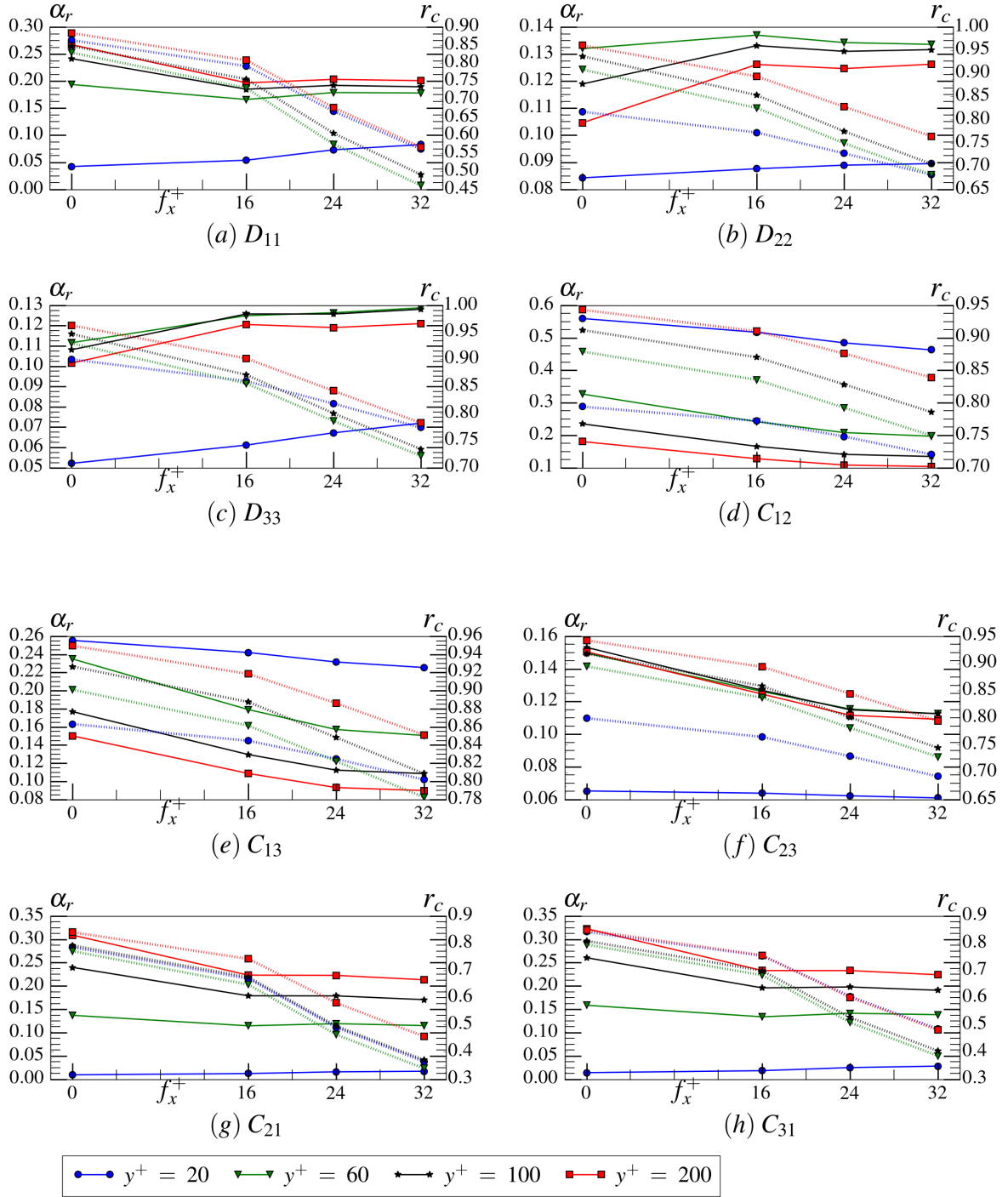


Fig. B.2 Effect of increasing the filter size in the span-wise direction (f_z^+) on α_r (solid lines) and r_c (dashed)

B.1.3 Effect of filter size in the stream-wise direction



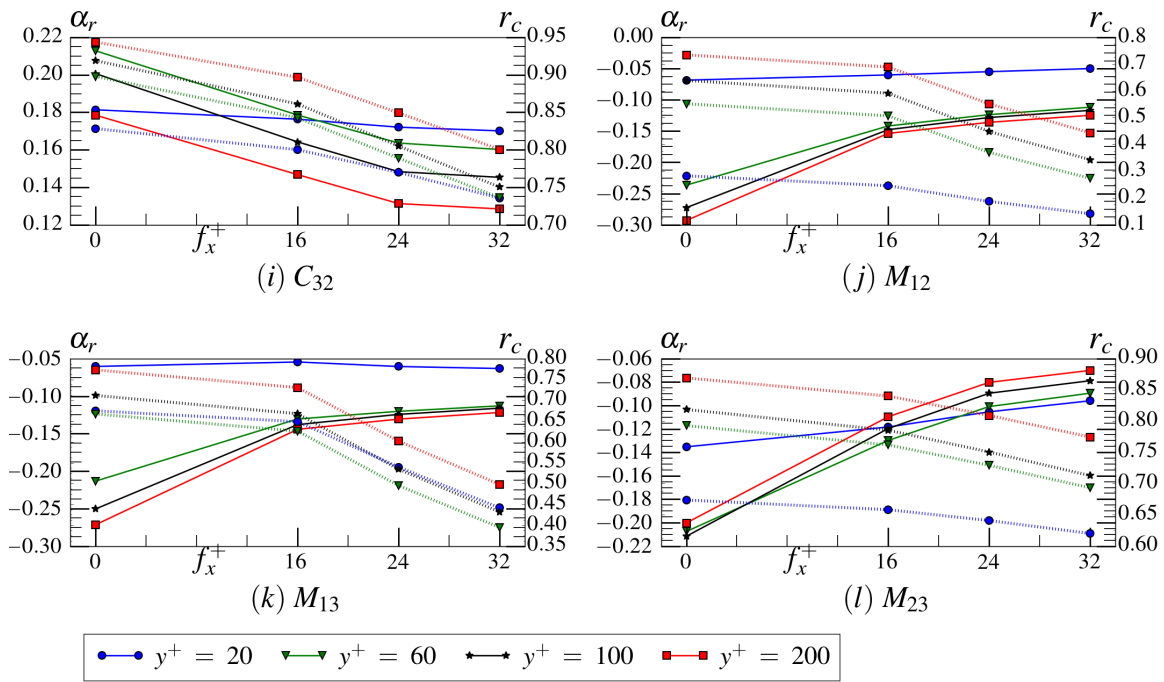


Fig. B.3 Effect of increasing the filter size in the stream-wise direction (f_x^+) on α_r (solid lines) and r_c (dashed)

Bibliography

- Abdel-Rahman, A., Tropea, C., Slawson, P., and Strong, A. (1987). On temperature compensation in hot-wire anemometry. *Journal of Physics E: Scientific Instruments*, 20(3):315.
- Antonia, R., Kim, J., and Browne, L. (1991). Some characteristics of small-scale turbulence in a turbulent duct flow. *Journal of Fluid Mechanics*, 233:369–388.
- Antonia, R., Zhu, Y., and Kim, J. (1994). Corrections for spatial velocity derivatives in a turbulent shear flow. *Experiments in Fluids*, 16(6):411–413.
- Atkinson, C., Buchmann, N. A., Amili, O., and Soria, J. (2014). On the appropriate filtering of PIV measurements of turbulent shear flows. *Experiments in Fluids*, 55(1):1654.
- Baldi, S., Hann, D., and Yianneskis, M. (2002). On the measurement of turbulence energy dissipation in stirred vessels with PIV techniques. In *11th Int. Symp. on Applications of Laser Techniques to Fluid Mech. Instituto superior técnico, Center for innovation, technology, and policy research, Lisbon, Portugal*.
- Bertens, G., van der Voort, D., Bocanegra-Evans, H., and van de Water, W. (2015). Large-eddy estimate of the turbulent dissipation rate using PIV. *Experiments in Fluids*, 56(5):89.
- Buschmann, M. H. and Gad-el Hak, M. (2006). Recent developments in scaling of wall-bounded flows. *Progress in Aerospace Sciences*, 42(5):419–467.
- Buxton, O., Laizet, S., and Ganapathisubramani, B. (2011). The effects of resolution and noise on kinematic features of fine-scale turbulence. *Experiments in Fluids*, 51(5):1417.
- Chang III, P. A., Piomelli, U., and Blake, W. K. (1999). Relationship between wall pressure and velocity-field sources. *Physics of Fluids*, 11(11):3434–3448.
- Chin, C., Hutchins, N., Ooi, A., and Marusic, I. (2009). Use of direct numerical simulation (DNS) data to investigate spatial resolution issues in measurements of wall-bounded turbulence. *Measurement Science and Technology*, 20(11):115401.
- Comte-Bellot, G. (1976). Hot-wire anemometry. *Annual review of fluid mechanics*, 8(1):209–231.
- Corrsin, S. (1963). Turbulence: experimental methods. *Handbuch der Physik*, 3:524–590.
- Corrsin, S. and Kovasznay, L. S. (1949). On the hot-wire length correction. *Physical Review*, 75(12):1954.
- Davidson, P. (2015). *Turbulence: an introduction for scientists and engineers*. Oxford University Press.
- De Jong, J., Cao, L., Woodward, S., Salazar, J., Collins, L., and Meng, H. (2009). Dissipation rate estimation from PIV in zero-mean isotropic turbulence. *Experiments in Fluids*, 46(3):499.

- Delafosse, A., Collignon, M.-L., Crine, M., and Toye, D. (2011). Estimation of the turbulent kinetic energy dissipation rate from 2D-PIV measurements in a vessel stirred by an axial mixer impeller. *Chemical Engineering Science*, 66(8):1728–1737.
- Doron, P., Bertuccioli, L., Katz, J., and Osborn, T. (2001). Turbulence characteristics and dissipation estimates in the coastal ocean bottom boundary layer from PIV data. *Journal of Physical Oceanography*, 31(8):2108–2134.
- Elsner, J. W. and Elsner, W. (1996). On the measurement of turbulence energy dissipation. *Measurement Science and Technology*, 7(10):1334.
- Forliti, D., Strykowski, P., and Debatin, K. (2000). Bias and precision errors of digital particle image velocimetry. *Experiments in Fluids*, 28(5):436–447.
- Foucaut, J.-M. and Stanislas, M. (2002). Some considerations on the accuracy and frequency response of some derivative filters applied to particle image velocimetry vector fields. *Measurement Science and Technology*, 13(7):1058.
- Fouras, A. and Soria, J. (1998). Accuracy of out-of-plane vorticity measurements derived from in-plane velocity field data. *Experiments in Fluids*, 25(5):409–430.
- Frenkiel, F. (1949). The influence of the length of a hot wire on the measurements of turbulence. *Physical Review*, 75(8):1263.
- Gabriele, A., Nienow, A., and Simmons, M. (2009). Use of angle resolved PIV to estimate local specific energy dissipation rates for up-and down-pumping pitched blade agitators in a stirred tank. *Chemical Engineering Science*, 64(1):126–143.
- George, W. K. and Hussein, H. J. (1991). Locally axisymmetric turbulence. *Journal of Fluid Mechanics*, 233:1–23.
- Gerolymos, G., Sénéchal, D., and Vallet, I. (2013). Wall effects on pressure fluctuations in turbulent channel flow. *Journal of Fluid Mechanics*, 720:15–65.
- Gerolymos, G. and Vallet, I. (2016). The dissipation tensor ϵ_{ij} in wall turbulence. *Journal of Fluid Mechanics*, 807:386–418.
- Hanjalic, K. and Launder, B. (1976). Contribution towards a reynolds-stress closure for low-reynolds-number turbulence. *Journal of Fluid Mechanics*, 76:593–610.
- Hinze, J. (1975). *Turbulence*. McGraw-Hill.
- Huang, H., Dabiri, D., and Gharib, M. (1997). On errors of digital particle image velocimetry. *Measurement Science and Technology*, 8(12):1427.
- Hultmark, M., Vallikivi, M., Bailey, S., and Smits, A. (2012). Turbulent pipe flow at extreme reynolds numbers. *Physical Review Letters*, 108(9):094501.
- Kim, J. (1989). On the structure of pressure fluctuations in simulated turbulent channel flow. *Journal of Fluid Mechanics*, 205:421–451.
- Kitsios, V., Sillero, J., Frederiksen, J., and Soria, J. (2015). Proposed stochastic parameterisations of subgrid turbulence in large eddy simulations of turbulent channel flow. *Journal of Turbulence*, 16(8):729–741.
- Kolmogorov, A. N. (1941). Dissipation of energy in locally isotropic turbulence. In *Dokl. Akad. Nauk SSSR*, volume 32, pages 16–18.

- Lee, M. and Moser, R. D. (2015). Direct numerical simulation of turbulent channel flow up to $Re_\tau \approx 5200$. *Journal of Fluid Mechanics*, 774:395–415.
- Lee, M. J. and Reynolds, W. C. (1987). On the structure of homogeneous turbulence. In *Turbulent Shear Flows 5*, pages 54–66. Springer.
- Lumley, J. L. (1979). Computational modeling of turbulent flows. *Advances in Applied Mechanics*, 18:123–176.
- Mansour, N., Kim, J., and Moin, P. (1988). Reynolds-stress and dissipation-rate budgets in a turbulent channel flow. *Journal of Fluid Mechanics*, 194:15–44.
- Mazellier, N. and Vassilicos, J. (2008). The turbulence dissipation constant is not universal because of its universal dependence on large-scale flow topology. *Physics of Fluids*, 20(1):015101.
- Mazellier, N. and Vassilicos, J. (2010). Turbulence without Richardson–Kolmogorov cascade. *Physics of Fluids*, 22(7):075101.
- Oberlack, M. (1997). Non-isotropic dissipation in non-homogeneous turbulence. *Journal of Fluid Mechanics*, 350:351–374.
- Philip, J., Hutchins, N., Monty, J. P., and Marusic, I. (2013). Spatial averaging of velocity measurements in wall-bounded turbulence: single hot wires. *Measurement Science and Technology*, 24(11):115301.
- Pope, S. B. (2001). *Turbulent flows*. Cambridge University Press.
- Richardson, L. F. (1922). Weather prediction by numerical process cambridge university press. *Cambridge Richardson Weather prediction by numerical process 1922*.
- Saarenrinne, P. and Piirto, M. (2000). Turbulent kinetic energy dissipation rate estimation from PIV velocity vector fields. *Experiments in Fluids*, 29:S300–S307.
- Saikrishnan, N., Marusic, I., and Longmire, E. K. (2006). Assessment of dual plane PIV measurements in wall turbulence using DNS data. *Experiments in Fluids*, 41(2):265–278.
- Segalini, A., Cimarelli, A., Rüedi, J., De Angelis, E., and Talamelli, A. (2011). Effect of the spatial filtering and alignment error of hot-wire probes in a wall-bounded turbulent flow. *Measurement Science and Technology*, 22(10):105408.
- Sharp, K. and Adrian, R. (2001). PIV study of small-scale flow structure around a rushton turbine. *AIChE Journal*, 47(4):766–778.
- Sheng, J., Meng, H., and Fox, R. (2000). A large eddy PIV method for turbulence dissipation rate estimation. *Chemical engineering science*, 55(20):4423–4434.
- Sreenivasan, K. R. and Antonia, R. (1997). The phenomenology of small-scale turbulence. *Annual Review of Fluid Mechanics*, 29(1):435–472.
- Uberoi, M. S. and Kovasznay, L. S. (1953). On mapping and measurement of random fields. *Quarterly of Applied Mathematics*, 10(4):375–393.
- Wyngaard, J. (1968). Measurement of small-scale turbulence structure with hot wires. *Journal of Physics E: Scientific Instruments*, 1(11):1105.
- Xu, D. and Chen, J. (2013). Accurate estimate of turbulent dissipation rate using PIV data. *Experimental Thermal and Fluid Science*, 44:662–672.

